Journal of the Anatomical Society of India

Print ISSN: 0003-2778

GENERAL INFORMATION

About the Journal

Journal of the Anatomical Society of India (ISSN: Print 0003-2778) is peer-reviewed journal. The journal is owned and run by Anatomical Society of India. The journal publishes research articles related to all aspects of Anatomy and allied medical/surgical sciences. Pre-Publication Peer Review and Post-Publication Peer Review Online Manuscript Submission System Selection of articles on the basis of MRS system Eminent academicians across the globe as the Editorial board members Electronic Table of Contents alerts Available in both online and print form. The journal is published quarterly in the months of January, April, July and October.

Scope of the Journal

The aim of the *Journal of the Anatomical Society of India* is to enhance and upgrade the research work in the field of anatomy and allied clinical subjects. It provides an integrative forum for anatomists across the globe to exchange their knowledge and views. It also helps to promote communication among fellow academicians and researchers worldwide. The Journal is devoted to publish recent original research work and recent advances in the field of Anatomical Sciences and allied clinical subjects. It provides an opportunity to academicians to disseminate their knowledge that is directly relevant to all domains of health sciences.

The Editorial Board comprises of academicians across the globe.

JASI is indexed in Scopus, available in Science Direct.

Abstracting and Indexing Information

The journal is registered with the following abstracting partners:

Baidu Scholar, CNKI (China National Knowledge Infrastructure), EBSCO Publishing's Electronic Databases, Ex Libris – Primo Central, Google Scholar, Hinari, Infotrieve, Netherlands ISSN center, ProQuest, TdNet, Wanfang Data

The journal is indexed with, or included in, the following:

SCOPUS, Science Citation Index Expanded, IndMed, MedInd, Scimago Journal Ranking, Emerging Sources Citation Index.

Impact Factor® as reported in the 2020 Journal Citation Reports® (Clarivate Analytics, 2021): 0.15

Information for Authors

Article processing and publication charges will be communicated by the editorial office. All manuscripts must be submitted online at https://review.jow.medknow.com/jasi.

Subscription Information

A subscription to JASI comprises 4 issues. Prices include postage. Annual Subscription Rate for non-members-

Rates of Membership (with effect from 1.1.2019)

	India	International
Ordinary membership	INR 1500	US $ 100
Couple membership	INR 2250	
Life membership	INR 8000	US $ 900
Subscription Rates (till 31st August)		
Individual	INR 6000	US $ 650
Library/Institutional Trade discount of 10% for agencies only	INR 12000	US $ 1000
Subscription Rates (after 31st August)		
Individual	INR 6500	US $ 700
Library/Institutional	INR 12500	US $ 1050

The Journal of Anatomical Society of India (ISSN: 0003-2778) is published quarterly **Subscriptions** are accepted on a prepaid basis only and are entered on a calendar year basis. Issues are sent by standard mail Priority rates are available upon request.

Information to Members/Subscribers

All members and existing subscribers of the Anatomical Society of India are requested to send their membership/existing subscription fee for the current year to the Treasurer of the Society on the following address: Prof (Dr.) Punit Manik, Treasurer, ASI, Department of Anatomy, KGMU, Lucknow - 226003. Email: punitamanik@yahoo.co.in. All payments should be made through an account payee bank draft drawn in favor of the **Treasurer, Anatomical Society of India,** payable at **Lucknow** only, preferably for **Allahabad Bank, Medical College Branch, Lucknow.** Outstation cheques/drafts must include INR 70 extra as bank collection charges.

All complaints regarding non-receipt of journal issues should be addressed to the Editor-in-Chief, JASI at editorjasi@gmail.com. The new subscribers may, please contact wkhlrpmedknow_subscriptions@wolterskluwer.com.

Requests of any general information like travel concession forms, venue of next annual conference, etc. should be addressed to the General Secretary of the Anatomical Society of India.

For mode of payment and other details, please visit www.medknow.com/subscribe.asp

Claims for missing issues will be serviced at no charge if received within 60 days of the cover date for domestic subscribers, and 3 months for subscribers outside India. Duplicate copies cannot be sent to replace issues not delivered because of failure to notify publisher of change of address. The journal is published and distributed by Wolters Kluwer India Pvt. Ltd. Copies are sent to subscribers directly from the publisher's address. It is illegal to acquire copies from any other source. If a copy is received for personal use as a member of the association/ society, one cannot resale or give-away the copy for commercial or library use.

The copies of the journal to the subscribers are sent by ordinary post. The editorial board, association or publisher will not be responsible for non receipt of copies. If any subscriber wishes to receive the copies by registered post or courier, kindly contact the publisher's office. If a copy returns due to incomplete, incorrect or changed address of a subscriber on two consecutive occasions, the names of such subscribers will be deleted from the mailing list of the journal. Providing complete, correct and up-to-date address is the responsibility of the subscriber.

Nonmembers: Please send change of address information to subscriptions@medknow.com.

Advertising Policies

The journal accepts display and classified advertising. Frequency discounts and special positions are available. Inquiries about advertising should be sent to Wolters Kluwer India Pvt. Ltd, advertise@medknow. com.

The journal reserves the right to reject any advertisement considered unsuitable according to the set policies of the journal.

The appearance of advertising or product information in the various sections in the journal does not constitute an endorsement or approval by the journal and/or its publisher of the quality or value of the said product or of claims made for it by its manufacturer.

Addresses

Editorial Office

Dr. Vishram Singh, Editor-in-Chief, JASI
OC-5/103, 1st floor, Orange County Society,
Ahinsa Khand-I, Indirapuram, Ghaziabad,
Delhi, NCR- 201014.
Email: editorjasi@gmail.com

Published by

Wolters Kluwer India Pvt. Ltd
A-202, 2nd Floor, The Qube,
C.T.S. No.1498A/2 Village Marol, Andheri (East),
Mumbai - 400 059, India.
Phone: 91-22-66491818
Website: www.medknow.com

Printed at

Nikeda Art Printers Pvt. Ltd.,
Building No. C/3 - 14,15,16, Shree Balaji Complex, Vehele Road,
Village Bhatale, Taluka Bhiwandi, District Thane - 421302, India.

Journal of the Anatomical Society of India

Print ISSN: 0003-2778

EDITORIAL BOARD

Journal of the Anatomical Society of India

Print ISSN: 0003-2778

EXECUTIVE COMMITTEE

Journal of the Anatomical Society of India

Volume 71 | Issue 3 | July-September 2022

CONTENTS

EDITORIAL

Vertebral Endplates, The Anatomically Discrete Structures of The Vertebral Column
Vishram Singh, B. V. Murlimanju, Rajanigandha Vadgaonkar 167

ORIGINAL ARTICLES

Carotid Intima–Media Thickness: An Independent Risk Factor for Stroke Prediction – A Call for Revised Framingham Score System
Garima Khatri, Mohan Singh, Sunita Bika, Khushboo Joshi, Nirmala Swami 169

Age- and Gender-Based Morphometric Variation of Macula in Indian Population using Optical Coherence Tomography
Pareesa Rabbani, Shalini Kumar, Taskin Khan, Shayama K. Razdan 178

Cardiac Morphometry in Healthy Young Indian Adult Males: An Evaluation of Chamber Thickness and Left Ventricular Cardiac Mass
Rohit Aggarwal, Ruchi Gautam, Abdul Raheem Sheik 186

Problem-based Learning Using Online Platforms: An Interactive Alternative to Mandatory E-learning during the COVID-19 Pandemic
Mamata Chimmalgi, S. Rajesh, K. V. Anil Kumar, U. V. Asha, Jesin Elsa Jose, Komalavallyamma Chandrakumari 191

Dimensional Accuracy of Medical Models of the Skull Produced by Three-Dimensional Printing Technology by Advanced Morphometric Analysis
Sharmila Aristotle, Shantanu Patil, Saikarthik Jayakumar 199

Gender Prediction with the Parameters Obtained from Pelvis Computed Tomography Images and Machine Learning Algorithms
Yusuf Secgin, Zulal Oner, Muhammed Kamil Turan, Serkan Oner 204

Description of an Atypical Vascular Arch in the Renal Parenchyma
Alberto Garcia Barrios, Ana Isabel Cisneros Gimeno, Jesus Obon Nogue, Jaime Whyte Orozco 210

Relationship between Digit Ratio of 2D:4D and The Physical Health among College Students of Han Ethnicity in Southern Fujian
Tongjun Chen, Jianmei Xiang, Shaokang Teng, Zhongqing Huang , Xiaoliang Li, Liping Huang, Huihua Chen, Baoying Luo 214

Variations of the Circle of Willis Determined via Magnetic Resonance Angiography: A Single-Center Analysis of the Serbian Population
Mimoza Đevukaj, Igor Nosek, Miloš Vuković, Duško Kozić 220

The Normal Vermiform Appendixin Adults: Its Anatomical Location, Visualization, and Diameter at Computed Tomography
Aysegul Altunkas, Fatma Aktas, Zafer Ozmen, Eda Albayrak, Osman Demir 225

REVIEW ARTICLE

An Anatomical Description of the Obturator Region with Clinical Aspects
Lidija Kocbek Šaherl, Mateja Rakuša 234

continued...

CASE REPORTS

True Hermaphrodite of Ovotestis in a 5-Year-Old Child
James Joseph Yahaya.....242

Bilateral Tripartite Dural Septation of the Jugular Foramen
Joastin Naidoo, Carmen Olivia Rennie, Lelika Lazarus 245

Multiple Intracranial Vessel Fenestrations: A Report of Two Cases from a Tertiary Care Center
Amlan Kusum Datta, Subhadeep Gupta.....248

Vertebral Endplates, The Anatomically Discrete Structures of The Vertebral Column

The vertebral endplates are anatomically discrete structures, which act as the interface between the body of the vertebra and the intervertebral disc. They are comprised of hyaline cartilage and are situated superior and inferior to each of the intervertebral discs.[1] Their function is to offer interlocking mechanically and puts the nucleus pulposus and bulging into the middle part of the vertebra.[2] Vertebral endplates are the hardest part of the intervertebral disc, however, they fail to work once there is fracture of the body of the vertebra.[3] They provide nutrition to the intervertebral disc by offering the nucleus pulposus and annulus fibrosus with the components, which preserve the intervertebral disc, keep them flourishing, and also prevent their degeneration.[4] In a computed tomography (CT)- and cadaveric-based study, many variations of concavity of the upper and lower vertebral endplates and variations due to age were found.[5] However, the dimensions of vertebral endplates can only be measured in the disarticulated fresh cadaveric vertebrae, which may be difficult. The geometric morphological analysis can be done with a goniometer. Huang *et al*.[6] reported that there is no gender difference in the curvature of the vertebral endplates. Other magnetic resonance imaging (MRI) and CT-based studies reported similar craniocaudal differences in the morphometry of the vertebral endplates; however, there are reports available that males have significantly larger geometric dimensions than females.[7,8] It is also important to understand that the concavity of the vertebral endplates increases linearly with aging and age-related degenerative changes including osteophytes add to the morphological variation.[9] A subanalysis corrected to the variation due to age is likely to remove the confounding due to age-related morphological changes in vertebral endplates. Asymptomatic individual can have age-related degenerative disc changes and intervertebral disc degenerative changes alter the morphology, surface area, and curvature of the vertebral endplates in the sagittal, coronal, and transverse axis.[10] The morphological data of the vertebral endplate can be studied, which will be not only useful in the field of neurosurgery, but are also extrapolated to specialties such as neurology and orthopedics, for the management of neurological and musculoskeletal disorders, which are a frequent cause of outpatient and emergency room visits.[5,7] The surgical implants should be devised as per the morphometric data of that particular population.[11] Characterizing the morphology of the spine among populations would allow personalizing the conditions under which each individual should be exposed, for example, at work, or also to determine a possible risk factor that explains the presence of a clinical picture in case of an injury at the spine level, thus modifying the decision-making in the clinical approach.

Vishram Singh, B. V. Murlimanju, Rajanigandha Vadgaonkar

Department of Anatomy, Kasturba Medical College, Mangalore, Manipal Academy of Higher Education, Manipal, Karnataka, India

Address for correspondence: *Dr. B. V. Murlimanju, Department of Anatomy, Kasturba Medical College, Mangalore - 575 004, Karnataka, India. E-mail: flutemist@gmail. com*

References

1. Moore RJ. The vertebral endplate: Disc degeneration, disc regeneration. Eur Spine J 2006;15 Suppl 3:S333-7.
2. Frost BA, Camarero-Espinosa S, Foster EJ. Materials for the spine: Anatomy, problems, and solutions. Materials (Basel) 2019;12:E253.
3. Lotz JC, Fields AJ, Liebenberg EC. The role of the vertebral end plate in low back pain. Global Spine J 2013;3:153-64.
4. Adams MA. Intervertebral Disc Tissues. In: Derby B, Akhtar R. Editors. Mechanical Properties of Aging Soft Tissues. Engineering Materials and Processes. Cham, Switzerland: Springer International Publishing; 2015.
5. Chen H, Jiang D, Ou Y, Zhong J, Lv F. Geometry of thoracolumbar vertebral endplates of the human spine. Eur Spine J 2011;20:1814-20.
6. Huang W, Wang H, Zhou P, Xie L, Huang Z, Zheng C, *et al.* Analysis of the curvature and morphologic features of the lumbar vertebral endplates through the transverse section: A radioanatomical study. World Neurosurg 2021;150:e500-10.
7. Tang R, Gungor C, Sesek RF, Foreman KB, Gallagher S, Davis GA. Morphometry of the lower lumbar intervertebral discs and endplates: Comparative analyses of new MRI data with previous findings. Eur Spine J 2016;25:4116-31.
8. Liu JT, Han H, Gao ZC, He CY, Cai X, Niu BB, *et al.* CT assisted morphological study of lumbar endplate. Zhongguo Gu Shang 2018;31:1129-35.
9. Shao Z, Rompe G, Schiltenwolf M. Radiographic changes in the lumbar intervertebral discs and lumbar vertebrae with age. Spine (Phila Pa 1976) 2002;27:263-8.
10. Louie PK, Espinoza Orías AA, Fogg LF, LaBelle M, An HS,

Andersson GBJ, *et al.* Changes in lumbar endplate area and concavity associated with disc degeneration. spine (Phila Pa 1976) 2018;43:E1127-34.

11. Prameela M, Prabhu LV, Murlimanju B, Pai MM, Rai R, Kumar CG. Anatomical dimensions of the typical cervical vertebrae and their clinical implications. Eur J Anat 2020;24:9-15.

Article Info

Received: 01 September 2022
Accepted: 01 September 2022
Available online: ***

Access this article online	
Quick Response Code:	**Website:** www.jasi.org.in
	DOI: 10.4103/jasi.jasi_118_22

How to cite this article: Singh V, Murlimanju B, Vadgaonkar R. Vertebral endplates, the anatomically discrete structures of the vertebral column. J Anat Soc India 2022;XX:XX-XX.

Original Article

Carotid Intima–Media Thickness: An Independent Risk Factor for Stroke Prediction – A Call for Revised Framingham Score System

Garima Khatri, Mohan Singh, Sunita Bika[1], Khushboo Joshi, Nirmala Swami

Departments of Anatomy and [1]Pathology, S.P. Medical College, Bikaner, Rajasthan, India

Abstract

Introduction: Stroke is the second leading cause of death globally, with more than 85% of deaths from stroke occurring in developing countries. It is also reported as the major sequel of head and neck irradiation and has not received the attention it deserves. The contribution of various risk factors to the burden of stroke worldwide is unknown, particularly in countries of low and middle income. We aimed to establish the association of known and emerging risk factors, the carotid intima–media thickness (IMT), with stroke in postradiotherapy patients with head and neck malignancies, also aimed to establish whether carotid IMT (cIMT) is an independent risk factor to predict future stroke. **Material and Methods:** The study recruited 501 subjects. 151 irradiated patients with head and neck malignancy, formed case group. Three hundred and fifty nonirradiated apparently healthy controls formed control group. Each group was subdivided into four subgroups on the basis of gender and presence or absence of classical atherogenic risk factors, i.e. totally 8 groups were structured. All subjects were measured for their cIMT by color Doppler, b-mode ultrasonography and were also made to complete a questionnaire to assess other cardiovascular risk factors. The Framingham score system was used to predict probability of stroke. **Results:** Study described higher values of cIMT and total points for risk factors in cases than in controls and the difference was again statistically significant ($P = 0.0001$). **Discussion and Conclusion:** CIMT clearly indicated to act as an independent risk factor to predict stroke and is suggested to be worked on to be incorporated in the Framingham score.

Keywords: *Cardiovascular risk factors, carotid intima–media thickness, stroke*

Introduction

Stroke is the second leading cause of death globally, with more than 85% of deaths from stroke occurring in developing countries.[1] Stroke has been reported the most common late circulatory disease after radiotherapy of head and neck malignancy.[2] The Indian subcontinent (including India, Pakistan, Bangladesh, Srilanka, and Nepal) has among the highest rates of cardiovascular diseases (CVDs)[3] stroke and coronary heart disease (CHD) contributes significantly to premature mortality and morbidity worldwide. Largely preventable, they demand prevention.[4]

Stroke is the major sequel of head and neck irradiation that has not received the attention it deserves. Radiotherapy as a part of the treatment regime of head and neck tumors increases the survival but also puts the patients at risk of radiation-related side effects. Of these, vascular side effects are serious and may be life-threatening. Radiation-induced thrombosis of carotid arteries and subsequent stroke is the most common complication after radiotherapy of head and neck malignancy.[2] The changes in carotid intima–media thickness (cIMT) are thought to occur in an accelerated manner; however, the time course of the appearance of clinical symptoms remains to be defined.

However, there has been little research to identify the causes of stroke in low-income and middle-income countries. An understanding of the risk factors for stroke in these countries is crucial, to determine priorities and strategies for reversing the rapidly rising rates of stroke mortality in developing countries.[1] The contribution of various risk factors to the burden of stroke worldwide is unknown, particularly in countries of low and middle income.[5] We aimed to establish the association of known risk factors and emerging risk factor, the cIMT, with stroke in postradiotherapy patients with head and neck malignancies. This study will aid in assessing the contribution of this risk factor to the burden

How to cite this article: Khatri G, Singh M, Bika S, Joshi K, Swami N. Carotid intima–media thickness: An independent risk factor for stroke prediction – A call for revised Framingham score system. J Anat Soc India 2022;XX:XX-XX.

Article Info

Received: 24 December 2021
Revised: 16 June 2022
Accepted: 05 July 2022
Available online: ***

Address for correspondence:
Dr. Garima Khatri, D-7 Nagnechi Scheme, UIT Colony, Bikaner, Rajasthan, India.
E-mail: khatri.g.04@gmail.com

Access this article online

Website: www.jasi.org.in
DOI: 10.4103/jasi.jasi_212_21
Quick Response Code:

of stroke and also explore the differences between risk factors for stroke and CVDs.

It is generally believed that atherosclerosis associated with radiation therapy, while histologically similar to spontaneous atherosclerosis, is clinically distinct because it is limited to the irradiated area and is less likely to be associated with atherogenic risk factors (i.e. aging, male sex, hypertension, cigarette smoking, diabetes, and hypercholesterolemia) and concomitant illnesses (i.e. coronary artery disease and peripheral vascular disease).[6,7]

The measurement of the cIMT is feasible with today's high-resolution ultrasound (US) machine. When US beam is at right angle to the carotid walls, two white lines are seen in the vessel, particularly on the far wall. The first-line corresponds to the blood-intima boundary and the second to the outer media-adventitia junction. The IMT is the distance between the two interfaces.[8,9]

Considering in view, the poor quality of the lives of cancer patients and the severe emotional trauma of their families, this study aimed first to determine the effect of radiations on cIMT in patients with head and neck malignancy in comparison with non-irradiated matched subjects. Second and more important, we aimed to establish whether cIMT is an independent risk factor to predict future stroke.

We postulated that cIMT increases after radiation therapy and acts as a good independent risk factor for stroke prediction, if this hypothesis is true, it will be an alarming call for recalibration or revision of Framingham and other risk scores for stroke prediction, which should give due place to cIMT as an individual risk factor in their risk score profiles. This will greatly help medical interventions to discriminate between future cases and noncases and help the clinicians to focus on those at highest risk because risk scores are not crystal balls for prophesying, they are for prioritizing preventive treatment.[4]

Material and Methods

Study design and participants

It was a cross-sectional study which recruited 501 subjects. 151 individuals were irradiated patients of head and neck malignancy, they constituted the case group. Three hundred and fifty individuals were nonirradiated apparently healthy controls formed the control group. Each group was further divided, first on the basis of gender, into two subgroups females and males. Each gender subgroup was then again further classified into two subgroups on the basis of the absence or presence of classical atherogenic risk factors. In this way, a total of 8 subgroups were structured as shown in Figure 1.

Distribution of study participants was classified into groups and subgroups:

A. Cases (E) (n = 151):
   a. Females (F) (n = 16):
      (i) Without risk factors (W) (n = 13)
      (ii) With risk factors (R) (n = 03)
   b. Males (M) (n = 135):
      (i) Without risk factors (W) (n = 26)
      (ii) With risk factors (R) (n = 109)

   i.e. 4 subgroups in cases, namely, EFW (n = 13), EFR (n = 03), EMW (n = 26), EMR (n = 109)

B. Controls (C) (n = 350):
   a. Females (F) (n = 60):
      (i) Without risk factors (W) (n = 44)
      (ii) With risk factors (R) (n = 16)
   b. Males (M) (290):
      (i) Without risk factors (W) (n = 188)
      (ii) With risk factors (R) (n = 102),

   i.e. four subgroups in controls, namely CFW (n = 44), CFR (n = 16), CMW (n = 188), CMR (n = 102)

Inclusion criteria for cases were that, they must have received radiation therapy to the carotid area for treatment of malignancy, radiotherapy to have occurred at least 1 year before US examination, may or may not have other atherogenic risk factors (i.e. diabetes mellitus, hypertension, hypercholesterolemia, obesity,and cigarette smoking habit), all cases were treated with cobalt therapy.

Inclusion criteria for the control group were that they were nonirradiated apparently healthy individuals with or without any major risk factors for atherosclerosis as mentioned before.

All cases and controls were made to complete a questionnaire to assess their cardiovascular risk factors, had their height, weight, and blood pressure measured and they also provided a blood sample for measurement of HDL, total cholesterol, and random blood sugar levels [Table 1]. Smoking history was assessed. The institutional ethics committee approved the protocol. The study obtained written, informed consent from all participants before enrolment.

Procedure

All scans were obtained by color Doppler and B mode US technique. All carotid US scans were carried out by one observer using previously standardized program incorporated in software package of the US equipment. Examination was performed after a rest period of 10 min with subjects in supine position and neck extended. Both common carotid arteries were examined along with their full visible length [Figure 2].

Sonological examination of common carotid artery (CCA) was done using L and T SEQUINA Color Doppler Scanner with a linear band probe of frequency 6.6–14 MHz. All scans were obtained at 12 MHz. All IMT measurements were made in the longitudinal plane at the point of maximum thickness on the far wall of the CCA along a 1 cm section of the artery, proximal to the carotid bulb [Figure 2]. The position of the carotid bulb is defined as the point at which the far wall deviates away from the parallel plane of the distal CCA. IMT was the distance between

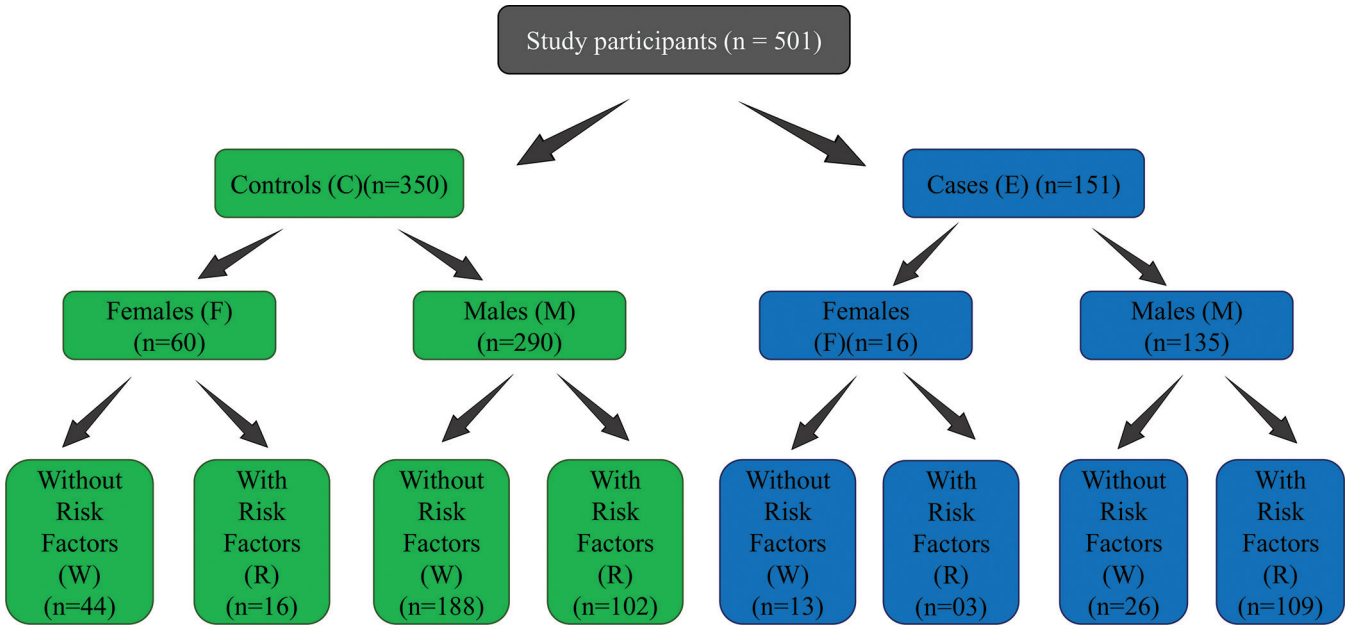

Figure 1: Classification of study participants into groups (on the basis of presence or absence of irradiations) and subgroups (on the basis of gender and absence or presence of atherogenic risk factors)

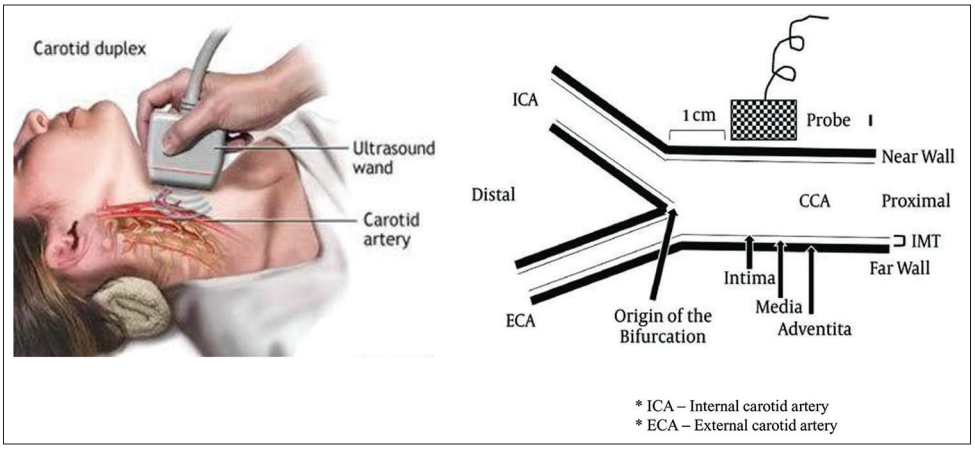

Figure 2: Schematic representation of cIMT on the far wall of CCA. cIMT: Carotid intima–media thickness, CCA: Common carotid artery

the inner echogenic line representing the intima-blood interface and the outer echogenic line representing the adventitia media junction [Figure 3]. After freezing the image, the measurements were made with electronic calipers [Figure 4].[9] The US images were magnified to improve the accuracy of caliper placement. Measurements were repeated three times, unfreezing the image on each occasion. The mean value of each set of three measurements, representing the mean IMT of each CCA was taken. The hard copy of images was obtained of each examination.

Statistical analysis

The data on cIMT were analyzed among all participants using INDOSTAT software. The mean values were compared using Student's *t*-test and their significance was assessed using *P* value. The $P < 0.05$ showed a significant difference among the cohorts.

Results

Our study enrolled 501 subjects. 350 individuals were nonirradiated control group [Table 1] and remaining 151 individuals were irradiated patients [Table 1] who underwent radiotherapy for head and neck region and also had CCA exposed to radiation during their treatment. Data obtained were put in Tables 1-3.

Table 1 describes the comparative baseline demographics of the cohorts with the prevalence of classical risk factors of atherosclerosis (i.e. age, hypercholesterolemia, diabetes mellitus, hypertension, and obesity). It makes evident that the values of all the risk factors were higher in groups with risk factors in comparison to groups without risk factors and the differences were statistically significant.

Table 1: Comparative baseline demographics of the cohorts

Parameters	Control females			Control males			Case females			Case males		
	Without risk factors (*n*=44), mean±SD	With risk factors (*n*=16), mean±SD	*P**	Without risk factors (*n*=188), mean±SD	With risk factors (*n*=102), mean±SD	*P**	Without risk factors (*n*=13), mean±SD	With risk factors (*n*=3), mean±SD	*P**	Case males without risk factors (*n*=26), mean±SD	Case males with risk factors (*n*=109), mean±SD	*P**
Age (years)	40.04±14.48	45.44±10.83	0.182	42.62±13.39	43.93±9.52	0.35	47.84±11.42	52.33±15.04	0.57	48.19±9.23	50.47±9.28	0.189
Height (cm)	159.09±4.16	157.81±2.56	0.254	173.70±4.32	173.64±3.78	0.906	162.46±2.53	161.0±3.61	0.415	174.46±2.83	175.35±4.15	0.304
Weight (kg)	57.70±4.68	67.31±8.67	0.0001	69.34±7.43	83.70±11.31	0.0001	58.23±4.02	61.5±9.19	0.334	66.46±5.22	70.24±13.55	0.166
Total cholesterol (mg/dl)	177.06±21.42	220.21±52.16	0.0001	184.24±23.82	203.51±36.01	0.0001	172.12±14.16	162.40±14.27	0.302	166.77±12.67	192.02±48.35	0.009
Random blood sugar (mg/dl)	89.52±23.84	125.56±70.25	0.004	94.83±23.31	104.72±37.75	0.003	92.86±9.51	142.46±65.67	0.01	99.30±19.93	115.77±48.10	0.091
Blood pressure systolic (mmHg)	125.90±7.01	151.43±22.81	0.0001	127.16±7.02	147.03±19.03	0.0001	128.15±8.02	130.0±10.0	0.74	130.34±9.19	141.58±17.38	0.001
Blood pressure diastolic (mmHg)	81.90±2.20	87.43±5.94	0.0001	82.29±2.21	87.34±6.48	0.0001	82.69±2.39	83.33±2.88	0.69	83.26±2.37	87.34±6.48	0.002
BMI	22.71±1.98	27.31±2.53	0.0001	22.99±1.91	27.73±3.58	0.0001	22.08±1.83	23.46±1.77	0.257	22.10±1.55	24.19±3.01	0.0001

*$P<0.05$ is statistically significant. Statistical comparison has been made between groups with and without risk factors. SD: Standard deviation, BMI: Body mass index

Table 2 shows higher values of cIMT and total points for risk factors in cases than in controls and the difference was again statistically significant.

Table 3 manifests comparative biometrics of all the 8 groups for cIMT and total points for risk factors. These total points for risk factors were calculated using a standard Framingham Stroke Risk Score[10] (being standard score, it has not been described here). Another alternative score for CVD risk calculation[11] which is less commonly used in standard books, gives more importance to modifiable risk factors such as physical activity and dietary factors, is described in Tables 4-6. Since this score is less commonly used currently but seems to be more relevant in the current scenario of changing lifestyles, especially in the Indian scenario, so we compared this score with Framingham score on a hypothetical subject in discussion section, to prove the rationale of our study.

In Table 3, when the female group was compared for their mean cIMT, it was found that CFW group (control females without risk factors) showed lower value (0.299 ± 0.049) than the CFR group (control females with risk factors) (0.425 ± 0.025) and the difference was highly significant (i.e. $P = 0.0001$).

When the baseline data of the above-mentioned groups were applied to the Framingham Stroke Risk Score[10] to calculate stroke probability for 10 years, the mean total points for Risk Factors in CFW group were 3.45 ± 0.76, and in CFR group, it was 7.31 ± 4.55 which was much higher than the former. The difference between the two groups was highly significant ($P = 0.0001$).

Similarly, when irradiated female groups were compared for the same data, then it was found that EFW group (case females without risk factors) showed lower mean cIMT value (0.689 ± 0.062) than the EFR group (case females with risk factors) (0.85 ± 0.06) and their difference was highly significant ($P = 0.0001$). In EFW group, Total Points for Risk Factors were recorded 4.0 ± 2.12 which was lower than EFR group (7.66 ± 1.52) and their difference was significant ($P = 0.014$).

When similar comparisons were made for males, then it is evident from Table 3 that CMW group (control males without risk factors) showed lower values of mean cIMT (0.313 ± 0.035) and total points for risk factors (2.88 ± 1.18) than the CMR group (control males with risk factors) (0.414 ± 0.036 and 6.99 ± 3.36. respectively). It is also clear from Table 2 that the difference in data between the two groups was found to be highly significant ($P = 0{\cdot}0001$).

In EMW group (case males without risk factors), the value of mean cIMT and total points for risk factors was lower (0.691 ± 0.068 and 3.35 ± 1.74, respectively) than EMR group (case males with risk factors) (0.826 ± 0.191 and 8.21 ± 3.15, respectively). The difference between both the variables was highly significant ($P = 0{\cdot}0001$).

Table 2: Mean intima-media thickness and mean total points for risk factors in controls and cases

Parameters	Mean±SD		*P*
	Controls without risk factors (*n*=232)	Cases without risk factors (*n*=39)	
Mean IMT (mm)	0.310±0.038	0.690±0.065	0.0001
Total points for risk factors	2.99±1.13	3.56±1.87	0.010
Parameters	**Controls with risk factors (*n*=118)**	**Cases with risk factors (*n*=112)**	***P***
Mean IMT (mm)	0.415±0.035	0.827±0.188	0.0001
Total points for risk factors	7.03±3.52	8.19±3.11	0.008

IMT: Intima-media thickness, SD: Standard deviation

Table 3: Mean intima-media thickness and mean total points for risk factors in different groups under study

Groups	Mean IMT (mm)±SD	*P*	Mean total points for risk factors	*P*
CFW: CFR	0.299±0.049:0.425±0.025	0.0001***	3.45±0.76:7.31±4.55	0.0001***
CMW: CMR	0.313±0.035:0.414±0.036	0.0001***	2.88±1.18:6.99±3.36	0.0001***
EFW: EFR	0.689±0.062:0.85±0.06	0.001**	4.0±2.12:7.66±1.52	0.014*
EMW: EMR	0.691±0.068:0.826±0.191	0.0001***	3.35±1.74:8.21±3.15	0.0001***

*Significant at 5%, **Moderately significant at 1%, ***Highly significant at 0.1%. CFW: Control females without risk factors, CFR: Control females with risk factors, CMW: Control males without risk factors, CMR: Control males with risk factors, EFW: Case females without risk factors, EFR: Case females with risk factors, EMW: Case males without risk factors, EMR: Case males with risk factors, SD: Standard deviation, IMT: Intima-media thickness

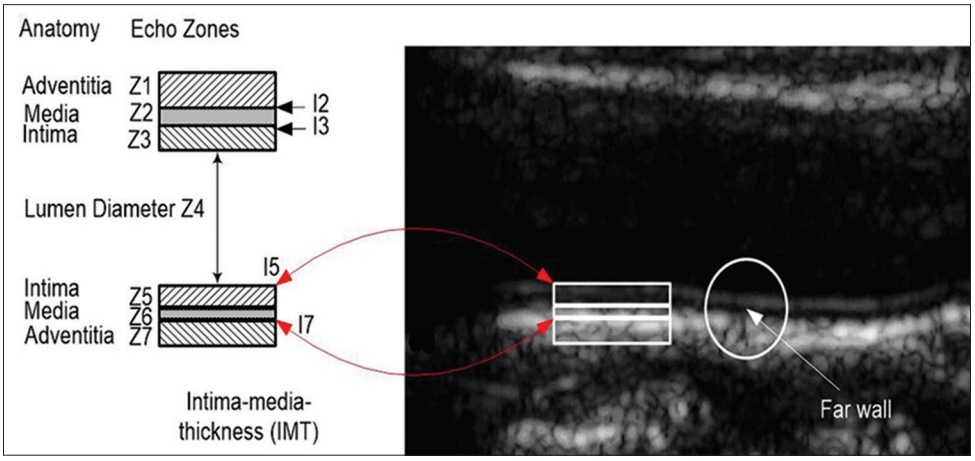

Figure 3: Illustration of IMC of far the wall of the common carotid artery. The IMC consists of the intima band (Z5), the media band (Z6) and the far wall adventitia band (Z7). The IMT complex is defined as the distance between the blood intima interface line and the media adventitia interface line. IMC: Intima–media complex, IMT: Intima–media thickness

Figures 5-7 show the data of cIMT, total points for risk factors, and cIMT versus total points for risk factors, respectively, in the form of a scatterplot. Figures 5 and 6 depict the increasing trends of these variables as we move from controls toward cases. Figure 7 clearly shows a positive linear correlation between the two plotted variables.

Discussion

Analysis of our data documents two major findings in support of the aim of this case–control study:

1. One is that there is thickening of the intima–media complex of CCA in patients with a history of radiations to the head and neck region compared with matched nonirradiated subjects (P = 0.0001). If there is the presence of any predisposing factors for atherosclerosis, then there is further increase in cIMT and cerebrovascular risk or stroke.[2,7-9,12-16] It was indicated when parameters under consideration of our study were compared for their mean in different groups. Table 3 shows that cIMT is independent of pressure of other conventional risk factors. Figure 5 favors this finding. It shows a clear increasing trend as we move from controls toward case groups.
2. Second finding surfaced from this study is an interesting one and opens up a new discussion on recalibration of the Framingham risk score for stroke and CVDs. It states that cIMT is not only a good predictor of future stroke but also appears to act as an independent factor for stroke prediction [Figure 7]. This can be easily understood by comparing the data for mean cIMT with that of Total Points for Risk factors, as calculated from the Framingham score, among different groups. Table 3

Table 4: Scoring for general risk factors[24]

General risk factor	Risk score	
	Present	Absent
History of hypertension	1	0
History of diabetes	1	0
History of stroke	1	0
Family history of hypertension	1	0
Family history of diabetes	1	0
Regular smoker	1	0
BMI ≥25	1	0
Hypertension		
Stage I	1	
Stage II	2	0
Stage III	3	

Maximum possible score=10, Minimum possible score=0. Stage I hypertension=Systolic: 140-159 mmHg/diastolic: 90-99 mmHg, Stage II hypertension=Systolic: 160-179 mmHg/diastolic: 100-109 mmHg, Stage III hypertension=Systolic ≥180 mmHg/diastolic ≥110 mmHg. BMI: Body mass index

Table 5: Physical activity scoring system[24]

Physical activity pattern	Risk score
Nature of work	
Sedentary	2
Moderate	1
Heavy	0
Mode of travelling for going to work place	
No travel required	3
Sitting/standing in a vehicle	2
Walking	1
Cycling	0
Physical activity not related to professional work	
No such physical activity	5
Slow walking	4
Brisk walking	3
Yoga/free hand/gym	2
Cycling	1
Physical activity games	0

Maximum possible score=10, Minimum possible score=0

apparently shows that the value of latter is more in groups with risk factors and furthermore in irradiated groups.

It is evident from Figures 5-7 that there is a positive linear relation between Total Points for risk factors as proposed in Framingham Stroke Risk Score, and cIMT, i.e. with increasing total points for risk factors, cIMT also increases, and thus, we can say that risk of stroke increases with increasing cIMT. Hence, this study indicates that besides all the conventional risk factors incorporated in Framingham Stroke Risk Score, cIMT appears to bag an independent position.

Although Figure 7 shows a positive correlation of cIMT and Framingham Stroke Risk Score, the scatter is wide. A more comprehensive scoring system may generate a better scatter plot.

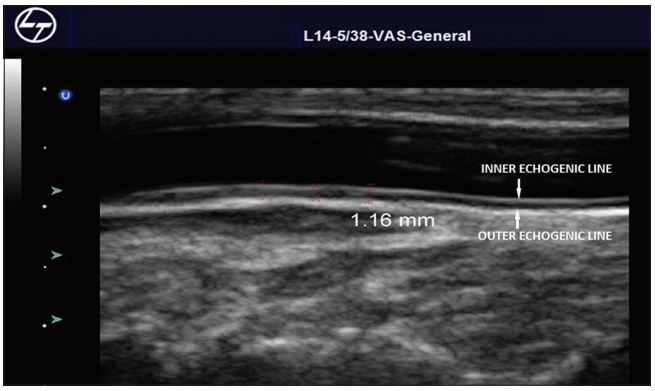

Figure 4: Ultrasound scan showing carotid intima–media thickness on the far wall of common carotid artery

This study is first to propose and suggest that cIMT appears to act [Figure 7] as a new independent factor for stroke prediction so it should be further worked on to be incorporated in the Framingham Stroke Risk Score.

As we know that stroke is one of the leading causes of serious, long-term disability and mortality in the developed as well as developing countries, this study is an alarming call for an improved scoring system for identifying patients at high risk of stroke, so as to prioritize the preventive treatments. Key to the usefulness of determining the likelihood of stroke by means of a risk score profile is evidence that the modification of several potential risk factors will reduce stroke probability.[17]

Many workers around the world are debating on Framingham and other risk scores such as ASSIGN, QRISK, REYNOLDS, and ABCD.[4,18-20] All these scores are working on conventional risk factors for predicting stroke and cardiovascular risk probability, but the ground fact with changing scenario is that besides classic risk factors, there are other determinants which play important role in the prediction of CVDs and stroke and they vary with geographical, environmental and lifestyle differences. If a score is to be globally adopted for preventive action, it should not neglect sections of the population at excess risk, for reasons incompletely identified by classic risk factors and score systems.

WHO in its surveillance study of risk factors for non-communicable diseases[21] has emphasized on risk factors amenable to intervention,[22,23] out of which physical inactivity and inappropriate diet are considered important.

The INTERHEART study[24] has also approved of the association of potentially modifiable risk factors with myocardial infarction.

The Framingham risk score profile for stroke and CVDs[10] has one major drawback that it has emphasized more on non-modifiable risk factors (e.g. age and sex) than the modifiable risk factors (e.g. cigarette smoking, high blood pressure, elevated serum cholesterol, diabetes, obesity, sedentary habits, and stress), while the latter is manageable

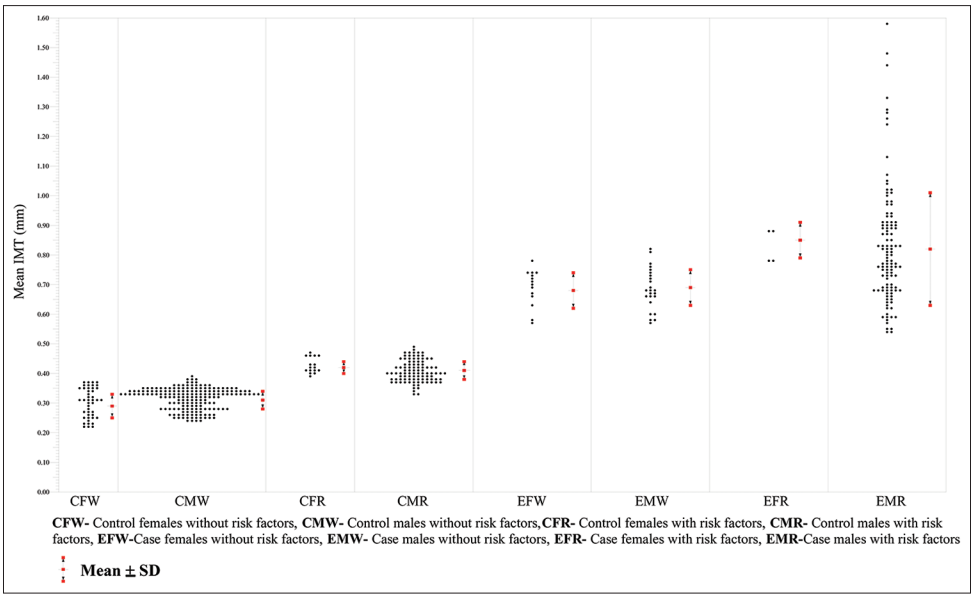

Figure 5: Scatterogram for mean carotid IMT. IMT: Intima–media thickness

by community action. This drawback can be better understood if we consider a hypothetical case, for example, a male, 30 years of age who is hypertensive (160/100 mm of Hg), diabetic, regular smoker, with a total cholesterol 150 mg/dl and HDL cholesterol value 50 mg/dl, is obese and leads a sedentary life with ridiculous dietary habits. He also exhibits family history of these diseases. In order to estimate CVD or CHD in this patient, we apply two different scoring systems. One is Framingham score and another is the score system [Tables 4-6] put forth in a hospital-based cross-sectional study at Apex Hospital in Kolkata, India.[11] The variation in results of two risk scores is shocking. The Framingham score gives us very low-risk estimation i.e. total points = 3/14 which means only 5% risk of CHD in the next 10 years, the latter score system for the same case manifests a high-risk warning, i.e. total points = 24/24 which means 100% risk of CVD in next 10 years. Such a wide difference in risk estimation is like playing with sensitive lives. This issue needs urgent attention and prompt action.

The role of physical activity and dietary habits seem to be underestimated in Framingham score, may be due to the fact that Framingham Heart Study[10] started long back in 1948 when the use of petrol-driven vehicles was limited and the physical activity of an average person was more. But with the changing lifestyle, the case is reversed. Sedentary life has taken over, leading to high vascular morbidity. This fact is also indicated by the higher vascular morbidity in urban population of India in comparison to the rural population which indicates toward higher physical activity in the lifestyle of latter.[25] Moreover, vigorous aerobic exercise has shown to be protective against ischemic heart diseases rather than the exercises such as long walks (the most convenient form of exercise for many).[26]

Table 6: Scoring for dietary risk factors[24]

Dietary pattern	Risk score
Number of days of vegetable intake/week	
<4	1
≥4	0
Number of days of fruit intake/week	
<4	1
≥4	0
Daily oil consumption/adult consumption unit (ml/day)	
≥20	1
<20	0
Extra salt intake in addition to salt in cooked food	
Yes	1
No	0

Maximum possible score=4, Minimum possible score=0

A leading newspaper in India[27,28], in 2014, published the scientific picture of Indian heart disease which comes from the American College of Cardiology and states that heart disease is hitting Indians early.[27] Another important fact is that CVD is no more an age-related problem as young patients with CVDs are being spotted in the OPDs in India. Halvor *et al*.[29] also emphasized the inclusion of individuals younger than 45 years of age so that the potential for primary prevention could be even greater. This also indicates toward the role of modifiable risk factors in a scoring system. The cIMT is a widely used surrogate marker for atherosclerosis and also a strong predictor of future cerebral and cardiovascular events, so a global standard for measuring cIMT is required for better understanding of its usefulness in clinical settings.[30,31] As Carotid IMT is indicated to play an independent factor for the prediction of future stroke in this study, it is suggested to be incorporated in the Framingham risk score.

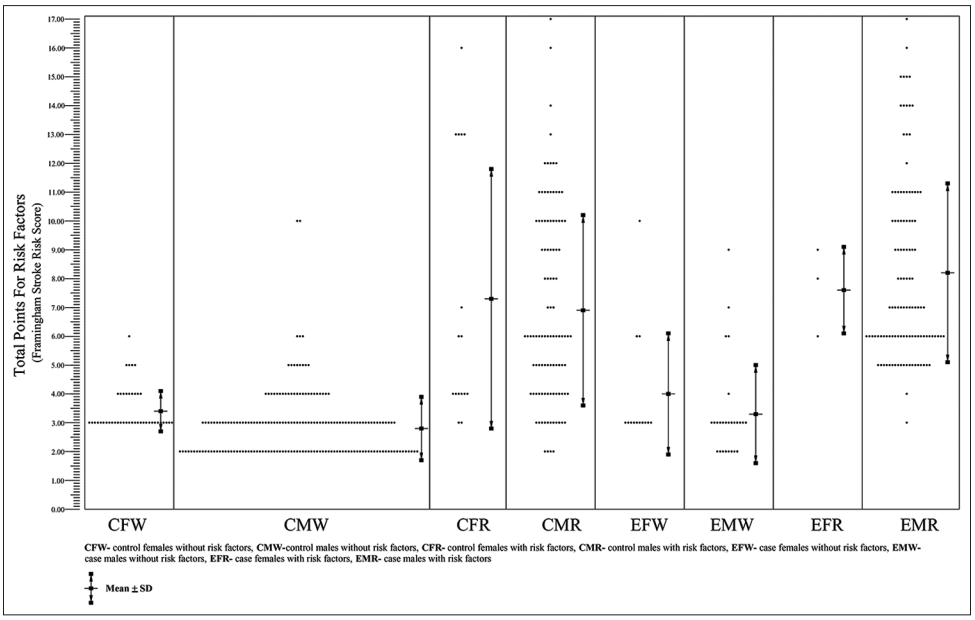

Figure 6: Scatterogram for total points for risk factors as per the Framingham Stroke Risk Score

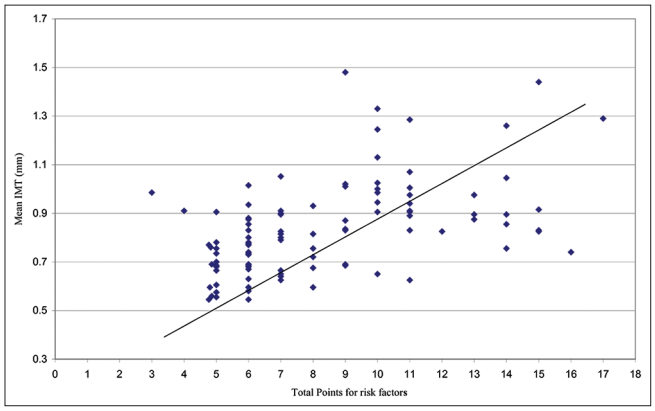

Figure 7: Scatterogram representing mean IMT versus total points for risk factors in case males with risk factors (EFR). IMT: Intima–media thickness

In recent studies at Apex Hospital and Urban Health care center in Kolkata, India,[11,32] a different score system is used to predict cardiovascular risk in which 60% burden is carried by physical activity and dietary factors and only 40% by general risk factors which seems to stand more appropriate in Asian scenario. In Framingham score, 100% contribution is by general risk factors which do not stand appropriate in the Indian subcontinent. Yusuf *et al*.[3] in their study of CVD burden in the Indian subcontinent, have clearly elaborated that there were important differences between risk factor profiles of South Asians compared with non-South Asians in INTERHEART STUDY.[24] Many researches are being conducted for genetic correlation and sex specific analysis of cIMT as well as for the prevention of stroke, so as to contribute to stratified medicine approaches.[33-35]

As the survival statistics of Asian, European, American, and other populations at the global level are different, so the same score system cannot be applicable to all.

Our study highlights the criticality of the situation and calls for an urgent need to produce such a comprehensive, flexible, and universal score system for stroke and CVDs which could be applicable to an individual in any corner of the world.

Conclusion

The main conclusions and recommendations of this study are that, as irradiation triggers atherosclerosis in carotid artery and causes carotid stenosis, it would appear prudent to exercise caution in recommending elective neck irradiation in patients if an alternative is feasible. Carotid IMT appears to act as good predictor and independent factor for stroke prediction so this study also recommends recalibration of Framingham stroke risk scoring system with suggestive follow-up researches to authenticate the incorporation of cIMT as an individual factor to make this score universally applicable to any individual, irrespective of geographical, environmental, and lifestyle differences. This study is an attempt to support INTERSTROKE[1,5] and like researches who are working to reduce stroke burden globally.

Acknowledgments

Departments of Sardar Patel Medical College and Associated Group of Hospitals at Bikaner (Rajasthan), India, supported in technical and administrative issues. We acknowledge the participants, clinical and non-clinical staff of the college and hospital. We thank all the people associated with this research in any which way.

Financial support and sponsorship

Nil.

Conflicts of interest

There are no conflicts of interest.

References

1. Tu JV. Reducing the global burden of stroke: INTERSTROKE. Lancet 2010;376:74-5.
2. Dorresteijn LD, Kappelle AC, Boogerd W, Klokman WJ, Balm AJ, Keus RB, *et al.* Increased risk of ischemic stroke after radiotherapy on the neck in patients younger than 60 years. J Clin Oncol 2002;20:282-8.
3. Goyal A, Yusuf S. The burden of cardiovascular disease in the Indian subcontinent. Indian J Med Res 2006;124:235-44.
4. Tunstall-Pedoe H. Cardiovascular risk and risk scores: ASSIGN, Framingham, QRISK and others: How to choose. Heart 2011;97:442-4.
5. O'Donnell MJ, Xavier D, Liu L, Zhang H, Chin SL, Rao-Melacini P, *et al.* Risk factors for ischaemic and intracerebral haemorrhagic stroke in 22 countries (the INTERSTROKE study): A case-control study. Lancet 2010;376:112-23.
6. Friedlander AH, Freymiller EG. Detection of radiation-accelerated atherosclerosis of the carotid artery by panoramic radiography. A new opportunity for dentists. J Am Dent Assoc 2003;134:1361-5.
7. Halak M, Fajer S, Ben-Meir H, Loberman Z, Weller B, Karmeli R. Neck irradiation: A risk factor for occlusive carotid artery disease. Eur J Vasc Endovasc Surg 2002;23:299-302.
8. King LJ, Hasnain SN, Webb JA, Kingston JE, Shafford EA, Lister TA, *et al.* Asymptomatic carotid arterial disease in young patients following neck radiation therapy for Hodgkin lymphoma. Radiology 1999;213:167-72.
9. Shariat M, Alias NA, Biswal BM. Radiation effects on the intima-media thickness of the common carotid artery in post-radiotherapy patients with head and neck malignancy. Postgrad Med J 2008;84:609-12.
10. Framingham Heart Study: Available from: https://www.framinghamheartstudy.org/fhs-risk-functions. [Last accessed on 2022 Jul 20].
11. Bisoi S, Chattopadhyay D, Bhattacharya N, Roy S, Pal B, Biswas B. A study on cardiovascular risk factors among care-providers of an apex hospital of Kolkata. J Indian Med Assoc 2011;109:623-6
12. Bots ML, Hoes AW, Hofman A, Witteman JC, Grobbee DE. Cross-sectionally assessed carotid intima-media thickness relates to long-term risk of stroke, coronary heart disease and death as estimated by available risk functions. J Intern Med 1999;245:269-76.
13. O'Leary DH, Polak JF, Kronmal RA, Manolio TA, Burke GL, Wolfson SK Jr. Carotid-artery intima and media thickness as a risk factor for myocardial infarction and stroke in older adults. Cardiovascular Health Study Collaborative Research Group. N Engl J Med 1999;340:14-22.
14. So NM, Lam WW, Chook P, Woo KS, Liu KH, Leung SF, *et al.* Carotid intima-media thickness in patients with head and neck irradiation for the treatment of nasopharyngeal carcinoma. Clin Radiol 2002;57:600-3.
15. Homma S, Hirose N, Ishida H, Ishii T, Araki G. Carotid plaque and intima-media thickness assessed by b-mode ultrasonography in subjects ranging from young adults to centenarians. Stroke 2001;32:830-5.
16. Abayomi OK. Neck irradiation, carotid injury and its consequences. Oral Oncol 2004;40:872-8.
17. Wolf PA, D'Agostino RB, Belanger AJ, Kannel WB. Probability of stroke: A risk profile from the Framingham study. Stroke 1991;22:312-8.
18. Tattersall MC, Gangnon RE, Karmali KN, Keevil JG. Women up, men down: The clinical impact of replacing the Framingham risk score with the reynolds risk score in the United States population. PLoS One 2012;7:e44347.
19. Coutts SB, Eliasziw M, Hill MD, Scott JN, Subramaniam S, Buchan AM, *et al.* An improved scoring system for identifying patients at high early risk of stroke and functional impairment after an acute transient ischemic attack or minor stroke. Int J Stroke 2008;3:3-10.
20. Cook NR, Paynter NP, Eaton CB, Manson JE, Martin LW, Robinson JG, *et al.* Comparison of the Framingham and reynolds risk scores for global cardiovascular risk prediction in the multiethnic Women's Health Initiative. Circulation 2012;125:1748-56, S1-11.
21. Bonita R, Courten M, Dwyer T, Jamrozik K, Winkelmann R. Surveillance of Risk Factors for Non-Communicable Disease: WHO STEP Wise Approach. Geneva: WHO; 2001.
22. Stamler J, Stamler R, Neaton JD, Wentworth D, Daviglus ML, Garside D, *et al.* Low risk-factor profile and long-term cardiovascular and noncardiovascular mortality and life expectancy: Findings for 5 large cohorts of young adult and middle-aged men and women. JAMA 1999;282:2012-8.
23. Engström G, Jerntorp I, Pessah-Rasmussen H, Hedblad B, Berglund G, Janzon L. Geographic distribution of stroke incidence within an urban population: Relations to socioeconomic circumstances and prevalence of cardiovascular risk factors. Stroke 2001;32:1098-103.
24. Yusuf S, Hawken S, Ounpuu S, Dans T, Avezum A, Lanas F, *et al.* Effect of potentially modifiable risk factors associated with myocardial infarction in 52 countries (the INTERHEART study): Case-control study. Lancet 2004;364:937-52.
25. Park K. Text Book of Preventive and Social Medicine. 20th ed. Jabalpur: Banarsidas Bhanot; 2009. p. 316.
26. Cardiovascular Disease In: Weatherall DJ, Ledingham JG, Warrell DA, editors. Oxford Textbook of Medicine. 3rd ed., Vol. 2, Sec. 15. New York: Oxford University Press Inc.; 1996. p. 2313.
27. Malathy Iyer. Heart disease is affecting Indians early, US study says. Times of India: Mumbai; 2014.
28. Heart at risk: Cholesterol levels worrisome in young & employed. Times of India: Pune; 2014.
29. Øygarden H. Carotid intima-media thickness and prediction of cardiovascular disease. J Am Heart Assoc 2017;6:e005313.
30. Nezu T, Hosomi N, Aoki S, Matsumoto M. Carotid intima-media thickness for atherosclerosis. J Atheroscler Thromb 2016;23:18-31.
31. Pereira VL Jr., Dobre M, Dos Santos SG, Fuzatti JS, Oliveira CR, Campos LA, *et al.* Association between carotid intima media thickness and heart rate variability in adults at increased cardiovascular risk. Front Physiol 2017;8:248.
32. Deb S, Dasgupta A. A study on risk factors of cardiovascular diseases in an urban health center of kolkata. Indian J Community Med 2008;33:271-5.
33. Strawbridge RJ, Ward J, Bailey ME, Cullen B, Ferguson A, Graham N, *et al.* Carotid intima-media thickness: Novel loci, sex-specific effects, and genetic correlations with obesity and glucometabolic traits in UK Biobank. Arterioscler Thromb Vasc Biol 2020;40:446-61.
34. Strong K, Mathers C, Bonita R. Preventing stroke: Saving lives around the world. Lancet Neurol 2007;6:182-7.
35. Feigin VL. Stroke in developing countries: Can the epidemic be stopped and outcomes improved? Lancet Neurol 2007;6:94-7.

Original Article

Age- and Gender-Based Morphometric Variation of Macula in Indian Population using Optical Coherence Tomography

Pareesa Rabbani, Shalini Kumar, Taskin Khan[1], Shayama K. Razdan

Departments of Anatomy and [1]Ophthalmology, HIMSR, New Delhi, India

Abstract

Introduction: Histological morphometric analysis of retinal layers has inherent limitations while processing the specimen. A new *in vivo* technique, optical coherence tomography (OCT), has been developed that can be used to analyze and differentiate normal and pathological retina. To do a morphometric analysis of normal macula in the adult population of India and study its variations on the grounds of sex and age. **Material and Methods:** One hundred (200 Eyes) healthy adult subjects (18–65 years) underwent macular cube scanning using Zeiss spectral-domain OCT (SD-OCT). Macular thickness from all nine regions of the Early Treatment Diabetic Retinopathy study map was documented for each subject. Their variations for age and sex were determined manually and automatically. Statistical analysis was done by entering into an MS Excel sheet using IBM SPSS Statistics for Windows,Version 25.0. Armonk, NY: IBM Corp. (2017). The data were also analyzed using an independent *t*-test and analysis of variance. **Results:** The mean age of the subjects was 34.2 ± 13 (range, 19–65) years. The mean Central Subfield Thickness (CST) measured automatically (foveal thickness) and manually was 239.52 ± 22.9 μm and 167.75 ± 21.94 μm, respectively, while mean macular thickness was 284.73 ± 15.7 μm and 276.76 ± 14.84 μm. Males were associated with greater foveal, central foveal thickness, and mean macular thickness than females ($P < 0.0001$). There was no significant correlation of CST, outer and inner ring, and mean macular thickness with increasing age (>30 years). However, with respect to gender in the inner ring (parafoveal region), all the quadrants except the inferior quadrant, CST was significantly ($P < 0.0001$) higher in males than females while in the outer ring (perifoveal region), it was the temporal quadrant that had statistically significant higher CST in males compared to females. **Discussion and Conclusion:** The results will add evidence and can serve as a normal database in morphometry of macula in Indians, created and found significantly different in already fed normal comparative data in SD-OCT machines. It will help analyze morphometry of macula and understand macular pathologies in Indian eyes.

Keywords: *Central subfield thickness, macular thickness, optical coherence tomography*

Introduction

The retina is a thin sheet of cells, ranging from <100 μm at its edge to a maximum of around 300 μm at the foveal rim. It lines the inner posterior surface of the eyeball, lying in between the choroid externally and the vitreous body internally, and terminates anteriorly at the Ora Serrata.[1] The total surface area of the retina is 266 mm². It is thickest near the disc, about 0.56 mm, and thinnest in the periphery, where it is approximately 0.18 mm wide at the equator and 0.3 mm at Ora Serrata.[2] The retina is derived embryologically from the two layers of the invaginated optic vesicle. The outer layer becomes a layer of cuboidal pigment cells that separates the choroid from the neural retina and therefore forms the outermost layer of the retina: the retinal pigment epithelium (RPE). The other nine layers of the retina develop from the inner layer of the optic vesicle and form the neural retina. Significant landmarks which are seen in the retina are[3] optic disc which is a round to oval well-defined structure about 1.5 mm in diameter where retinal layers terminate except the nerve fibers which pass through the lamina cribrosa to run into the optic nerve. The center contains a depression or pit called the physiological cup. Another landmark is area centralis (Macula Lutea) or anatomical macula which is the part of the retina lying lateral to the optic disc, demarcated by superior and inferior temporal arteries with an average diameter of 5.5 mm. It corresponds to approximately 15° of the visual field where the fovea is a depression in the center. The foveola constitutes its

How to cite this article: Rabbani P, Kumar S, Khan T, Razdan SK. Age- and gender-based morphometric variation of macula in Indian population using optical coherence tomography. J Anat Soc India 2022;XX:XX-XX.

Article Info

Received: 12 December 2021
Revised: 16 May 2022
Accepted: 05 June 2022
Published: ***

Address for correspondence:
Dr. Shalini Kumar, Department of Anatomy, Hamdard Institute of Medical Sciences and Research (HIMSR), Hamdard University, New Delhi - 110 062, India.
E-mail: drshalini94@gmail.com

Access this article online

Website: www.jasi.org.in
DOI: 10.4103/jasi.jasi_205_21
Quick Response Code:

floor surrounded by a parafoveal and perifoveal ring around it. The peripheral retina is an area which lies outside the macula. The retina comprises various epithelial, neural, and glial cell types, whose distribution is divided into ten layers.[1] Microscopic structure of the retina, as seen under light microscopy, can be distinguished into ten layers.[4,5]

Since times immemorial retinal studies were being done by fundus photography, angiography, B-Scan ultrasonography, and various histological techniques, but all these techniques have inherent limitations like dehydration of tissue and retinal detachment. Moreover, histological techniques are not *in vivo* studies and also there are limited cadaveric studies on human and primate eyes. Hence, these layers can be seen *in vivo* using a newly emerged technique known as optical coherence tomography (OCT), which uses backscattered light to visualize layers by differences in their optical scattering properties. Each distinct retinal layer can be visualized by OCT that corresponds well to histological studies[6] On OCT, the retinal layers can be seen with different color coding as well. The hyperreflective lines are seen as bright (red or white). Those layers with minimum reflectivity are shown as dark (blue or black), and intermediate reflectivity is green. OCT scan identifies the following hyper-reflective layers which are nerve fiber layer, inner plexiform layer, outer plexiform layer, external limiting membrane, RPE, ellipsoid zone, inter digitation zone. The hyporeflective layers which can be seen are ganglion cell layer, inner nuclear layer, outer nuclear layer, Henle's nerve fiber layer at the macula, outer segments of photoreceptors, myoid zone, chorio capillaries, and inner and outer choroidal layers as shown in Figure 1a-c.

The most important landmark of the retina where images are formed is known as the anatomical macula or macula lutea. It has the highest concentration density of cones responsible for color vision and central vision. Several retinal diseases can affect the macula, leading to vision loss if they are not treated earlier. Therefore, to lower down morbidity by analyzing diseases such as diabetic retinopathy and macular degenerations earlier assessment of change in macular anatomy is necessary and can be assessed using OCT.[7] Whereas the light microscopic structure of macula has the outermost layer of RPE,consisting of a single layer of hexagonal cells as in the retina elsewhere but in the macular area, they are taller and denser. The outer nuclear layer contains the nuclei of cones at the fovea centralis as rods are absent. Here the cones are covered by an internal limiting membrane (ILM). Outer Plexiform Layer is thickest at the macula, formed by inner fibers of cones known as Henle's layer , which are arranged obliquely.The Ganglion cell layer in the macula is about 6-8 layers thick, seen only at the edge of the foveola. This layer is absent at the foveola and optic disc.[8]

Variations have been reported in macular structure concerning age, gender, ethnicity, and various ocular diseases and systemic comorbidities like diabetes and hypertension before the development of retinopathies These variations are perhaps because of the normative database that has been created and developed in different OCT machines based on studies conducted mostly on Caucasians.[9] Hence, it is imperative to assess and overcome the inherent limitations faced during the preparation and processing of slides. It is necessary to have normative data based on Indian eyes to distinguish between normal anatomical variants from macular pathology *in vivo*. However, a normative database for variations in normal macular anatomy on OCT remains lacking on Indian eyes.[10] The present study serves as a baseline for OCT data of normal macular morphology in healthy Indian eyes.

Material and Methods

A cross-sectional study was conducted on the subjects reporting to the department of ophthalmology outpatient department in the age group of 18–65 years. After getting ethical approval from institutional ethical committee and informed written consent from the study subjects. A complete ophthalmic examination was done including best-corrected visual acuity, slit-lamp examination, and dilated fundus examination to rule out any ocular disease. The subjects who had clear ocular media with best-corrected visual acuity of 20/20, a refractive error with the spherical equivalent of less than or equal to ±6D, intraocular pressure of <21 mm Hg, and without any signs of glaucoma or any other ocular and systemic disorder that would affect eye were included in the study. Those who had undergone ocular surgeries or corneal transplantation and subjects with maculopathies or retinopathies were excluded from the study. The sample size taken was 100 subjects (200 eyes), the study duration was 1 year.

The selected subjects underwent dilated macular imaging using OCT spectral-domain OCT (SD-OCT) (Carl Zeiss, Primus 200).

Macular thickness was defined as the distance between the ILM and the inner boundary of RPE in each of the nine regions as defined by Early Treatment Diabetic Retinopathy Study[11] using Carl Zeiss SD-OCT. The inner and outer rings were segmented into 4 quadrants, with radii of 1.5 mm and 3 mm, respectively. Foveal thickness was defined as the average thickness in the central 1000-μm diameter of the Early Treatment Diabetic Retinopathy Study layout. Central foveal thickness was defined as the mean thickness at the point of intersection of the 6 radial scans. Automatic measurements were taken in all nine regions and were documented. The anatomical landmarks of the macula on OCT imaging were manually determined based on the International Nomenclature for OCT Panel[12] based on relative reflectivity by the structures The manually determined central foveal thickness measurements were compared with the values generated by the software. The macular thickness of the central foveal area and all four

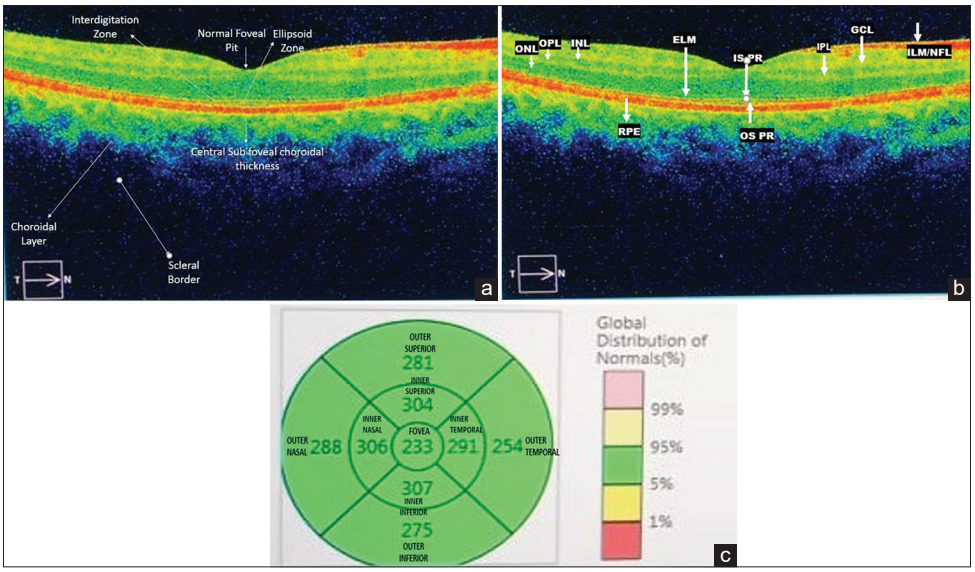

Figure 1: (a) Representative OCT image from a healthy subject of the right eye. (b) Layers seen on SD-OCT, These hyperreflective layers should be identified while evaluating an OCT scan: NFL, IPL, OPL, ELM, RPE, Ellipsoid zone, and Inter digitation zone. The hypo reflective layers are GCL, INL, ONL and Henle's nerve fiber layer at the macula, OSPR, and ISPR and myoid zone–Chorio capillaries and inner and outer choroidal layers. (c) Standard ETDRS. This is a representation of standard ETDRS map showing map diameters centered on the fovea and nine standard ETDRS Map ETDRS regions: Outer and inner superior quadrant, outer and inner inferior quadrant, outer temporal quadrant, inner temporal quadrant, outer nasal quadrant and INQ. The macular thickness was defined as the distance between the ILM and the inner boundary of RPE in each of the nine regions. OCT: optical coherence tomography, SD-OCT: Spectral-domain optical coherence tomography, NFL: Nerve fiber layer, IPL: Ganglion cell layer Inner plexiform layer, OPL: Outer plexiform layer, ELM: External limiting membrane, GCL: Ganglion cell layer, INL: Inner nuclear layer, ONL: Outer nuclear layer, OSPR: Outer segments of photoreceptors, ISPR: inner segment of photoreceptors, ETDRS: Early treatment diabetic retinopathy study, INQ: inner nasal quadrant, RPE: Retinal pigment epithelium, ILM: Internal limiting membrane

quadrants (superior, inferior, nasal, and temporal) of the outer and inner rings were evaluated. Statistical analysis of the data collected was done using SPSS version 25. The data were also analyzed using an independent *t*-test and statistically tested using appropriate tests of significance.

Results

The total number of subjects enrolled in the study was 100 (200 eyes). The number of males and females was 50 each (total of 200 eyes). The age of the subjects ranged from 18 to 65 years (mean 34.2 ± 13 years).

Average morphometric parameters of macula of 100 subjects (200 eyes) in the study are represented in Table 1.

As shown in Table 1, the mean foveal thickness (measured automatically) was 239.52 ± 22.9 μm, while measured manually, the central foveal thickness was found to be 167.75 ± 21.94 μm, 72 μm less than automatically measured data. The mean thickness in both parafoveal region (inner ring) and perifoveal region (outer ring) of Macula, the nasal quadrant was found to be thickest, with values of 311.7 ± 20.6 micrometer and 293.29 ± 18.6micrometer ,respectively,while the superior quadrant of the two regions it was 309.81 ± 19.5 micrometer and 276.73 ± 16.91 micrometer.

The mean macular thickness was 284.73 ± 15.7 μm for automatically fed data while on manual evaluation; it was 276.76 ± 14.84 μm as shown in Figure 2.

The mean central subfield foveal thickness was found to be 239.52 μm when measured automatically and manually it was found to be 167.75 μm, 72 μm less than automatically fed data as shown in Figure 3a. According to Bland–Altman plot of Central Subfield Thickness, the mean was found to be 71.77 as shown in Figure 3b.

The overall nasal quadrant was thickest followed by superior and inferior quadrant as shown in Figure 4. Furthermore, it was seen that the temporal quadrant was thinnest in the perifoveal (outer) ring.

Table 2 shows the macular parameters evaluated on the grounds of gender. The mean foveal thickness in males was 248.54 μm, higher as compared to females, 230.5 μm. The mean central foveal thickness in males was 172.51 μm and in females, it was 162.99 μm. The mean macular thickness measured automatically was higher in males, 290.16 μm compared to females, 279.31 μm. These values are statistically significant ($P < 0.001$). In the perifoveal region, only the temporal quadrant showed higher thickness (being higher in males) that was statistically significant, the superior, inferior, and nasal quadrants did not show any statistically significant difference. While in the parafoveal region, all the quadrants except inferior quadrant was statistically significant ($P < 0.001$).

As shown in Figure 5, the mean macular thickness (both automatic and manual) was higher in males as compared to females.

Table 1: Average morphometric parameters of macula of 100 subjects (200 eyes)

Outcome variables	Number of subjects (*n*)	Mean value (μm)	Minimum value (μm)	Maximum value (μm)	SD	Significance
Foveal thickness (Automatic)	100 (200 eyes)	239.52	168	298	22.9	<.0001
Central foveal thickness (Manual)	100 (200 eyes)	167.75	115	240	21.94	<.0001
Macular thickness (Automatic)	100 (200 eyes)	284.73	251	324.56	15.7	<.0001
Macular thickness (manual)	100 (200 eyes)	276.76	243.33	316.22	14.84	<.0001
Parafovea (inner ring) (3mm diameter)						
Superior	100 (200 eyes)	309.81	268	362	19.85	<.0001
Inferior	100 (200 eyes)	308.63	246	364	20.04	<.0001
Nasal	100 (200 eyes)	311.76	266	395	18.62	<.0001
Temporal	100 (200 eyes)	297.64	239	357	20.06	<.0001
Perifovea (outer ring) (6mm diameter)						
Superior	100 (200 eyes)	276.73	222	336	16.91	<.0001
Inferior	100 (200 eyes)	267.4	205	351	20.46	<.0001
Nasal	100 (200 eyes)	293.29	226	352	16.6	<.0001
Temporal	100 (200 eyes)	257.8	217	302	18.6	<.0001

SD: Standard deviation

Table 2: Morphometric analysis of macula on grounds of gender

Outcome variables	Gender	Number of subjects (*n*)	Minimum value (μm)	Maximum value (μm)	Mean value (μm)	SD	Significance
Foveal thickness	Males	100 (200 eyes)	168	298	248.54	22.26	<.0001
	Females	100 (200 eyes)	182	295	230.5	19.87	<.0001
Central foveal thickness	Males	100 (200 eyes)	133	225	172.51	21.95	<.0001
	Females	100 (200 eyes)	115	240	162.99	20.97	<.0001
Macular thickness	Males	100 (200 eyes)	251	324.56	290.16	15.2	<.0001
	Females	100 (200 eyes)	253	320.89	279.31	14.28	<.0001
Perifovea (outer ring)							
Superior	Males	100 (200 eyes)	241	336	280	15.95	0.005
	Females	100 (200 eyes)	222	324	273.45	17.28	0.005
Inferior	Males	100 (200 eyes)	231	321	270.85	18.81	0.016
	Females	100 (200 eyes)	205	351	263.96	21.54	0.016
Temporal	Males	100 (200 eyes)	229	302	262.97	16.5	<.0001
	Females	100 (200 eyes)	217	292	252.64	15.09	<.0001
Nasal	Males	100 (200 eyes)	235	352	295.5	18.86	0.093
	Females	100 (200 eyes)	226	329	291.08	18.17	0.093
Parafovea (inner ring)							
Superior	Males	100 (200 eyes)	275	362	316.57	19.63	<.0001
	Females	100 (200 eyes)	268	358	303.05	17.72	<.0001
Inferior	Males	100 (200 eyes)	246	364	313.89	20.54	0.0002
	Females	100 (200 eyes)	247	347	303.37	18.15	0.0002
Temporal	Males	100 (200 eyes)	265	357	304.58	16.87	<.0001
	Females	100 (200 eyes)	239	338	290.69	17.75	<.0001
Nasal	Males	100 (200 eyes)	278	395	318.51	21.42	<.0001
	Females	100 (200 eyes)	266	360	305.01	17.38	<.0001

SD: Standard deviation

As shown in Table 3, the mean foveal thickness, central foveal thickness, macular thickness, parafoveal, and perifoveal thickness did not correlate significantly with increasing age.

Discussion

OCT has emerged as a useful imaging technique by providing new high-resolution images of retina. It is clinically relevant for the diagnosis of a variety of diseases such as glaucoma, macular degeneration, and macular edema.

It is important to have a normative data to be able to distinguish between normal anatomical variants from macular pathology. The study of normal morphology of each distinctive layer of retina using OCT is important to analyze variations and correlate it clinically such as in cases of

retinopathies, maculopathies. It is an important noninvasive, rapid, *in vivo*, technique that helps in determining anatomical changes in retina by producing cross-sectional images. Each distinct layer of retina can be visualized on OCT that corresponds well to histological appearance.[3]

A number of studies have found variations in normal macular anatomy with regard to age, gender, and ethnicity besides also in various ocular diseases.

Natung *et al*. in 2016,[10] assessed macular thickness in healthy Indian subjects aged 18–65 years and found that foveal thickness was more in males than females while no significant correlation was found on grounds of age. The foveal thickness was 240.40 ± 18.26 μm, and mean macular thickness was 287.87 ± 18.07 μm. Males had greater foveal thickness and mean macular thickness compared to females ($P < 0.05$). There was statistical association of foveal and mean macular thickness with sex ($P < 0.05$) but not with age. Liu *et al*., 2011,[13] assessed 192 eyes of subjects aged 20–90 years using Cirrhus OCT. They found that foveal thickness never exceeded 308 μm in healthy controls. The macular thickness did decrease with age but foveal thickness did not change significantly with age similar to the results seen in the present study. The values were higher in males as compared to females. They stated that CST ranged from 216.8 μm to 308 μm in normal eyes. These results are consistent with our study where foveal thickness never exceeded 239.52 ± 22.9. The mean foveal thickness varied statistically significantly with sex ($P < 0.0001$) but not with age. The macular thickness was 284.73 ± 15.7 μm reported higher in males (290.16 ± 15.2) as compared to females (279.31 ± 14.28) but had no statistical relation with age. The findings of a study by Gupta *et al*. in 2013,[14] differ from our findings as they stated that macular thickness correlates with age and it was thinner in older people, this could be because the mean age in their study was 53.17 years and maximum age was 80 years while in the present study the average age is 34.2 years and maximum age of the subject is 65 years.

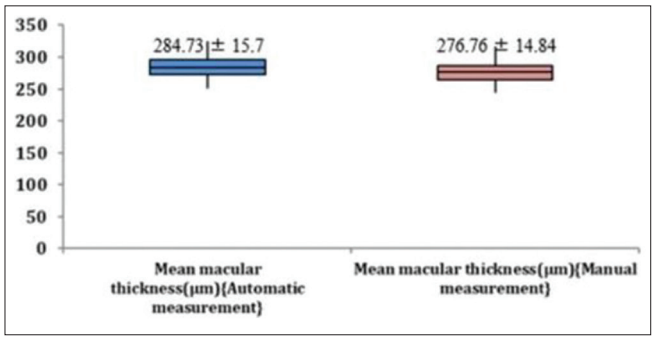

Figure 2: Descriptive statistics of mean macular thickness (μm) (automatic measurement) and mean macular thickness (μm) (manual measurement) of study subjects

Chan *et al*. in 2006,[15] reported macular thickness measurements in 37 healthy controls using OCT 3. In their study, macular thickness was thinner at center of fovea. The temporal quadrant was found to be thinner than the nasal quadrant. Waris *et al*. 2015[16] assessed 20 subjects who underwent complete ophthalmic examination followed by macular assessment using OCT 3. Macular thickness measurements were thinnest at the center of the fovea,

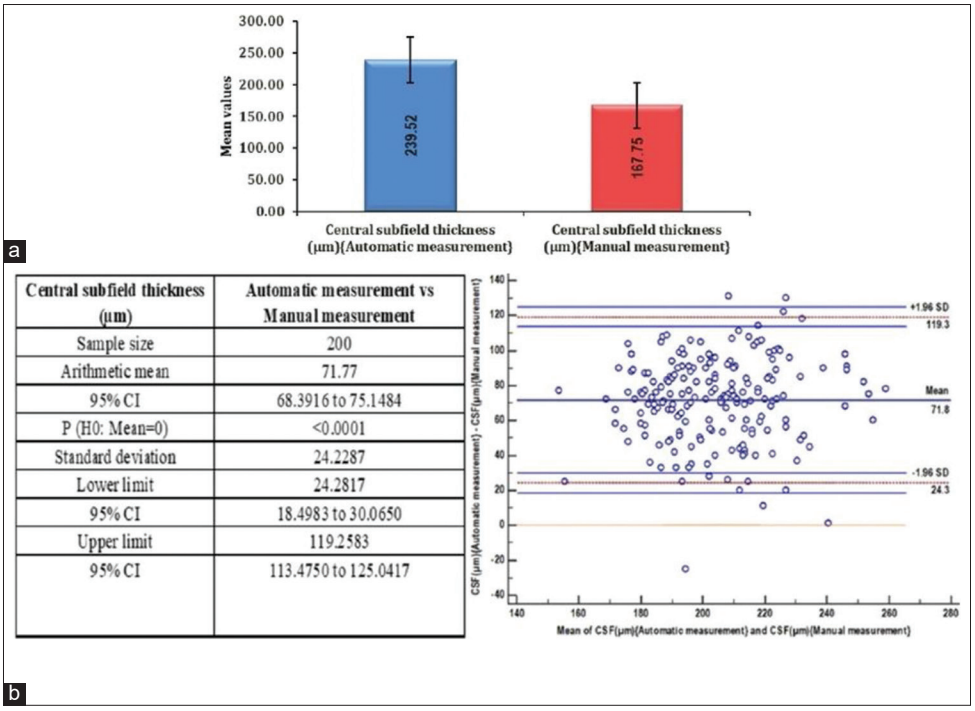

Central subfield thickness (μm)	Automatic measurement vs Manual measurement
Sample size	200
Arithmetic mean	71.77
95% CI	68.3916 to 75.1484
P (H0: Mean=0)	<0.0001
Standard deviation	24.2287
Lower limit	24.2817
95% CI	18.4983 to 30.0650
Upper limit	119.2583
95% CI	113.4750 to 125.0417

Figure 3: (a) Comparison of central subfield thickness between automatic and manual measurement. (b) Bland-Altman plot of central subfield thickness to compare measurements of automatic and manual

Table 3: Morphometric analysis of macula on the basis of age

Outcome variables	Age (years)	Number of subjects (*n*)	Minimum value (μm)	Maximum value (μm)	Mean value (μm)	SD	Significance
Foveal thickness	< 30	102 (204 eyes)	168	298	240	22.2	0.763
	>30	98 (196 eyes)	182	295	239.02	23.73	0.763
Central foveal thickness	< 30	102 (204 eyes)	124	240	170.6	22.92	0.06
	>30	98 (196 eyes)	115	216	164.79	20.56	0.06
Macular thickness	< 30	102 (204 eyes)	256.11	317.78	285.87	13.96	0.294
	>30	98 (196 eyes)	251	324.56	283.54	17.3	0.294
Perifoveal thickness							
Superior	< 30	102 (204 eyes)	245	336	277.91	14.86	0.314
	>30	98 (196 eyes)	222	324	275.49	18.8	0.314
Inferior	< 30	102 (204 eyes)	234	317	268.77	15.54	0.339
	>30	98 (196 eyes)	205	351	265.98	24.57	0.339
Temporal	< 30	102 (204 eyes)	226	300	257.2	14.16	0.599
	>30	98 (196 eyes)	217	302	258.44	18.86	0.599
Nasal	< 30	102 (204 eyes)	266	352	296.47	15.35	0.013
	>30	98 (196 eyes)	226	329	289.98	21.04	0.013
Parafoveal thickness							
Superior	< 30	102 (204 eyes)	268	357	310.87	18.39	0.441
	>30	98 (196 eyes)	272	362	308.7	21.3	0.441
Inferior	< 30	102 (204 eyes)	247	364	310.77	19.85	0.122
	>30	98 (196 eyes)	246	360	306.4	20.09	0.122
Temporal	< 30	102 (204 eyes)	256	339	297.76	16.24	0.92
	>30	98 (196 eyes)	239	357	297.5	20.9	0.92
Nasal	< 30	102 (204 eyes)	279	359	313.1	19.34	0.349
	>30	98 (196 eyes)	266	395	310.37	21.85	0.349

SD: Standard deviation

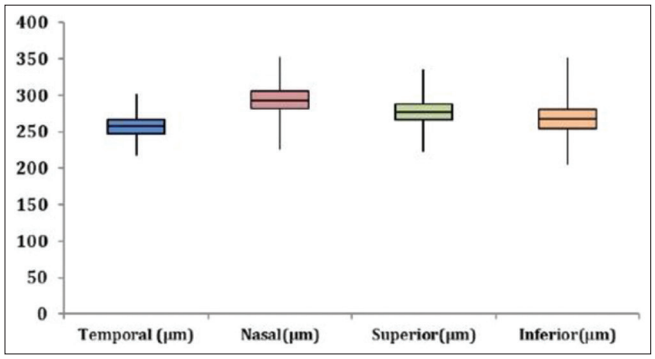

Figure 4: Descriptive statistics of temporal (μm), nasal (μm), superior (μm) and inferior (μm) quadrants of outer ring of study subjects

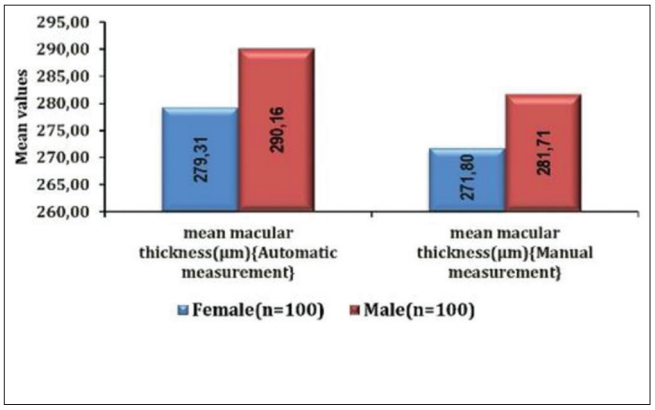

Figure 5: Mean macular thickness on grounds of gender

thickest within 3-mm diameter of the center, and reduced toward the periphery of the macula. The temporal quadrant was thinner than the nasal quadrant. This might be due to anatomical relationship of the converging of nerve fibers with the optic disc. The results were similar to our study where temporal quadrant was thinner than nasal quadrant. In our study, only the temporal quadrant was statistically significant on grounds of gender. In the parafoveal region, all the quadrants except inferior quadrant were statistically significant ($P < 0.001$) on the basis of gender.

In our study, foveal thickness was found to be 239.52 ± 22.9 μm and central foveal thickness was found to be 167.75 ± 21.94 μm which was 72 μm lower than automatically obtained values. The Bland–Altman plot as depicted in Figure 3a and b in the present study also shows that the automatic measurements of foveal thickness obtained are higher than those measured manually. This reflects the difference in approach between the manual method and the automatic method of the OCT mapping software. The software automatically determines the mean and standard deviation thickness for the center point where all 6 scans intersect, whereas we manually located the minimum point on each separate radial scan and averaged those values. This is a significant finding while determining

and interpreting normal from abnormal macular parameters when doing OCT scan by automatic method.

Massin *et al*. 2002[17] found that the mean macular thickness was not affected significantly by age or laterality, but it was significantly higher in men than women (P = 0.0139). It has been suspected that increasing age shows decreased macular thickness but no such correlation was found in our study. The results vary from a study done by Tewari *et al*.[18] who reported a positive correlation with minimum foveal thickness, but not with average foveal thickness.

Anastasia *et al*. (2014),[19] assessed macular layer morphology in healthy controls using high-resolution SD-OCT across ethnicities comparing Asian (i.e., Indian subcontinent) and Caucasian individuals. One hundred and thirty-three healthy volunteers (67-Asian, 66-Caucasian) underwent examination using SD-OCT. The analysis of the measurements of each retinal layer at the macula was determined using tomographs obtained by SD-OCT. They found a significant difference in macular structure in Asian and Caucasian subjects. Caucasian subjects had thicker inner segment (P = 0.015 in the central region), outer segment (P = 0.04 in the temporal region), and outer nuclear (P = 0.021 and P = 0.03 for the central and temporal regions, respectively) layers, while Asians demonstrated thicker retinal pigment epithelial layer (P = 0.004 for the temporal region). They suggested that the differences in macular morphology due to ethnicity should be taken into consideration for determining control values for diagnostic purposes, and also to assess risk and prognosis of macular diseases.

A number of studies have been reported on normative data for macular thickness using different OCT machines with varying results. This might be due to the variation in the ethnicity of the study group, the OCT model (prototype, OCT 2, OCT 3), the scan (radial vs. linear), and analysis protocol. This discrepancy concludes the importance of paying attention to the above-mentioned variables before assessing OCT parameters.

Our study provides a normative database for macular thickness and volume parameters in Indian eyes by OCT. The automatic method overestimates the mean macular thickness and central foveal thickness and it is significantly associated with gender as well. This could be beneficial in assessment, early diagnosis, and management of macular disorders and retinal pathologies.

Conclusion

Various studies have reported on normative data for macular thickness using different OCT machines. Although our results are variable from previously reported values it might be due to the variation in the ethnicity of the study group, the OCT model (prototype, OCT 2, OCT 3), the scan (radial vs. linear) and analysis protocol. This discrepancy concludes the importance of paying attention to the above-mentioned variables before assessing OCT parameters.

The present study provides a normative database for macular thickness in Indian eyes by OCT SD-OCT and compares both manual with automatic methods. It also compares the differences observed with age and gender. This could be beneficial in early assessment, diagnosis, and management of macular disorders and retinal pathologies.

Financial support and sponsorship

Nil.

Conflicts of interest

There are no conflicts of interest.

References

1. Standring S, Borley NR, Gray H. Gray's Anatomy: The Anatomical Basis of Clinical Practice. 41st ed., Anniversary Edition. Edinburgh: Churchill Livingstone/Elsevier; 2008.
2. Singleman J, Ozanics V. Retina. In: Jakobiec, editor. Ocular Anatomy, Embryology and Tetralogy. Philadelphia: Harper and Row; 1982.
3. Tripathi RC, Tripathi BJ. Anatomy of human eye, orbit and adnexa. In: Davson H, editor. The Eye. 3rd ed. London: Academic Press; 1984.
4. Pushplatha K. Inderbir Singh's Text Book of Human Histology. 9th ed. New Delhi: Jaypee Brothers Medical Publishers: 2019.
5. Ross MH, Pawlina W. Histology: A Text and Atlas Book, with Correlated Cell and Microbiology. 6th ed. Philadelphia: Lippencott Williams and Wilkins; 2011.
6. Ferguson LR, Grover S, Dominguez JM 2nd, Balaiya S, Chalam KV. Retinal thickness measurement obtained with spectral domain optical coherence tomography assisted optical biopsy accurately correlates with *ex vivo* histology. PLoS One 2014;9:e111203.
7. Eagle RC Jr. Optical coherence tomography: Clinicopathologic correlations – The 2016 Gordon K. Klintworth Lecture. Ocul Oncol Pathol 2018;4:203-12.
8. Khurana AK, Khurana AK, Bhawna K. Comprehensive Ophthalmology. DL: Jaypee Brothers Medical Publishers; 2015.
9. Manassakorn A, Chaidaroon W, Ausayakhun S, Aupapong S, Wattananikorn S. Normative database of retinal nerve fiber layer and macular retinal thickness in a Thai population. Jpn J Ophthalmol 2008;52:450-6.
10. Natung T, Keditsu A, Lyngdoh LA, Dkhar B, Prakash G. Normal macular thickness in healthy Indian eyes using spectral domain optical coherence tomography. Asia Pac J Ophthalmol (Phila) 2016;5:176-9.
11. Early treatment diabetic retinopathy study design and baseline patient characteristics. ETDRS report number 7. Ophthalmology 1991;98 5 Suppl: 741-56.
12. Staurenghi G, Sadda S, Chakravarthy U, Spaide RF; International Nomenclature for Optical Coherence Tomography (IN•OCT) Panel. Proposed lexicon for anatomic landmarks in normal posterior segment spectral-domain optical coherence tomography: the IN•OCT consensus. Ophthalmology 2014;121:1572-8.
13. Liu T, Hu AY, Kaines A, Yu F, Schwartz SD, Hubschman JP. A pilot study of normative data for macular thickness and volume measurements using cirrus high-definition optical coherence tomography. Retina 2011;31:1944-50.
14. Gupta P, Sidhartha E, Tham YC, Chua DK, Liao J, Cheng CY, *et al*. Determinants of macular thickness using spectral

domain optical coherence tomography in healthy eyes: The Singapore Chinese eye study. Invest Ophthalmol Vis Sci 2013;54:7968-76.
15. Chan A, Duker JS, Ko TH, Fujimoto JG, Schuman JS. Normal macular thickness measurements in healthy eyes using Stratus optical coherence tomography. Arch Ophthalmol 2006;124:193-8.
16. Waris A, Asghar A, Yunus SM, Malakar M. Normal macular thickness measurements in normal eyes using Fourier domain optical coherence tomography. IOSR J Dent Med Sci (IOSR-JDMS) 2015;14:63-6.
17. Massin P, Erginay A, Haouchine B, Mehidi AB, Paques M, Gaudric A. Retinal thickness in healthy and diabetic subjects measured using optical coherence tomography mapping software. Eur J Ophthalmol 2002;12:102-8.
18. Tewari HK, Wagh VB, Sony P, Venkatesh P, Singh R. Macular thickness evaluation using the optical coherence tomography in normal Indian eyes. Indian J Ophthalmol 2004;52:199-204.
19. Pilat AV, Proudlock FA, Mohammad S, Gottlob I. Normal macular structure measured with optical coherence tomography across ethnicity. Br J Ophthalmol 2014;98:941-5.

Original Article

Cardiac Morphometry in Healthy Young Indian Adult Males: An Evaluation of Chamber Thickness and Left Ventricular Cardiac Mass

Rohit Aggarwal, Ruchi Gautam[1], Abdul Raheem Sheik

Department of Radiology, 7 Airforce Hospital, Kanpur Cantonment, Kanpur, Uttar Pradesh, [1]Department of Radiology, Command Hospital Air Force (Bangalore), Bengaluru, Karnataka, India

Abstract

Introduction: Measurement of cardiac chambers is an important tool in the assessment of cardiac disease. Cardiac imaging can be used for the accurate assessment of these parameters. The primary objective of this study is to estimate various clinically relevant cardiac measurements including the left ventricular (LV) myocardial mass using cardiac magnetic resonance imaging (CMRI). The secondary objective is to correlate these measurements with the patient's body mass index (BMI). **Material and Methods:** A descriptive cross-sectional observational study was done at a tertiary care hospital. A total of 100 healthy young Indian adult males between 18 and 30 years of age underwent cardiac MRI on a 1.5Tesla Magnetic Resonance Imaging scanner. The thickness of various cardiac chambers and LV cardiac mass was measured. The results were compared with BMI. **Results:** Mean left atrial wall thickness is 1.6 mm in End -systole (ES)) and 1.5 mm in end diastole (ED). Mean Right atrial thickness is 1.5 mm (ES) and 1.8 mm (ED). Mean left ventricular wall thickness is 17.7 mm in End -systole (ES)) and 10.9 mm in end diastole (ED). Mean Right ventricular thickness is 6.9 mm (ES) and 3.2 mm (ED). Mean interventricular wall thickness is 14/9.7 mm in ES and ED, respectively. LV cardiac mass is 119.97 g. There is weak-to-moderate association between cardiac chambers and BMI. **Discussion and Conclusion:** Assessment of cardiac chamber thickness and LV cardiac mass in healthy adults can be made using CMRI. These values can be used as baseline to compare with measurements in various diseases of the heart.

Keywords: *Cardiac imaging techniques, heart diseases, magnetic resonance imaging, myocardium*

Introduction

Diseases of the cardiovascular system (CVS) are the leading cause of mortality.[1] Evaluation of the heart is an important component of CVS diseases, which has evolved over time from mere palpation and auscultation to advanced cardiac imaging. At present, standard structural evaluation of the heart comprises electrocardiography (ECG), echocardiography, and angiography. Cardiac magnetic resonance imaging (CMRI) of the heart has gained popularity in the recent past due to its excellent temporal and spatial resolution, lack of ionizing radiation, and noninvasiveness. Various diseases of CVS like hypertension cause structural changes in the size and morphologies of cardiac chambers.[2] Accurate evaluation of these changes involves various measurements of cardiac chambers and their comparison with known values in the healthy population. Conventionally, the cardiac chambers are evaluated on echocardiography. However, its accuracy is operator dependent and affected by the shape of cardiac chambers and the availability of sufficient field of view (FOV). These limitations can be addressed by CMRI which allows standardized measurements of various cardiac chambers on a 3-Dimensional (3D) dataset. Most clinically, relevant cardiac chamber measurements are the thickness of various cardiac chambers and left ventricular (LV) myocardial mass. There is limited literature on normal values of these parameters, especially in the Indian population. Thus, the primary objective of this study is to estimate various clinically relevant cardiac measurements including the LV myocardial mass. The secondary objective is to correlate these measurements with the patient's body mass index (BMI).

Material and Methods

This study is a descriptive cross-sectional observational study. The study is conducted in a tertiary care hospital catering to population representing various states of India. A total of 100 healthy volunteering

How to cite this article: Aggarwal R, Gautam R, Sheik AR. Cardiac morphometry in healthy young Indian adult males: An evaluation of chamber thickness and left ventricular cardiac mass. J Anat Soc India 2022;XX:XX-XX.

Article Info

Received: 21 April 2021
Revised: 03 January 2022
Accepted: 09 June 2022
Available online: ***

Address for correspondence:
Dr. Abdul Raheem Sheik, Department of Radiology, 7 Airforce Hospital, Nathu Singh Road, Kanpur Cantonment, Kanpur - 208 004, Uttar Pradesh, India.
E-mail: rohitaggy@gmail.com

Access this article online

Website: www.jasi.org.in
DOI: 10.4103/jasi.jasi_77_21
Quick Response Code:

participants were enrolled in the study. All the participants were aged between 18–30 years of age. Participants with a known history of hypertension and cardiac disease were excluded from the study. The study conforms to widely accepted ethical principles guiding human research. The study design was approved by the institutional ethics committee. Informed written consent was obtained from all the participants after explaining the purpose of the study and methodology. Patients who were unable to undergo CMRI evaluation or who could not complete the study due to various reasons like claustrophobia were excluded from the study. Patients underwent CMRI evaluation on a Siemens, Magentom Avanto1.5 Tesla Magnetic Resonance Imaging (MRI) scanner (Siemens medical systems, Erlangen, Germany). ECG-gated cine imaging of the heart was done in three planes, namely short-axis (SA), vertical long axis, and horizontal long axis (four chamber view). For half-Fourier acquisition single-shot turbo spin-echo sequences, the following parameters used were Time to Relaxation (TR) = 750 mS, Time to Echo (TE) = 46 mS, and FOV 234 mm × 340 mm. For cine SA, the following parameters were used TR = 45 mS, TE = 1.3 mS, FOV = 276 mm × 340 mm. After the images were acquired, they were transferred to dedicated workstation (Leonardo©). Images were analyzed by using the specific post-processing tool (Argus©) available in the workstation.

The wall thickness of all four chambers was recorded. The left atrial (LA) and right atrial (RA) wall thickness were measured in four-chamber views [Figure 1]. The average of maximum anterior and posterior wall thicknesses was recorded in end-systole (ES) and end-diastole (ED) frames of the cine sequence. The ventricular thickness was measured on ES and ED frames of cine sequence [Figures 2 and 3]. The right ventricular (RV) thickness was measured by measuring the mean of free wall thickness. The LV wall thickness was measured on four-chamber views by taking the maximum wall thickness. The LV ventricular cardiac mass was calculated on ED image frames by manually drawing epicardial and endocardial borders [Figure 4]. The mean thickness of the interventricular septum (IVS) was also estimated in the systolic and diastolic phases. The myocardial mass was calculated automatically on the "Argus®" by using estimated volume and predetermined assumed density of myocardium. The mean, range, and 95% confidence interval (CI) of the above-mentioned values were estimated. Statistical analysis was performed by estimating the Pearson correlation coefficient and statistical significance was estimated by taking a $P < 0.05$ as statistically significant. The estimated measurements were compared with similar studies in published literature.

Results

The demographic details and thickness of various cardiac chambers were recorded and tabulated. The demographic details of the participants including age, weight, BMI, pulse, systolic and diastolic blood pressure are tabulated in Table 1. The thickness (mean, range, and 95% CI) of various cardiac chambers, interventricular septal thickness, and LV myocardial mass are tabulated in Table 2. The various cardiac chamber measurements were correlated with BMI using the Pearson correlation coefficient to see the relationship with the BMI. The findings (*r* value and *P* value) are tabulated in Table 3.

Table 1: The demographic details of subjects

	Mean	Range	95% CI
Age (years)	24.86	19-30	6.78
Weight (kg)	68.6	47-86	16.22
BMI	23.14	18-28.1	4.6
Height (cm)	172	157-183	9.2
Pulse	73.80	60-86.00	11.26
Systolic blood pressure (mmHg)	114.19	110-130.00	10.02
Diastolic blood pressure (mmHg)	75.51	60-86	9.2

BMI: Body mass index, CI: Confidence interval

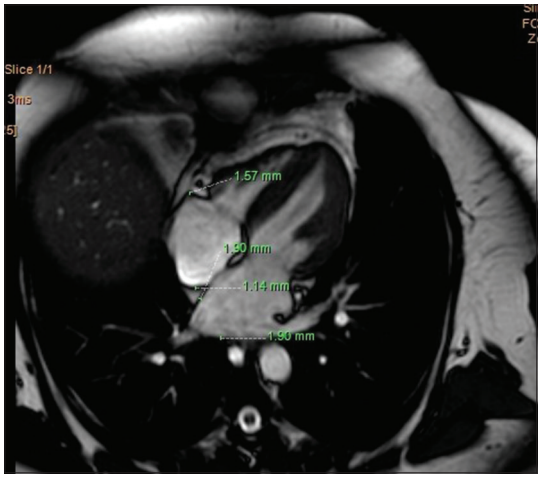

Figure 1: Measurement of atrial thickness

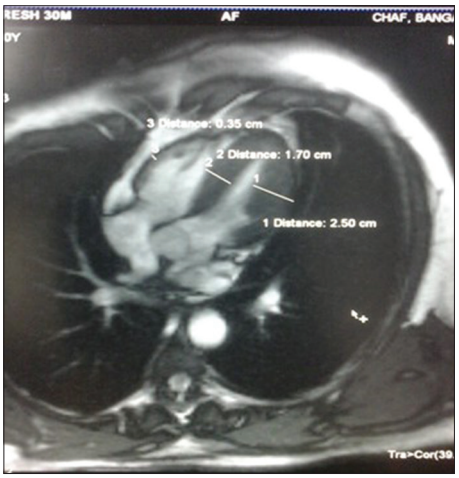

Figure 2: Measurement of ventricular and inter-ventricular septum thickness in end systole

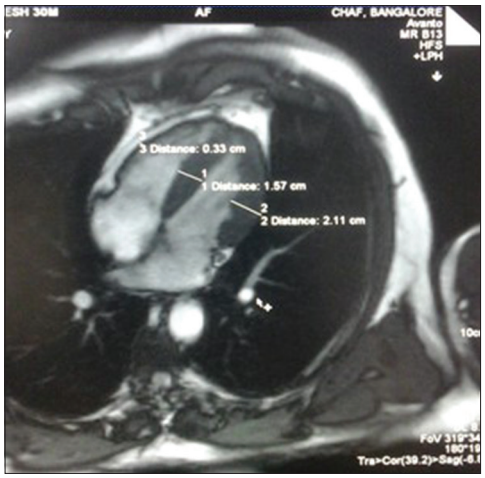

Figure 3: Measurement of ventricular and inter-ventricular septum thickness in end diastole

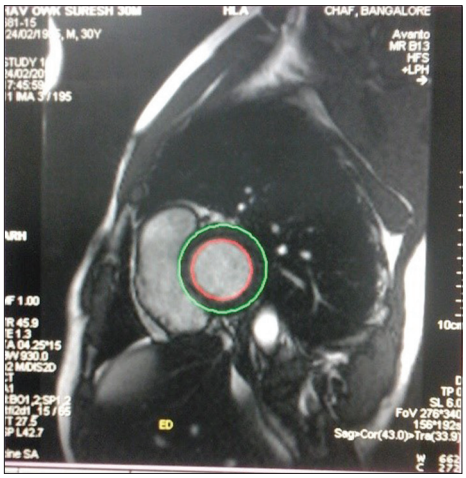

Figure 4: Measurement of endocardial mass in ED. Measured value on Argus software: 124.32 gm

Discussion

The study evaluated the thickness of various cardiac chambers and IVS in ES and ED frames. The LV myocardial mass was also estimated. Further, the study examined the relationship between the chamber thicknesses and LV cardiac mass with the BMI of the participants. The findings of our study were compared with similar studies in the available literature.

The mean thickness of LA in our study was 1.6 mm in ES and 1.5 mm in ED. Various authors have studied the relationship between LA wall thickness in patients with cardiac arrhythmias, especially atrial fibrillation (AF). Imada *et al*. have studied the LA wall thickness (LAWT) in patients of AF (16 chronic AF and 17 paroxysmal AF) using CT scan.[3] In their study, the mean thickness of the LA wall was 2.6 mm. They also observed thinning of the LA wall in the chronic AF group as compared to the paroxysmal AF group. Similarly, Nakamura *et al*. have studied LAWT in 186 participants belonging to chronic AF, paroxysmal AF and normal controls and observed that patients with paroxysmal AF have higher LAWT than chronic AF and healthy controls.[4] The mean LAWT in healthy controls in their study was 1.9 ± 0.2 mm. The results compare well with our study (1.5–1.6 mm). They also observed that the transition from Paroxysmal AF to Chronic AF was more frequent in patients with LAT <2.4 mm than LAT ≥2.4 mm suggesting LAWT can be a useful predictor of transition from PAF to CAF. Pan *et al*. have studied LAWT in 180 patients undergoing Multidetector computed tomography (CT) evaluation for coronary artery disease.[5] They observed that in the age group of 50–80 years, the LAWT increases with age and also observed the anterior wall thickness is consistently greater than the posterior wall thickness. In this study, the observed LAWT in population <40 years of age is 2.0 ± 0.9 mm (anterior wall) and 0.7 ± 0.2 mm (posterior wall). In the year 2019, Zuo *et al*. studied the relationship between the LAWT and response to catheter ablation in patients with persistent AF.[6] They observed that there is

Table 2: Cardiac chamber thickness and myocardial mass

	Mean	Range	95% CI
LA thickness in ES (cm)	0.16	0.10-0.30	0.14
LA thickness in ED (cm)	0.15	0.10-0.30	0.12
RA thickness in ES (cm)	0.15	0.10-0.30	0.10
RA thickness in ED (cm)	0.18	0.10-3.30	0.64
LV thickness in ES (cm)	1.77	0.60-2.20	0.50
LV thickness In ED (cm)	1.09	0.70-1.50	0.34
RV thickness in ES (cm)	0.69	0.40-1.00	0.26
RV thickness in ED (cm)	0.32	0.10-0.60	0.20
IVS in ES (cm)	1.4	0.6-1.90	0.56
IVS in ED (cm)	0.97	0.20-1.40	0.40
LV myocardial mass (g)	119.97	95-160.00	25.86

LA: Left atrial, RA: Right atrial, LV: Left ventricular, RV: Right ventricular, ES: End systole, ED: End diastole, IVS: Inter-ventricular septum, CI: Confidence interval

Table 3: Correlation of body mass index with cardiac chamber measurements

Pearson correlation coefficient	*r*	*P*
BMI (kg/m^2) versus LV thickness in ES (mm)	0.363	<0.001**
BMI (kg/m^2) versus LV thickness in ED (mm)	0.209	0.037*
BMI (kg/m^2) versus LA thickness in ES (mm)	0.194	0.054$^+$
BMI (kg/m^2) versus LA thickness in ED (mm)	0.213	0.034*
BMI (kg/m^2) versus RV thickness in ES (mm)	0.173	0.085$^+$
BMI (kg/m^2) versus RV thickness in ED (mm)	0.172	0.087$^+$
BMI (kg/m^2) versus RA thickness in ES (mm)	0.208	0.037*
BMI (kg/m^2) versus RA thickness in ED (mm)	0.125	0.214
BMI (kg/m^2) versus IVS thickness in ES (mm)	0.124	0.219
BMI (kg/m^2) versus IVS thickness in ED (mm)	0.111	0.270
BMI (kg/m^2) versus LV myocardial mass (g)	0.235	0.018*

**Strong association, *Weak association, $^+$No association. LA: Left atrial, RA: Right atrial, LV: Left ventricular, RV: Right ventricular, ES: End systole, ED: End diastole, IVS: Inter-ventricular septum, BMI: Body mass index

a negative association between the LAWT and response to ablation and LA roof thickness >3.10 mm might be the predictor of poor response to ablation.

The mean RA wall thickness in our study was around 1.5 mm in ES and 1.8 mm in ED. This compares well with other studies. In a post-mortem study by Wolf CM *et al*. the mean RA thickness was 1.8 ± 0.4 mm.[7] Varela *et al*. have used a novel MRI technique to non-invasively measure atrial wall thickness (AWT) in 10 healthy volunteers and 2 patients with AF.[8] They generated a whole atrial AWT atlas and measured mean AWT using this atlas. The mean Right AWT in their study was 2.7 ± 0.7 mm in healthy controls and 3.1 ± 1.3 mm in patients of AF with structural heart disease. Similarly, another study by Ginami G *et al*. quantified the AWT on CMR.[9] The observed RAWT in this study was 2.54 ± 0.87 mm. The difference in the AWT could be due to the difference in the method of estimation of AWT and the difference in the investigative modality used.

In our study, the mean free wall thickness of RV was 3.2 mm (ED). In a study by Foale *et al*. using echocardiography on 41 normal adults, the mean RV thickness in ED was 3–5 mm.[10] In our study, the mean ES RV thickness was 6.9 mm (4.0–10.0 mm). Similarly, Prakash has studied the correlation between the echocardiography and necropsy findings of the RV wall thickness in ES and ED.[11] In their study, the mean ED and ES RV wall thickness were 3.0 ± 0.92 cm and 5.1 ± 1.64 cm, respectively. These findings correlate well with our study.

The mean LV wall thickness in our study was 10.9 mm (ED) and 17.7 mm (ES). Haag *et al*. compared the LV wall thickness on CMRI in systole and diastole with 2-Dimensional (2D) echocardiography and digital subtraction angiography (DSA).[12] They observed that MR overestimates the wall thickness as compared to 2D echo and DSA. Using CMR, Dawson *et al*. have studied age- and sex-related morphometric changes in the thickness of LV in 120 healthy volunteers.[13] They studied these changes with respect to ES versus ED as well as trabeculated versus compacted segment. They observed that the total wall thickness is neither sex nor age dependent. Further, they observed that compacted layer thickens and trabeculated layers thins out with age. The compact layer is thicker in systole, in males and in participants above 40 years of age as compared to diastole, females and younger participants. The average wall thickness in this study was 9.7 mm (ED) and 14 mm (ES), respectively. The difference could be due to the difference in the method of estimation of LV wall thickness.

The mean IVS thickness in our study was 9.7 mm in ED and 14 mm in ES. In a study by Hergan *et al*., the normal measurement of IVS was calculated in 56 volunteers.[14] In males, the mean IVS thickness in diastole was 9.9 ± 1.2 mm, while in systole, it was 13.6 ± 1.9 mm. The findings correlate well with our study. Lorenz *et al*. have done CMR of 75 healthy adults and proposed normative data on the mass and function of LV and RV.[15] They also assessed the gender differences in these parameters. Sandstede *et al*. have studied LV and RV cardiac mass in 36 healthy volunteers of four different age and gender groups of 09 in each group.[16] The mean cardiac mass in LV was 155 ± 18 g, respectively. These values compare well with our study (119.9 g). They also found no difference in the cardiac mass between >45 years and <45 years age groups but significant gender differences with cardiac mass being high in males. Bhambhani *et al*. have estimated LA and LV cardiac chamber measurements in 133 healthy Indian adults using 3D echocardiography.[17] In their study, the estimated LV mass was 119.79 g ± 23.95 g. These findings match closely the findings of our study (119.97 ± 25.86 g). They also noted significant gender differences in the mean LV mass, but this difference disappeared after indexing the values for body surface area.

The association with BMI and various measured cardiac chamber thickness showed weak to moderate association (*r*-value ranging from 0.11–0.36) between various parameters, as shown in Table 3. There is significant correlation between Left cardiac chamber thicknesses and LV cardiac mass in our study. Similarly, Fuchs *et al*. studied normal values of cardiac chambers and LV mass in 569 healthy controls. They also observed a significant association between LV cardiac mass and BMI.[18] However, in another study by Krishnan *et al*., no correlation was found between LV thickness and BMI.[19]

The main strength of our study is the use of CMRI for the estimation of various cardiac chambers. CMRI is free from ionizing radiation. It is not operator dependent and not limited by the orientation and shape of the cardiac chambers in comparison to echocardiography. It is also not limited by the availability of scanning window and can be done without the use of contrast. Limited data are available studying the racial differences in cardiac mass and only two studies have been done in India till date to the knowledge of authors.[17,19] However, CMR has certain drawbacks. The resolution of CMRI is less as compared to CT scan thus the measurements done on MRI would be less accurate than cardiac CT measurement. Breathing artifacts can significantly compromise the quality of images, especially in patients with poor breath hold. The study did not assess the inter-observer and intra-observer variability. Previous similar studies have shown that this observer bias is not statistically significant. Nevertheless, the involvement of more than one observer and the calculation of inter- and intra-observer variability would have further improved the value of the study. The study included only the male population due to administrative convenience. The absence of data from female participants might preclude generalization to the entire population. We

only studied the cardiac chamber thickness and cardiac mass in the 18–30 years of age group. A study representing a wide range of age groups would have improved the generalizability of the study. While estimating the LV cardiac mass in our study, the mass of the individual components of the LV free wall and IVS were not measured separately. This could have been useful in conditions like transposition of great arteries and hypertrophic constrictive cardiomyopathy.

Conclusion

Measurement of various cardiac chamber thicknesses and LV mass can be done reliably using CMRI. This study evaluated these values using CMRI which is more reliable than echocardiography. Data on India-specific normal values of these cardiac chamber measurements are valuable for evaluating the changes in various disease processes.

Financial support and sponsorship

Nil.

Conflicts of interest

There are no conflicts of interest.

References

1. The Top 10 Causes of Death; 2020. Available from: https://www.who.int/news-room/fact-sheets/detail/the-top-10-causes-of-death. [Last accessed on 2020 Dec 13].
2. Santos M, Shah AM. Alterations in cardiac structure and function in hypertension. Curr Hypertens Rep 2014;16:428.
3. Imada M, Funabashi N, Asano M, Uehara M, Ueda M, Komuro I. Anatomical remodeling of left atria in subjects with chronic and paroxysmal atrial fibrillation evaluated by multislice computed tomography. Int J Cardiol 2007;119:384-8.
4. Nakamura K, Funabashi N, Uehara M, Ueda M, Murayama T, Takaoka H, *et al*. Left atrial wall thickness in paroxysmal atrial fibrillation by multislice-CT is initial marker of structural remodeling and predictor of transition from paroxysmal to chronic form. Int J Cardiol 2011;148:139-47.
5. Pan NH, Tsao HM, Chang NC, Chen YJ, Chen SA. Aging dilates atrium and pulmonary veins: Implications for the genesis of atrial fibrillation. Chest 2008;133:190-6.
6. Zuo K, Li K, Liu M, Li J, Liu X, Liu X, *et al*. Correlation of left atrial wall thickness and atrial remodeling in atrial fibrillation: Study based on low-dose-ibutilide-facilitated catheter ablation. Medicine (Baltimore) 2019;98:e15170.
7. Wolf CM, Seslar SP, den Boer K, Juraszek AL, McGowan FX, Cowan DB, *et al.* Atrial remodeling after the Fontan operation. Am J Cardiol 2009;104:1737-42.
8. Varela M, Morgan R, Theron A, Dillon-Murphy D, Chubb H, Whitaker J, *et al.* Novel MRI technique enables non-invasive measurement of atrial wall thickness. IEEE Trans Med Imaging 2017;36:1607-14.
9. Ginami G, Lòpez K, Mukherjee RK, Neji R, Munoz C, Roujol S, *et al.* Non-contrast enhanced simultaneous 3D whole-heart bright-blood pulmonary veins visualization and black-blood quantification of atrial wall thickness. Magn Reson Med 2019;81:1066-79.
10. Foale R, Nihoyannopoulos P, McKenna W, Kleinebenne A, Nadazdin A, Rowland E, *et al.* Echocardiographic measurement of the normal adult right ventricle. Br Heart J 1986;56:33-44.
11. Prakash R. Determination of right ventricular wall thickness in systole and diastole. Echocardiographic and necropsy correlation in 32 patients. Br Heart J 1978;40:1257-61.
12. Haag UJ, Hess OM, Maier SE, Jakob M, Liu K, Meier D, *et al*. Left ventricular wall thickness measurements by magnetic resonance: A validation study. Int J Card Imaging 1991;7:31-41.
13. Dawson DK, Maceira AM, Raj VJ, Graham C, Pennell DJ, Kilner PJ. Regional thicknesses and thickening of compacted and trabeculated myocardial layers of the normal left ventricle studied by cardiovascular magnetic resonance. Circ Cardiovasc Imaging 2011;4:139-46.
14. Hergan K, Schuster A, Mair M, Burger R, Töpker M. Normal cardiac diameters in cine-MRI of the heart. Rofo 2004;176:1599-606.
15. Lorenz CH, Walker ES, Morgan VL, Klein SS, Graham TP Jr. Normal human right and left ventricular mass, systolic function, and gender differences by cine magnetic resonance imaging. J Cardiovasc Magn Reson 1999;1:7-21.
16. Sandstede J, Lipke C, Beer M, Hofmann S, Pabst T, Kenn W, *et al*. Age- and gender-specific differences in left and right ventricular cardiac function and mass determined by cine magnetic resonance imaging. Eur Radiol 2000;10:438-42.
17. Bhambhani A, John N, Mathew A. Real-time three-dimensional echocardiographic left heart parameters in healthy Indian adults. Indian Heart J 2018;70:642-8.
18. Fuchs A, Mejdahl MR, Kühl JT, Stisen ZR, Nilsson EJ, Køber LV, *et al*. Normal values of left ventricular mass and cardiac chamber volumes assessed by 320-detector computed tomography angiography in the Copenhagen General Population Study. Eur Heart J Cardiovasc Imaging 2016;17:1009-17.
19. Krishnan R, Becker RJ, Beighley LM, López-Candales A. Impact of body mass index on markers of left ventricular thickness and mass calculation: Results of a pilot analysis. Echocardiography 2005;22:203-10.

Original Article

Problem-based Learning Using Online Platforms: An Interactive Alternative to Mandatory E-learning during the COVID-19 Pandemic

Mamata Chimmalgi, S. Rajesh, K. V. Anil Kumar, U. V. Asha, Jesin Elsa Jose, Komalavallyamma Chandrakumari

Department of Anatomy, Sree Gokulam Medical College and Research Foundation, Trivandrum, Kerala, India

Abstract

Introduction: Problem-based learning (PBL) helps in contextual and experiential learning. PBL using online platforms (PBL-op) was introduced to counter the declining interest in the mandatory e-learning during the COVID-19 pandemic. The purpose of this study was to determine the effect of PBL-op on learning outcome; student perception of PBL-op; effect of communication and motivation on learning outcome; and performance in PBL-op. **Material and Methods:** Study participants were introduced PBL-op and the control group to PBL in classroom setting. Five-way assessment was done: learning outcome by pre-and postintervention tests; performance by project reports and presentations; communication skills; motivation; and student satisfaction through an anonymous survey. Data were analyzed using descriptive statistics, paired or independent *t*-tests to compare paired variables, Spearman's correlation to establish association, and theme-based analysis for qualitative inputs. **Results:** Students showed better learning outcome with PBL op than with e learning ($t = 11.199$; $P < 0.001$*), traditional teaching ($t = 12.193$; $P < 0.001$*) and PBL in classroom setting ($t = -15.493$; $P < 0.001$*; d = 1.83). Women outperformed men with PBL-op ($t = -2.74$; $P = 0.0034$*; d = 0.48). Performance in PBL was better when conducted using online platforms than in classroom setting ($t = 8.5471$; $P < 0.001$*; d = 1.01). However, learning outcome and performance in PBL-op did not show a significant association with motivation or communication skills. Students favored PBL-op as it offered them an opportunity for active participation. **Discussion and Conclusion:** PBL-op offers all the advantages of PBL and allows productive teamwork using familiar online platforms and freedom from restrictive class timings. It is, therefore, suggested that PBL-op may be used as a feasible and effective alternative to PBL even after the pandemic.

Keywords: *Asynchronous e-learning, communication, motivation, problem-based learning, soft skills*

Introduction

Background

Problem-based learning (PBL) provides context to learning by connecting the concepts in anatomy with clinical experiences.[1-3] By encouraging research, it inculcates the practice of scientific enquiry, critical thinking, and evidence-based decision-making.[4] By collaborative and self-directed learning, it trains the future physician to be a life-long learner.[5-8] By enhancing motivation and underscoring communication skills, it paves the way for better clinical practice.[9-11]

Soft skills include social skills, communication skills, and professional and ethical attitudes. Good communication ensures greater compliance by the patients and greater job satisfaction for the clinicians.[12-14] Significance of communication skills in medical education is emphasized in international consensus statements[15] and standards for clinical practice.[16] This has led to development of various guidelines for teaching and assessing communication skills[13,14,17-20] and integration soft skills in the curriculum by the medical schools.[12-14,21]

Motivation determines how well the student engages in learning, which in turn defines his learning approach and academic performance. Different theories of motivation, e.g., Maslow's hierarchy of needs theory, Murray's need to achieve theory, Atkinson's expectancy value theory, Bandura's social cognitive theory, Pintrich's goal theory, and Deci and Ryan's self-determination theory, emphasize on different key factors or constructs.[22] Tools that measure strength of motivation

How to cite this article: Chimmalgi M, Rajesh S, Kumar KV, Asha UV, Jose JE, Chandrakumari K. Problem-based learning using online platforms: An interactive alternative to mandatory e-learning during the COVID-19 pandemic. J Anat Soc India 2022;XX:XX-XX.

Article Info

Received: 17 January 2022
Revised: 08 May 2022
Accepted: 09 June 2022
Available online: ***

Address for correspondence:
Dr. Mamata Chimmalgi, Department of Anatomy, Sree Gokulam Medical College and Research Foundation, Venjaramoodu, Trivandrum – 695 607, Kerala, India.
E-mail: mamatachimmalgi@gmail.com

Access this article online

Website: www.jasi.org.in
DOI: 10.4103/jasi.jasi_13_22
Quick Response Code:

rely on these motivational constructs. Motivation is broadly classified as intrinsic (behavior driven by what an individual perceives as valuable or enjoyable) and extrinsic (behavior driven by a promise of reward or a threat of punishment).[22-30] Some of the other constructs used to measure the strength of motivation include task value (how useful the task is), expectancy (belief that performance goals are achievable by one's efforts), interest (situational or individual), instrumentality (belief that one receives appropriate reward if performance meets the expectation), and cost value (negative aspects of choosing the task over alternatives).[31-36]

Context

Implementation of competency-based undergraduate curriculum in India from the academic year 2019–2020 initiated working with various teaching–learning methods that simultaneously addressed cognitive, psychomotor, affective, and/or communication domains. However, the concomitant onset of COVID-19 pandemic imposed a shift to obligatory e-learning. Although students welcomed e-learning with enthusiasm, initial excitement was soon replaced by disinterest, evidenced by declining attendance and learning outcome. Hence, a need was felt to change the passive instructive method to an interactive method that could work under the lockdown situation. This led to introducing "PBL using online platforms" (PBL-op) to the 1st-year medical students. Since the students were secluded in their homes under the duress of COVID pandemic, their motivation to participate in the activity was assessed. Since students were interacting using online platforms, their ability to communicate productively on the online platforms was assessed. The purpose of this study was to determine the (a) effect of PBL-op on learning outcome, (b) effect of different modes of interaction (online or offline) on the performance in PBL, (c) effect of communication and motivation on learning outcome and performance in PBL-op, (d) gender difference in learning outcome and motivation, and (d) if PBL-op was perceived favorably.

Material and Methods

Design and sample

An experimental study was conducted during 2020–2021, for the duration of about 15 days each year in the department of anatomy following approval from the institutional ethics committee. Study participants were recruited within the cohort of 1st-year medical students of 2019–2020 batch (n = 150, 55 men, 95 women, age range 18y7m-23y, average±Std. Dev=20.01±0.89). At the time of the study, they were at home due to pandemic and were engaged in lecture series on neuroanatomy using asynchronous e-learning. The control group were recruited within the cohort of 1st-year medical students of 2020–2021 batch, who at the time of the study had completed lecture series on development of cardiovascular system using classroom teaching (n = 150, 49 men, 101 women, age range 18y2m-22y9m, average±Std. Dev=20.62±0.77). Participation in online or offline PBL was part of the training program. Participation in the questionnaire was voluntary following informed consent.

Procedure

Study participants and controls were randomly divided into performance-matched, smaller subgroups. Study participants were divided into ten groups of 15 students each and controls were divided into six groups of 25 students each. Each subgroup was assigned a clinical scenario (anatomy of the brainstem and associated brainstem lesions for the study participants and development of cardiovascular system and associated congenital heart diseases for the control group). Members of each subgroup were instructed to collaborate, plan individual contributions, research information from various resources (textbooks, scientific articles, web pages, blogs, YouTube videos, etc.), discuss and analyze the data, and develop solutions and content over the next 10 days. Study participants were instructed to conduct all their discussions pertaining to planning, execution, and submission within the allocated WhatsApp group for each subgroup, whereas the controls discussed in the classroom setting with face-to-face interactions. Each subgroup was closely monitored by one of the investigators to assess communication and contribution by individual student. At the end of 10 days, all the subgroups were instructed to submit a project report (minimum thousand-worded document file) and a video (study group) or a live (controls) presentation.

Data collection

Learning outcome was assessed by average percentage scores in the pre- and posttests. Pre- and posttests were conducted using objective questions of multiple-choice questions type and single-word response type. Performance in PBL-op or PBL was assessed by the average percentage scores for the project reports and presentations. Project reports and the presentations were assessed independently by all the faculty members. Assessment was based on prior selected criteria (e.g. Content, clinical correlation, new or additional information, organisation/format, style of presentation, diagrams, references, and use of AV aids (for presentation)). Average percentage scores were awarded.

Communication among the study participants was assessed based on twenty statements from SEGUE framework and Kalamazoo consensus statement.[17-20] Each statement was assigned ordinal value of one or zero for yes or no responses, respectively, and an average score (max. score of 20) was awarded.

Motivation of the study participants was assessed by a survey containing twenty-eight statements adapted from Motivation Strategies for Learning Questionnaire (MSLQ) and motivation section of phase 1 survey by McCord

and Matusovich.[31,35,37] Statements belonged to one of the seven constructs: internal goal orientation (statements 1–3), external goal orientation (4–6), task value (7–11), expectancy (12–17), interest (18–20), cost (21–23), and instrumentality (24–28). As the statements were from valid and reliable instruments, only internal consistency reliability was evaluated. Cronbach's alpha coefficient for all the statements was 0.955, suggesting excellent internal consistency. Each statement required the students to respond on a five-point Likert scale with assigned ordinal values of 1–5. Average scores for overall motivation (all the 28 statements) and for different constructs were calculated.

Perception regarding PBL-op was assessed by an anonymous survey. It collected data regarding perception about ease of using online media and resources, and about the comparative merits of PBL-op, e-learning, and traditional teaching. It also collected responses to open-ended questions about what they liked or did not like about PBL-op.

Data analysis

Learning outcome was assessed by comparing the average percentage scores in pre- and posttests using paired *t*-test. Effect of mode of interaction during PBL (online or offline) on learning outcome was assessed by comparing the average scores of the two groups in posttests using independent *t*-test. The SPSS statistical package, version 16.0 (SPSS Inc., Chicago, IL, USA) was used for the statistical analysis. Level of significance was set at 0.05. Performance in PBL by study participants (online) and controls (offline) was assessed by comparing the average percentage scores in the project reports and presentations using independent *t*-test. Effect of communication and motivation on learning outcome and on performance in PBL-op was determined using Spearman's correlation. Gender difference in learning outcome and motivation was assessed by comparing the average scores for the two genders using the independent *t*-test. Perception regarding PBL-op was inferred by the descriptive statistics for the categorical data and theme-based analysis of the narrative responses for the open-ended questions. Investigator triangulation was adopted for the latter to improve validity.

Results

Learning outcome was found to be significantly better with PBL using online platforms than with classroom settings (average posttest scores for study group = 65.48 ± 15.09 and controls = 36 ± 17; t = −15.493; P < 0.001*; d = 1.83, suggesting large effect size). Students showed better academic performance with PBL-op than with asynchronous e-learning (average scores in pretest = 49.55 ± 12.79 and posttest = 65.48 ± 15.09; t = 11.199; P < 0.001*) or traditional teaching (average scores in pretest = 44.53 ± 13.27 and posttest = 65.48 ± 15.09; t = 12.193; P < 0.001*). However, PBL in classroom setting did not improve academic performance when compared to traditional teaching (average scores for control group for traditional teaching = 55.00 ± 16.00 and PBL = 36 ± 17; t = −9.6402; P < 0.001*).

Students showed better performance in the project reports and presentations when PBL was conducted using online interactions than in classroom settings (average percentage scores for the study group = 66.68 ± 6.14 and the controls = 61 ± 5; t = 8.5471; P < 0.001*; d = 1.01 suggesting large effect size).

Enhanced motivation was expected to improve communication, leading to better performance in PBL-op and ultimately improved academic performance. However, findings were mostly contrary to the expectations. Although overall motivation was high (3.81 ± 1.07), it did not show significant association with communication (rs = −0.357, P = 0.310). Similarly, performance in PBL-op did not show a significant association with motivation (rs = −0.40122, P = 0.2505) and showed a weak negative association with communication (rs = −0.3054, P = 0.00014*). Learning outcome also did not show a significant association with overall motivation (rs = −0.45732, P = 0.18389) or communication (rs = −0.06733, P = 0.41936) or performance in PBL-op (rs = 0.19453, P = 0.59021). When different constructs of motivation were considered, expectancy and instrumentality showed a strong positive association with communication (rs = 0.648, P = 0.043* and rs = 0.733, P = 0.016*, respectively). Cost value showed a significant negative association with performance in PBL-op (rs = −0.705, P = 0.023*). Expectancy showed a strong negative association with learning outcome (rs = −0.669, P = 0.035*).

Women showed better academic performance following PBL-op than men (average posttest scores of women = 68.04 ± 15.03, men = 60.94 ± 14.30; t = −2.74, P = 0.0034*, d = 0.48). However, there was no significant difference between the genders in overall motivation (women = 105.39 ± 19.39, men = 108.93 ± 18.61, t = 1.082, P = 0.281) or intrinsic goal orientation (women = 3.2 ± 0.7, men = 3.39 ± 1.32, t = −1.256, P = 0.112) or extrinsic goal orientation (women = 3.48 ± 0.62, men = 3.52 ± 1.56, t = −0.253, P = 0.401).

Total 147 students (54 males, 93 females) responded to the survey (98% response rate). Most students were using personal smart phones and perceived no difficulty in accessing the online resources (64.63%) or communicating with the peers using online platforms (84.27%) [Figures 1a-d and 2]. When didactic lectures, e-learning and PBL-op were compared, and majority observed that PBL-op would maximize attention to the task and help them become a better clinician, but didactic lectures helped them perform better in exams [Figure 3].

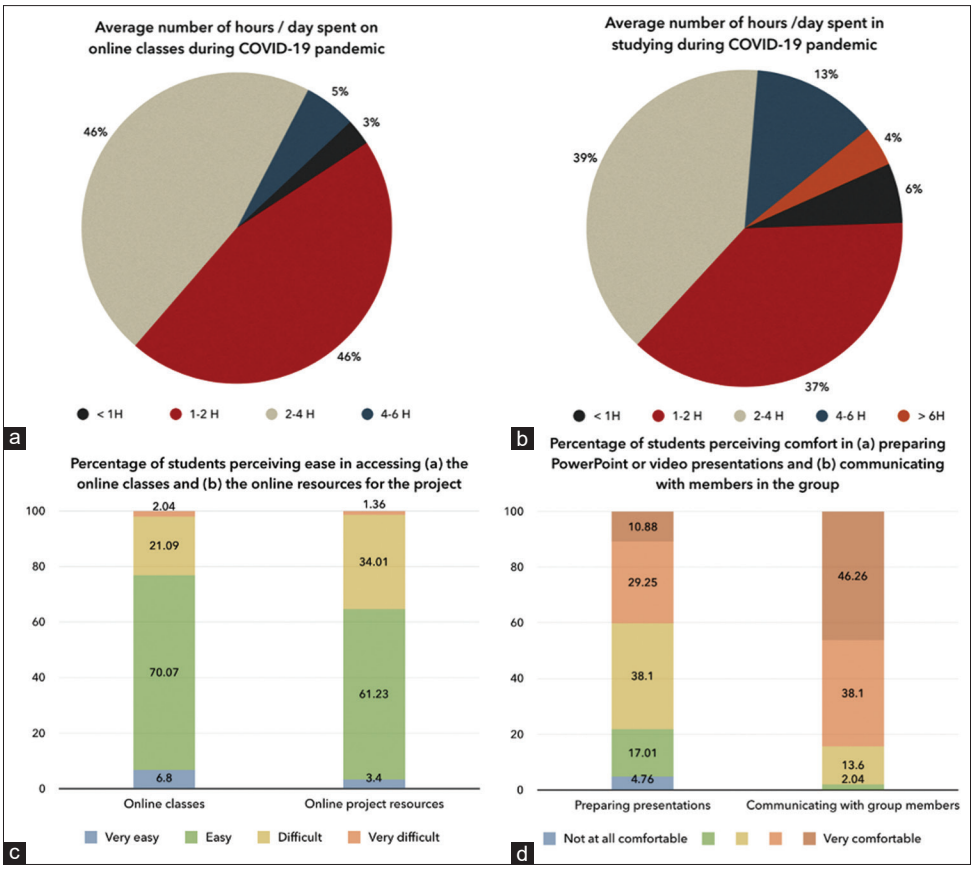

Figure 1: (a and b) Average number of hours the students spent per day in accessing online classes and resources, (c) ease of accessing online resources, and (d) comfort in preparing PowerPoint or video presentations and communicating with the peers

Analysis of qualitative data revealed six major themes each for "what they liked" and "what they did not like" about PBL-op. Some of the narrative comments to the open-ended questions are listed in Table 1. What students liked about PBL-op was an opportunity for problem-solving, interaction with team members, and involvement of self in the process. What they liked least about PBL-op was that it was time-consuming.

Discussion

Mandatory e-learning imposed by the COVID pandemic had a diametrically opposite effect on the progression of its two principal participants. With time, the instructors gained expertise by overcoming technophobia and infrastructure limitations. Students, on the contrary, showed steadily diminishing interest and learning outcome, and on occasions, the participation in the class was limited to only digital presence. PBL-op was, therefore, introduced as a remedial method, designed to trigger and maintain situational interest.[34] Participants enjoyed this interactive learning experience using familiar online discussion platform and found the method beneficial to learn tougher areas like structure of brainstem ("Working under a surveillance in a team seems more effective. Neuroanatomical structures are more clear when discussing among ourselves"). Majority opined that PBL-op provided an opportunity for critical thinking through its problem-solving approach ("It made us think and question, above all to find the solutions for all those problems") and allowed them to search from various sources ("I could refer (to sources) other than books. whereas normal learning keep us within our (text) books itself…"). They perceived that PBL-op was more interesting than didactic teaching ("Each case gave us an opportunity to understand more about that topic… Routine classes sometimes seem boring as we are listening to lectures continuously"). Other advantages cited included opportunity for interaction, team work, involvement of self, better understanding, and clinical correlation. On the downside, they perceived that the method was time-consuming. A few had difficulty in navigating through intersource differences in information ("Different resources give different points about the topic. It is a little confusing"). However, almost a third of the students opined that they did not find any downsides about PBL-op ("Nothing at all. Literally that much I enjoyed finishing this project").

Assessment in a problem-based approach focuses on evaluating application of the reasoning process rather than recall and requires use of several methods to evaluate different domains, as was done in the current study.[38] Learning outcome was assessed based on questions on application of reasoning (e.g., likely site of

lesion or anatomical basis for clinical case scenarios). In addition to knowledge of anatomy, performance in PBL op also assessed the ability to conduct basic research, creativity, presentation skills, working as a team member and technological know how. As PBL-op was being conducted for the first time, students ability to communicate productively on online platforms and their motivation levels were also assessed.

Effect of PBL on learning outcome has been reported by different studies as both positive[38-40] and negative.[2,5,6,41,42] In the current study, academic performance of the study group with PBL-op agreed with the former observation, whereas academic performance of the control group following PBL in classroom setting agreed with the latter. Academic performance following PBL-op was not only superior to traditional teaching, but was also superior to e-learning and PBL in classroom setting. This was possibly because the students engaged more earnestly in PBL-op as they were relatively free from the robust academic training activities and perceived PBL-op as a relief from the monotony of passive e-learning. This prompts us to suggest that effect of PBL on the learning outcome is influenced by several factors outside the ambit of the merits of the method itself, e.g., situational interest, concomitant academic burden, mode of interaction, and perceived complexity of the topic.

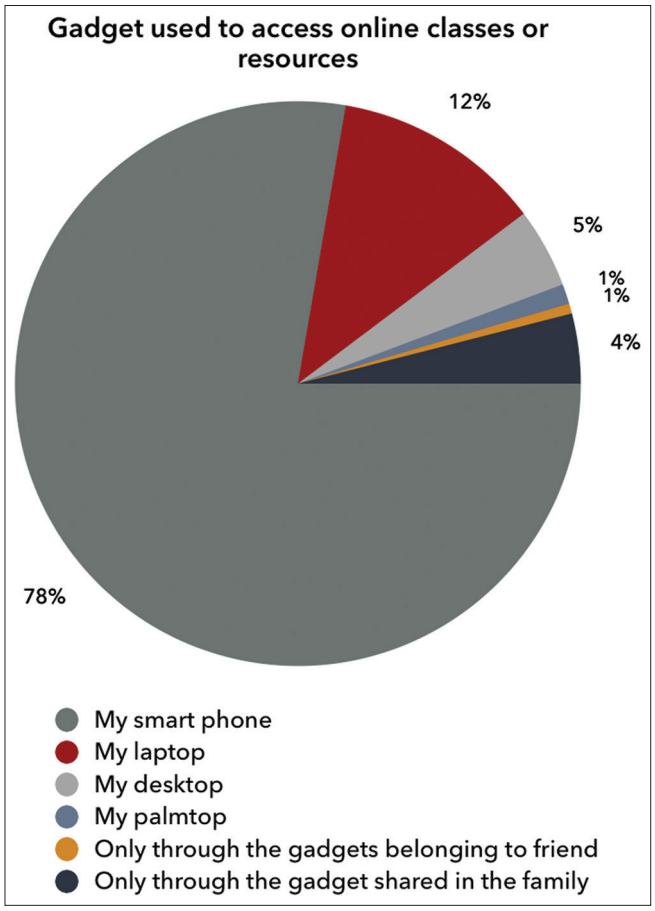

Figure 2: The gadget used by the students to access online classes or resources

Motivation is affected by situation, mood, goal and tool.[28] Educationists are interested in motivation, as it is purported to influence the performance in learning activities and learning outcome.[22] Although motivation and academic achievements are recognized as mutually inducing,[43,44] different studies have reported the association between the two as not significant[45] or directly positive[25,28] or indirectly positive through study strategy and study efforts[27] or as positive only for intrinsic motivation.[30] Our findings agree with those of Luqman, as overall motivation did not show a significant association with learning outcome (rs = −0.45732, $P = 0.18389$).[45] Moreover, "expectancy," despite showing a strong positive association with communication, showed a strong negative association with learning outcome (rs[8] = −0.669, $P = 0.035$*). This means, the students who were motivated by the belief that performance goals were achievable by one's efforts contributed more to the discussions, but, they did not show corresponding improvement in academic performance. Similar findings have been reported by Kusurkar *et al*., where the study efforts did not show a significant association with academic performance.[27] In addition, in the present study, overall motivation did not show a significant association with performance in PBL-op (rs = −0.40122, $P = 0.2505$), although cost value showed a strong negative association with it (rs[8] = −0.705, $P = 0.023$*), suggesting that negative perception toward choosing PBL-op over other

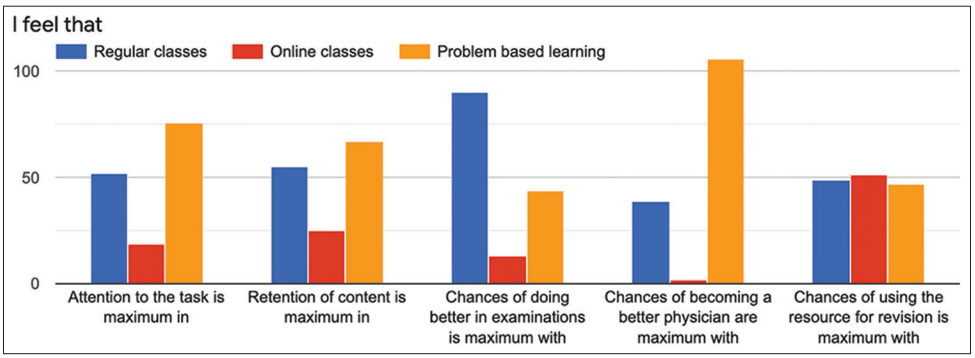

Figure 3: The comparison between the perceptions regarding traditional teaching, e-learning, and problem-based learning

Table 1: Narrative responses of the students about problem-based learning using online platforms

Theme	Responses
What I liked best about PBL-op?	
Critical thinking and problem solving	1. "I could refer other than books.it was a wide platform. whereas normal learning keep us within our books itself…."
	2. "It made us think and question above all to find the solutions for all those problems"
Better understanding and retention	1. "Each case gave us an opportunity to understand more about that topic. Communication between our group mates was interesting. Routine classes sometimes seems boring as we are listening to lectures continuously"
	2. "Working under a surveillance in a team seems more effective. Neuroanatomical structure are more clear when discussing among ourselves"
Self-involvement and self-learning	1. "We could add our innovative ideas"
	2. "The main difference is that we are preparing the notes. We are searching and referring the content in different textbooks. So that we are able to understand the topic clearly"
Teamwork and interactive	1. "Group discussion and contribution to it as a member helped build my team skills"
	2. "The way we could interact with teammates. During each presentation we got opportunity to ask any doubts freely and get it cleared"
Interesting task and a different experience	1. "It is a new experience and raised curiosity"
	2. "Problem based learning is more interesting than routine classes"
Clinical correlation or useful for clinical practice	1. "Through problem based learning, we will become more aware about the clinical aspects of each case"
	2. "Instead of just understanding the topic we were able to relate the topic with someone's clinical condition so that we will never forget (it) and (it will) help us not only to pass the examination but also will help us massively during clinical postings"
What I liked least about PBL-op?	
Time consuming	1. "It was time consuming and I had to set aside my learning hours for this"
	2. "Time consuming, I got many of my works pending. In between all online classes, tests and assignments it was heavy load for me"
Difficult to understand	1. "Some concepts were not clear"
	2. "The different resources give different points about the topic. It is little confusing"
Difficult to gather information	1. "Collection of resources was bit difficult where books of our choice was not available"
	2. "To collect some resources we worked really hard as it was not easily available neither in books nor in sites. Other than that everything was good and I recommend to give us more such projects. Thank you"
Technical drawbacks	1. "Difficulty in using apps for the making of project"
	2. "Difficulty in using smartphones to make reports"
	3. "As communication is through indirect methods like texting, it can be a bit difficult to put facts across"
Getting friends on board	1. "Bringing everyone's idea to a single project"
	2. "Having disagreements about the project layout and content"
Confined to one topic	1. "We become aware of only the topic we prepare for. Less interested to go through other projects which seem bulkier"
	2. "We get confined to our own topic.and we spend more time in a single topic….even though there are more topics"
Nothing	1. "Nothing at all. Literally that much I enjoyed finishing this project"
	2. "Nothing, I like all the aspects of problem based learning"

PBL-op: Problem-based learning using online platforms

activities had a stronger influence on performance in learning activities. Thus, our findings implore re-examining the effects of motivation on the performance in the learning activities and on learning outcome.

Good communication skills play an important role in effective delivery of health care, making comprehensive training and assessment of communication skills a necessity in the medical curriculum.[12-14,46] In the current study, communication skills showed a strong positive association with both expectancy (rs[8] = 0.648, P = 0.043*) and instrumentality (rs (8) =0.733, P = 0.016*), indicating that the students who believed that they could reach the performance goals through their efforts and receive appropriate rewards made an active effort to communicate better. However, better communication did not translate into better learning outcome (rs = −0.06733, P = 0.41936) or performance in PBL-op (rs = −0.3054, P = 0.00014). While the role of communication in clinical practice cannot be overemphasized, the results of the study suggest that the immediate outcomes of PBL for the 1st-year medical students, namely, cognitive learning, critical thinking, or content creation, are independent of their ability to communicate. Yet again, these findings demand a rethink about highlighting the significance of communication when selecting a newer teaching–learning method for the 1st-year medical students in the competency based undergraduate curriculum.

Gender is one of the important predictors for motivation. Studies comparing gender difference in motivation and academic performance have all reported better academic performance by the women, although observations on

motivation are varied. Some studies have reported higher overall and intrinsic motivation in women and higher extrinsic motivation in men,[27,44] whereas others have reported higher intrinsic motivation in men with no significant gender difference in extrinsic motivation.[30] Our findings are in concurrence with these studies in learning outcome as women showed significantly better academic performance ($t = -2.74$, $P = 0.0034$*, d = 0.48). However, our results differ regarding motivation, in that there was no significant gender difference in overall motivation, intrinsic motivation, or extrinsic motivation. This further supports our initial observation that motivation did not show a significant association with learning outcome.

Limitations of the study

The study with PBL-op was conducted as a single session in a single institution using a small sample size. Results may have been confounded by the novelty factor and the pandemic induced lockdown.

Conclusion

PBL-op offered a feasible and interactive alternative to the enforced e-learning during the COVID pandemic. Academic performance with PBL-op was significantly better than with asynchronous e-learning, traditional teaching, or PBL in classroom setting. Although PBL-op enhanced motivation, neither performance in PBL-op nor learning outcome was influenced by greater motivation. Similarly, better communication did not result in better performance in PBL-op or learning outcome. Women showed significantly better academic performance, although there was no gender difference in motivation. These findings suggest that communication or motivation need not be the defining factors in selecting the teaching–learning methods for the 1st -year medical students in competency-based undergraduate curriculum.

PBL-op offered all the benefits of PBL, e.g., opportunity for critical thinking and evidence-based decision-making, improved academic performance, enhanced motivation, clinical correlation, and sensitizing the students to the importance of research and communication skills. In addition, the method also offered the benefits of learning through familiar online platforms, freedom from restrictive class hours, and better academic performance. Hence, it is suggested that PBL-op may be used as an alternative to PBL even after the COVID-19 pandemic.

Acknowledgments

The authors wish to express their gratitude to Dr. P Chandramohan, Dean, for inputs on PBL, Dr. Manju L, Associate Professor (Statistics), for her contributions to statistical analysis, Dr. Regi Jose, Professor, Community Medicine, for valuable suggestions, and the first-year medical students (2019-20 and 2020-21 batches) for their enthusiastic participation.

Financial support and sponsorship

Nil.

Conflicts of interest

There are no conflicts of interest.

References

1. Fincham AG, Shuler CF. The changing face of dental education: The impact of PBL. J Dent Educ 2001;65:406-21.
2. Prince KJ, van Mameren H, Hylkema N, Drukker J, Scherpbier AJ, van der Vleuten CP. Does problem-based learning lead to deficiencies in basic science knowledge? An empirical case on anatomy. Med Educ 2003;37:15-21.
3. McHarg J, Kay EJ. The anatomy of a new dental curriculum. Br Dent J 2008;204:635-8.
4. Kaufman A, Mennin S, Waterman R, Duban S, Hansbarger C, Silverblatt H, *et al.* The New Mexico experiment: Educational innovation and institutional change. Acad Med 1989;64:285-94.
5. Hinduja K, Samuel R, Mitchell S. Problem-based learning: Is anatomy a casualty? Surgeon 2005;3:84-7.
6. Nayak S, Ramnarayan K, Somayaji N, Bairy KL. Teaching anatomy in a problem-based learning (PBL) curriculum. Neuroanatomy 2006;5:2-3.
7. Yiou R, Goodenough D. Applying problem-based learning to the teaching of anatomy: The example of Harvard Medical School. Surg Radiol Anat 2006;28:189-94.
8. Azer SA, Eizenberg N. Do we need dissection in an integrated problem-based learning medical course? Perceptions of first- and second-year students. Surg Radiol Anat 2007;29:173-80.
9. Pawlina W, Romrell LJ, Rarey KE, Larkin LH. Problem-based learning with gross anatomy specimens: One year trial. Clin Anat 1991;4:298-306.
10. Koh GC, Khoo HE, Wong ML, Koh D. The effects of problem-based learning during medical school on physician competency: A systematic review. CMAJ 2008;178:34-41.
11. Onyon C. Problem-based learning: A review of the educational and psychological theory. Clin Teach 2012;9:22-6.
12. Taveira-Gomes I, Mota-Cardoso R, Figueiredo-Braga M. Communication skills in medical students – An exploratory study before and after clerkships. Porto Biomed J 2016;1:173-80.
13. Radziej K, Löchner J, Engerer C, Niglio de Figueiredo M, Freund J, Sattel H, *et al*. How to assess communication skills? Med Educ Online 2017;22:1392823.
14. Brouwers M, Custers J, Bazelmans E, van Weel C, Laan R, van Weel-Baumgarten E. Assessment of medical students' integrated clinical communication skills: Development of a tailor-made assessment tool. BMC Med Educ 2019;19:118.
15. Simpson M, Buckman R, Stewart M, Maguire P, Lipkin M, Novack D, *et al*. Doctor-patient communication: The Toronto consensus statement. BMJ 1991;303:1385-7.
16. Tate P, Foulkes J, Neighbour R, Campion P, Field S. Assessing physicians' interpersonal skills via videotaped encounters: A new approach for the Royal College of General Practitioners Membership examination. J Health Commun 1999;4:143-52.
17. Makoul G. Essential elements of communication in medical encounters: The Kalamazoo consensus statement. Acad Med 2001;76:390-3.
18. Makoul G. The SEGUE Framework for teaching and assessing communication skills. Patient Educ Couns 2001;45:23-34.
19. Rider EA, Hinrichs MM, Lown BA. A model for communication skills assessment across the undergraduate curriculum. Med

Teach 2006;28:e127-34.
20. Modi JN, Anshu, Chhatwal J, Gupta P, Singh T. Teaching and assessing communication skills in medical undergraduate training. Indian Pediatr 2016;53:497-504.
21. Staden CV, Joubert PM, Pickworth GE, Roos JL, Bergh AM, Krüger C, *et al.* The conceptualisation of "soft skills" among medical students before and after curriculum reform. Afr J Psych 2006;9:33-7.
22. Kusurkar RA, Ten Cate TJ, van Asperen M, Croiset G. Motivation as an independent and a dependent variable in medical education: A review of the literature. Med Teach 2011;33:e242-62.
23. Ryan RM, Deci EL. Intrinsic and extrinsic motivations: Classic definitions and new directions. Contemp Educ Psychol 2000;25:54-67.
24. Sobral DT. What kind of motivation drives medical students' learning quests? Med Educ 2004;38:950-7.
25. Vansteenkiste M, Zhou M, Lens W, Soenens B. Experiences of autonomy and control among Chinese learners: Vitalizing or immobilizing? J Educ Psych 2005;97:468-83.
26. Artino AR, La Rochelle JS, Durning SJ. Second-year medical students' motivational beliefs, emotions, and achievement. Med Educ 2010;44:1203-12.
27. Kusurkar RA, Ten Cate TJ, Vos CM, Westers P, Croiset G. How motivation affects academic performance: A structural equation modelling analysis. Adv Health Sci Educ Theory Pract 2013;18:57-69.
28. Yousefy A, Ghassemi G, Firouznia S. Motivation and academic achievement in medical students. J Educ Health Promot 2012;1:4.
29. Wouters A, Croiset G, Galindo-Garre F, Kusurkar RA. Motivation of medical students: Selection by motivation or motivation by selection. BMC Med Educ 2016;16:37.
30. Wu H, Li S, Zheng J, Guo J. Medical students' motivation and academic performance: The mediating roles of self-efficacy and learning engagement. Med Educ Online 2020;25:1742964.
31. Pintrich PR, Smith DAF, Garcia T, McKeachie WJ. A Manual for the Use of the Motivated Strategies for Learning Questionnaire (MSLQ). Technical Report No. 91-08-004. University of Michigan National Center for Research to Improve Postsecondary Teaching and Learning, Ann Arbor, MI: The Regents of the University of Michigan.
32. Wigfield A, Eccles JS. Expectancy-value theory of achievement motivation. Contemp Educ Psychol 2000;25:68-81.
33. Husman J, Pitt Derryberry W, Michael Crowson H, Lomax R. Instrumentality, task value, and intrinsic motivation: Making sense of their independent interdependence. Contemp Educ Psychol 2004;29:63-76.
34. Hidi S, Renninger KA. The four-phase model of interest development. Educ Psychol 2006;41:111-27.
35. McCord R, Matusovich HM. Developing an instrument to measure motivation, learning strategies and conceptual change. 2013. ASEE Annual Conference & Exposition, Atlanta, Georgia, USA. 2013. p. 23.92.1-23.92.22. [Doi: 10.18260/1 2 19406].
36. Priniski SJ, Hecht CA, Harackiewicz JM. Making learning personally meaningful: A new framework for relevance research. J Exp Educ 2018;86:11-29.
37. Jackson CR. Validating and adapting the Motivated Strategies for Learning Questionnaire (MSLQ) for STEM courses at an HBCU. AERA Open 2018;4:1-16.
38. Nyemb PM. Studying anatomy through a problem-based learning approach. MOJ Anat Physiol 2017;4:377-9.
39. Khaki AA, Tubbs RS, Zarrintan S, Khamnei HJ, Shoja MM, Sadeghi H, *et al.* The first year medical students' perception of and satisfaction from problem-based learning compared to traditional teaching in gross anatomy: Introducing problem-based anatomy into a traditional curriculum in Iran. Int J Health Sci (Qassim) 2007;1:113-8.
40. Yuvaraj BJ, Iyer PB. Problem based learning in anatomy – Our experience. Natl J Integr Res Med 2016;7:92-7.
41. Bergman EM, Prince KJ, Drukker J, van der Vleuten CP, Scherpbier AJ. How much anatomy is enough? Anat Sci Educ 2008;1:184-8.
42. Potu B, Hla Shwe W, Jagadeesan S, Aung T, Peh SC. Scope of anatomy teaching in problem-based learning (PBL) sessions of integrated medical curriculum. Int J Morphol 2013;31:899-901.
43. Nieuwhof MG, ThJ Ten Cate O, Oosterveld P, Soethout MB. Measuring strength of motivation for medical school. Med Educ Online 2004;9:4355.
44. Kunanitthaworn N, Wongpakaran T, Wongpakaran N, Paiboonsithiwong S, Songtrijuck N, Kuntawong P, *et al*. Factors associated with motivation in medical education: A path analysis. BMC Med Educ 2018;18:140.
45. Luqman M. Relationship of academic success of medical students with motivation and pre-admission grades. J Coll Physicians Surg Pak 2013;23:31-6.
46. Tabish SA. Assessment methods in medical education. Int J Health Sci (Qassim) 2008;2:3-7.

Original Article

Dimensional Accuracy of Medical Models of the Skull Produced by Three-Dimensional Printing Technology by Advanced Morphometric Analysis

Sharmila Aristotle, Shantanu Patil[1], Saikarthik Jayakumar[2,3]

Departments of Anatomy and [1]Translational Medicine, SRM Medical College Hospital and Research Center, Kattankulathur, Tamil Nadu, India, Departments of [2]Basic Medical Science and [3]Medical Education, College of Dentistry, Majmaah University, Al Zulfi, Riyadh, Saudi Arabia

Abstract

Introduction: Three-dimensional (3D) printing creates a design of an object using software, and the process involves by converting the digital files with a 3D data using the computer-aided design into a physical model. The aim of the study was to investigate the accuracy of human printed 3D skull models from computed tomography (CT) scan data via a desktop 3D printer, which uses fused deposition modeling (FDM) technology. **Material and Methods:** Human anatomical cadaver skulls were CT scanned in 128-slice CT scanner with a slice thickness of 0.625 mm. The obtained digital imaging and communications in medicine files were converted to 3D standard tessellation language (STL) format by using MIMICS v10.0 software (Materialise, Leuven, Belgium) program. The 3D skull model was printed using a Creatbot DX desktop 3D FDM printer. The skull model was fabricated using polylactic acid filament with the nozzle diameter of 0.4 mm and the resolution of the machine was maintained at 0.05 mm. The accuracy was estimated by comparing the morphometric parameters measured in the 3D-printed skull with that of cadaver skull and with CT images to ensure high accuracy of the printed skull. Fourteen morphometric parameters were measured in base and cranial fossa of the skull based on its surgical importance. **Results:** Analysis of measurements by inferential statistical analysis of variance for all three groups showed that the 3D skull models were highly accurate. Reliability was established by interobserver correlation for measurements on cadaver skull and the 3D skulls. Dimensional error was calculated, which showed that the errors between three groups were minimal and the skulls were highly reproducible. **Discussion and Conclusion:** The current research concludes that a 3D desktop printer using FDM technology can be used to obtain accurate and reliable anatomical models with negligible dimensional error.

Keywords: *Computed tomography scan, fused deposition modeling, morphometry, skulls, three-dimensional printing*

Introduction

Additive manufacturing technology refers to three-dimensional (3D) printing technology that produces 3D objects, which are digitally defined by computer-aided design.[1] This 3D printing technology has now extended its hands representing a big opportunity in the medical field helping the health care workers. This technology is gaining much importance in the field of medicine recently to supplement human donor organs, to preplan surgical procedures, to produce cost-effective surgical tools, and to improve the lives of those reliant on prosthetic limbs.[2,3] Inexpensive 3D-printed models can also be used as teaching aid-simulating surgical models, which are very useful to impart surgical skills especially for oromaxillary and neurosurgical procedures that involve complex anatomy. They are also used as educative aids to explain the area involved for patients before surgery.[4]

The major advantage of this technology involves manufacturing models that can be patient specific, and it can be customized for transplant, implants, and prosthesis.[5] The 3D printing applications in the coronavirus disease 2019 outbreak help in the development of various stable and compatible masks such as N95, facial shields, coronavirus specimen collection apparatus, valves used for ventilators, fabricated 3D-printed pills, and many more applications.[6]

Despite significant and wide advances in medicine involving 3D printing, notable scientific and regulatory challenges

How to cite this article: Aristotle S, Patil S, Jayakumar S. Dimensional accuracy of medical models of the skull produced by three-dimensional printing technology by advanced morphometric analysis. J Anat Soc India 2022;XX:XX-XX.

Article Info

Received: 07 December 2021
Revised: 30 June 2022
Accepted: 26 July 2022
Available online: ***

Address for correspondence:
Dr. Sharmila Aristotle, Department of Anatomy, SRM Medical College Hospital and Research Center, Kattankulathur - 603 203, Tamil Nadu, India.
E-mail: drsharmiaris@gmail.com

Access this article online

Website: www.jasi.org.in
DOI: 10.4103/jasi.jasi_202_21
Quick Response Code:

remain, demanding the accuracy, reproducibility, and biocompatibility for the usage of 3D-printed models on large scales. Currently, there are no gold standard measurements for the accuracy of medical models. With all these developing technologies, performing manual segmentation of the medical images and the process of conversion of the digital imaging and communications in medicine (DICOM) to standard tessellation language (STL) format demands detailed knowledge of anatomy to avoid a potential source of error.[7] Several parameters such as width of the fused ceramic/polymer filament, layer thickness, placement and direction of the target area, printing speed, and raster angle are required for achieving the desired quality of the product.[8]

Hence, the study was carried out for validating the accuracy of the medical models of the skulls by standardizing the measurements taken from the original cadaver skulls. This study uses fused deposition technique (FDM) for creating the models since this technique is widely used, easily available, and produces cost-effective models.

Material and Methods

The study was approved by the Scientific and the Institutional Ethical Committee with ethical clearance no.: 1162/IEC/2017 of SRM Institute of Science and Technology, Kattankulathur, Chennai.

Study design

Analytical cross-sectional study.

Fabrication of three-dimensional skull

Twenty cadaver skulls with intact measurable areas were procured from the Department of Anatomy, SRM Medical College Hospital and Research Center. The skulls were CT scanned in a 128-slice computed tomography (CT) scanner with a slice thickness of 0.625 mm. The DICOM files were then processed and converted into Standard Tessellation Language (STL) files using the MIMICS v10.0 software (Materialise, Leuven, Belgium). The generated STL files of the 3D model were further cleaned up by CreatWare v 6.4.6, (CreatBot, Zhengzhou city, China), a customized GUI software, and the skull was printed. The material used was polylactic acid (PLA) using the fused deposition modeling (FDM) method.

Fourteen parameters were selected in the posterior cranial base and the middle cranial fossa of the skull. These skeletal landmarks used are highly relevant, clinically based on the literature. The 14 measurements were taken in all three groups of 20 cadaver skulls, 20 CT images, and 20 fused deposition skulls.

The parameter measurements taken in the base of the skull were (1) occipital condyle length for the right and left sides; (2) occipital condyle width for the right and left sides; (3) anterior intercondylar distance; (4) posterior intercondylar distance; (5) anteroposterior diameter of foramen magnum; and (6) transverse diameter of foramen magnum [Figure 1].

The measurements were taken in the cranial fossa: (1) sella turcica; (2) clivus; (3) distance between anterior clinoid processes (ACP); (4) distance between posterior clinoid processes; (5) distance between foramen ovale and apex of the petrous part of the temporal bone on the right side; and (6) distance between foramen ovale and apex of the petrous part of the temporal bone on the left side [Figure 2].

For cadaver skull, and 3 D-printed skulls measurements

High-resolution digital photographs of the cadaver skulls and 3D-printed skull models were taken using a digital camera Nikon D 5600 digital SLR camera. Both the cadaver skulls and printed skulls were calibrated by placing in the same position under a regular grid sheet by drawing a straight line measuring 10 μm as known measurement.

The measurements were taken using the digital image analysis program known as Digimizer Software version 4.3.0. The morphometric measurements obtained in the Digimizer programmer window were taken into database. The mean and standard deviation were obtained for all variables measured.

For computed tomography image measurements

The raw data collected were reformatted in the axial, coronal, and sagittal plane, and then 3D images were created using the Radiant software version 5.5.0. Distance for linear measurement on the CT determined with the internal digital caliper of the workstation was recorded. All the measurements were taken by two independent observers at different intervals for ensuring reliability.

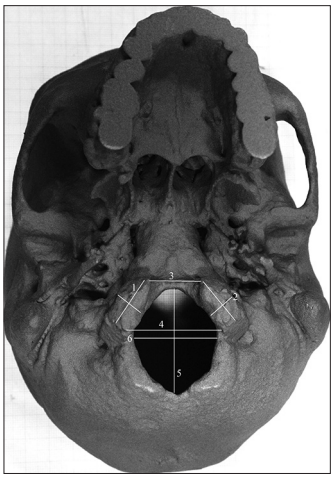

Figure 1: The measurements taken in the base of skull. 1: Occipital condyle length; 2: Occipital condyle width; 3: Anterior intercondylar distance; 4: Posterior intercondylar distance; 5: Anteroposterior diameter of foramen magnum; 6: Transverse diameter of Foramen magnum

Results

Statistical analysis was done using the statistical software package SPSS Statistics for Windows, Version 19.0 Armonk, New York: IBM Corporation and a probability level of $P < 0.05$ was considered statistically significant.

The results are tabulated in Tables 1 and 2. Comparison of means across three groups using analysis of variance showed that there was no statistically significant difference ($P > 0.05$) between the means scores of all three groups across all 14 parameters.

Analysis of the data demonstrated that the morphometric measurement values obtained from 3D print were similar with those obtained from CT scan and cadaver skull, thus proving that the 3D-printed skulls models are accurate replicas of the original skull. To assess the reliability of the independent observers, intraclass correlation coefficient was calculated independently for the cadaver skull, CT, and 3D-printed skull. A high degree of reliability was found between the three groups measured between the two observers [Supplementary Table 1]. To analyze the dimension errors, absolute and relative difference was calculated by comparing the measurements of 3D models with the measurements of cadaver skull and CT measurements. The dimension error measured in terms of absolute and relative difference is summarized in Supplementary Table 2. It is pertinent to point out that the errors between three groups were minimal. The parameters OC-T-R; OC-AP-L; AIC, PIC, FM-AP, Sella turcica, PCP, FO-APT-R, FO-APT-L has least errors, when compared between the 3D skull model and cadaver skull. Whereas, these parameters OC-AP-R; OC-T-L; FM-T-R; clivus and ACP measurements got least error when compared with the CT measurements. Figures 3 and 4 show the absolute and relative error difference of 3D-printed skull in comparison with dry skull (blue bar) and CT skull (orange bar) measurements.

Discussion

Different printing technologies can lead to different manufacturing errors; inaccuracy in any form in worst case may harm the patient and may lead to fatal errors.[9] This study evaluates the accuracy and reliability of FDM skulls, which can be used for clinical practice. Threes groups were compared here to ensure the accuracy of the printed models. Moreover, the morphometric parameters chosen for measurements are highly relevant surgically and begin used in various craniovertebral junction surgeries, transoral, and trans-sphenoidal surgeries. The parameters, which are chosen for measurements to determine the accuracy of the

Table 1: Measurements in base of the skull for all the three groups

Parameter	Mean±SD			*F*	*P*
	Cadaver skull (mm)	CT (mm)	3D skull (mm)		
OC-AP-R	20.327±4.422	20.380±2.286	20.558±2.195	0.03	0.971
OC-T-R	12.470±1.356	12.572±1.229	12.426±1.010	0.08	0.926
OC-AP-L	21.739±3.592	21.580±3.336	21.663±3.270	0.01	0.989
OC-T-L	13.293±2.754	12.839±3.193	12.997±1.285	0.06	0.849
AIC	19.158±4.329	19.025±2.716	19.330±1.781	0.05	0.953
PIC	41.333±4.321	41±3.373	41.7±3.503	0.35	0.705
FM-AP	33.463±3.994	33.420±2.396	33.612±3.734	0.02	0.983
FM-T	27.72±5.43	27.962±1.998	28.455±2.143	0.22	0.801

SD: Standard deviation, CT: Computed tomography, 3D: Three dimensional, OC: Occipital condyles, FM: Foramen magnum, AP: Anteroposterior, T: Transverse diameter, R: Right, L: Left, AIC: Anterior intercondylar distance, PIC: Posterior intercondylar distance

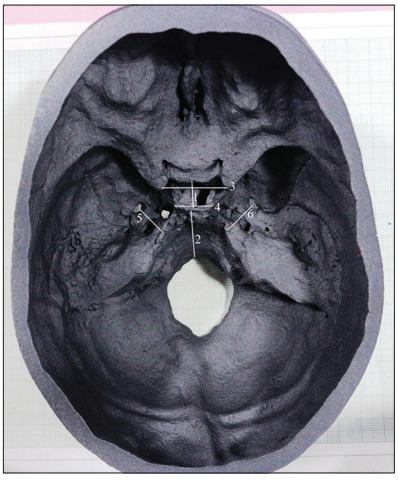

Figure 2: The measurements taken in the cranial fossa. 1: Sella turcica; 2: Clivus; 3: Distance between ACP; 4: Distance between posterior clinoid processes; 5: Distance between foramen ovale and apex of the petrous part of the temporal bone on the right side; 6: Distance between foramen ovale and apex of the petrous part of the temporal bone on the left side. ACP: Anterior clinoid processes

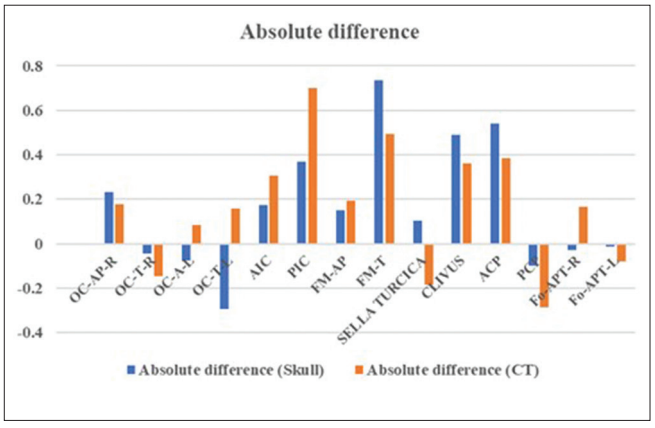

Figure 3: : The absolute difference of 3D-printed skull in comparison with Dry skull(blue bar) and CT skull(orange bar) measurements . CT: Computed tomography, 3D: Three dimensional. OC: Occipital condyles, FM: Foramen magnum, AP: Anteroposterior, T: Transverse diameter, R: Right, L: Left, AIC: Anterior intercondylar distance, PIC: Posterior intercondylar distance, ACP: Anterior clinoid process, PCP: Posterior clinoid process, FO: Foramen ovale, APT: Apex of petrous part of temporal bone

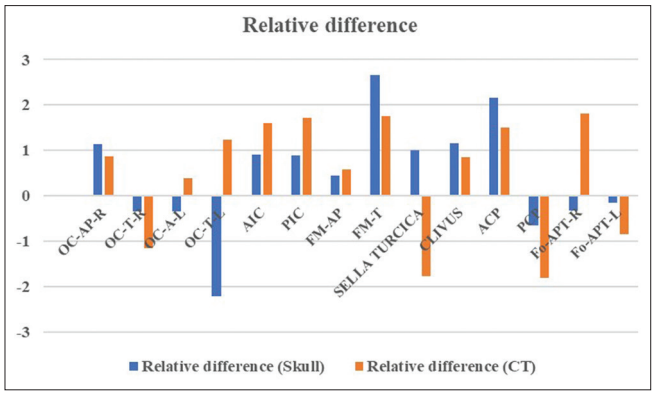

Figure 4: The relative difference of 3D-printed skull in comparison with dry skull(blue bar) and CT skull(orange bar) measurements. CT: Computed tomography, 3D: Three dimensional, OC: Occipital condyles, FM: Foramen magnum, AP: Anteroposterior, T: Transverse diameter, R: Right, L: Left, AIC: Anterior intercondylar distance, PIC: Posterior intercondylar distance, ACP: Anterior clinoid process, PCP: Posterior clinoid process, FO: Foramen ovale, APT: Apex of petrous part of temporal bone

fabricated skulls, are not reported in the literature to the best of our knowledge.

Nizam *et al*. studied the dimensional accuracy of four adult human skull models produced by rapid prototyping technology using stereolithography apparatus; eight linear measurements were measured on each of the original skull and the 3D-printed skull model using an electronic digital caliper and found that the skull models were accurate but with high standard deviation.[10] El-Katatny *et al*. determined the accuracy of skull and mandibular models using FDM and noted an outstanding accuracy using FDM process, which coincides with our study for accuracy with FDM skulls.[11] Huotilainen *et al*. who compared physical medical skull models fabricated at three different institutes from an identical DICOM data set showed a large variation in dimensions of the physical skull models.[7]

Inaccuracy in dimensional values of 3D-printed anatomical mandibular models using five different printing technology, which can be utilized for clinical purposes, was determined by Msallem *et al*.[9] However, Ibrahim *et al*. mandibular models showed greater dimensional accuracy details, which can reproduce more accurately in selective laser sintering (SLS) than polyjet and 3D-printing.[12]

Therapeutic methods of craniofacial bone repair were studied in a systematic review of about 43 relevant clinical trials and case series including human and animal studies of about 81 patients for short- and long-term effectiveness of 3D printing strategies for skull bone repair by Maroulakos *et al*.[13]

Accuracy of skull models for craniofacial skeleton repair by SL technology produces accurate results; however, midface parameters in the maxilla were prone to more error than those of other regions of skulls due to thin bony walls.[14] For structures, demanding higher accuracy

Table 2: Measurements in cranial fossa of all the three groups

Parameters	Mean±SD			*F*	*P*
	Cadaver skull (mm)	CT (mm)	3D skull (mm)		
Sella Turcica	10.123±1.802	10.41±2.120	10.225±1.625	0.46	0.633
Clivus	42.002±1.271	42.13±4.76	42.490±4.087	0.09	0.911
ACP	25.176±1.922	25.335±1.14	25.718±3.655	0.25	0.777
PCP	15.581±1.465	15.765±2.320	15.480±2.010	0.11	0.898
FO-APT-R	9.345±2.414	9.1±1.649	9.315±1.584	0.28	0.760
FO-APT-L	9.390±3.115	9.455±2.22	9.375±2.434	0.01	0.995

SD: Standard deviation, ACP: Anterior clinoid process, PCP: Posterior clinoid process, FO: Foramen ovale, APT: Apex of petrous part of temporal bone, R: Right, L: Left

improvement can be achieved by utilizing smaller pixel resolution in the CT images. SLA models can be utilized in any complex surgeries for preoperative surgical planning.[15]

Brouwers *et al*. validated the 3D-printed anatomical models using two PLA printers. Nine anatomic specimens were chosen including three pelvis, three hands, and three feet. The replicated models were compared with that of original specimens. They found that the printed models were accurate in both printers.[16] Brown *et al*. used digital light processing and polyjet printing techniques for determining the accuracy of the scaffolds in dental models and reported that both printers produced clinically acceptable models with high accuracy.[17] However, high accuracy was noted in SLS printer with a similar study done for determining the accuracy in 10-tooth replica models. Armin Andreas Sokolowski *et al*. and Ibrahim *et al*.'s mandibular models also showed high validated anatomical details, using SLS and polyjet when compared to 3D-printing.[12,18]

Various scholars have determined the accuracy of the fabricated models based on various software used for printing and even the accuracy was identified for the printing direction used. Gendviliene *et al*. assessed the morphology and dimensional accuracy of 3D-printed models using different synthetic materials used for printing, with a similar study of Anthony Tahayeri *et al*.[19,20] Antonino Lo Giudice *et al*. evaluated the accuracy of the printed mandible in four different types of software for the semiautomatic segmentation and compared with manual segmentation.[21] Zhang *et al*. studied the influence of the 3D printing technique and different printing layer thicknesses on dental models.[22]

An inaccurate 3D-printed model can result in inappropriate surgical outcome, leading to severe consequences for both the patient and surgeons. However, accuracy and reliability are currently mentioned in only a small number of literature, and errors can occur during any time of the process like imaging, segmentation, postprocessing, and 3D printing steps. Accuracy has to be verified and validated

in areas involving thin bones, small foramina, and some acute bony tubercles and landmarks of the skull.[23] A mean variation of ±0.5% for the size of 100 mm is considered as a negligible error and the accuracy of the 3D model is acceptable for clinical purposes.[10]

Conclusion

To produce an accurate and error-free biomodel, the factors determining the accuracy should be kept in mind before printing. The major component of human error of accuracy is the nature of the anatomical structure of interest, defining the exact location of the anatomical landmarks placed to be captured by the CT scanner. This study measured various clinically relevant parameters and noted that the 3D-printed models are accurate and reliable.

Financial support and sponsorship

Nil.

Conflicts of interest

There are no conflicts of interest.

References

1. Abdulhameed O, Al-Ahmari A, Ameen W, Mian SH. Additive manufacturing: Challenges, trends, and applications. Adv Mech Eng 2019;11:1-27.
2. Ventola CL. Medical applications for 3D printing: Current and projected uses. *P* T 2014;39:704-11.
3. Paulsen SJ, Miller JS. Tissue vascularization through 3D printing: Will technology bring us flow? Dev Dyn 2015;244:629-40.
4. Werz SM, Zeichner SJ, Berg BI, Zeilhofer HF, Thieringer F. 3D Printed Surgical Simulation Models as educational tool by maxillofacial surgeons. Eur J Dent Educ 2018;22:e500-5.
5. Yan Q, Dong H, Su J, Han J, Song B, Wei Q, *et al*. A review of 3D printing technology for medical applications. Engineering 2018;4:729-42.
6. Ishack S, Lipner SR. Applications of 3D printing technology to address COVID-19-related supply shortages. Am J Med 2020;133:771-3.
7. Huotilainen E, Jaanimets R, Valášek J, Marcián P, Salmi M, Tuomi J, *et al.* Inaccuracies in additive manufactured medical skull models caused by the DICOM to STL conversion process. J Craniomaxillofac Surg 2014;42:e259-65.
8. Han Y, Wei Q, Chang P, Hu K, Okoro OV, Shavandi A, *et al*. Three-dimensional printing of hydroxyapatite composites for biomedical application. Crystals 2021;11:353.
9. Msallem B, Sharma N, Cao S, Halbeisen FS, Zeilhofer HF, Thieringer FM. Evaluation of the dimensional accuracy of 3D-printed anatomical mandibular models using FFF, SLA, SLS, MJ, and BJ printing technology. J Clin Med 2020;9:817.
10. Nizam A, Gopal R, Naing L, Hakim AB, Samsudin AR. Dimensional accuracy of the skull models produced by rapid prototyping technology using stereolithography apparatus. Arch Orofac Sci 2006;1:60-6.
11. El-Katatny I, Masood SH, Morsi YS. Error analysis of FDM fabricated medical replicas. Rapid Prototyp J 2010;16:36-43.
12. Ibrahim D, Broilo TL, Heitz C, de Oliveira MG, de Oliveira HW, Nobre SM, *et al.* Dimensional error of selective laser sintering, three-dimensional printing and PolyJet models in the reproduction of mandibular anatomy. J Craniomaxillofac Surg 2009;37:167-73.
13. Maroulakos M, Kamperos G, Tayebi L, Halazonetis D, Ren Y. Applications of 3D printing on craniofacial bone repair: A systematic review. J Dent 2019;80:1-14.
14. Chang PS, Parker TH, Patrick CW Jr., Miller MJ. The accuracy of stereolithography in planning craniofacial bone replacement. J Craniofac Surg 2003;14:164-70.
15. Barker TM, Earwaker WJ, Lisle DA. Accuracy of stereolithographic models of human anatomy. Australas Radiol 1994;38:106-11.
16. Brouwers L, Teutelink A, van Tilborg FA, de Jongh MA, Lansink KW, Bemelman M. Validation study of 3D-printed anatomical models using 2 PLA printers for preoperative planning in trauma surgery, a human cadaver study. Eur J Trauma Emerg Surg 2019;45:1013-20.
17. Brown GB, Currier GF, Kadioglu O, Kierl JP. Accuracy of 3-dimensional printed dental models reconstructed from digital intraoral impressions. Am J Orthod Dentofacial Orthop 2018;154:733-9.
18. Sokolowski AA, Sokolowski AA, Kammerhofer J, Madreiter-Sokolowski CT, Payer M, Koller M, *et al.* Accuracy assessment of 3D-printed tooth replicas. Int J Comput Dent 2019;22:321-9.
19. Gendviliene I, Simoliunas E, Rekstyte S, Malinauskas M, Zaleckas L, Jegelevicius D, *et al.* Assessment of the morphology and dimensional accuracy of 3D printed PLA and PLA/HAp scaffolds. J Mech Behav Biomed Mater 2020;104:103616.
20. Tahayeri A, Morgan M, Fugolin AP, Bompolaki D, Athirasala A, Pfeifer CS, *et al.* 3D printed versus conventionally cured provisional crown and bridge dental materials. Dent Mater 2018;34:192-200.
21. Lo Giudice A, Ronsivalle V, Grippaudo C, Lucchese A, Muraglie S, Lagravère MO, *et al.* One step before 3D printing-evaluation of imaging software accuracy for 3-dimensional analysis of the mandible: A comparative study using a surface-to-surface matching technique. Materials (Basel) 2020;13:2798.
22. Zhang ZC, Li PL, Chu FT, Shen G. Influence of the three-dimensional printing technique and printing layer thickness on model accuracy. J Orofac Orthop 2019;80:194-204.
23. Silva DN, Gerhardt de Oliveira M, Meurer E, Meurer MI, Lopes da Silva JV, Santa-Bárbara A. Dimensional error in selective laser sintering and 3D-printing of models for craniomaxillary anatomy reconstruction. J Craniomaxillofac Surg 2008;36:443-9.

Supplementary Table 1: Intraclass correlation coefficient for the three groups

Parameter	Intraclass correlation	95% CI		Value	*P*
		Lower bound	Upper bound		
CT					
OC-AP-R	0.999	0.999	1.00	1985.24	0.000
OC-T-R	0.998	0.996	0.999	573.75	0.000
OC-AP-L	1.000	1.000	1.000	-	0.000
OC-T-L	1.000	1.000	1.000	-	0.000
AIC	0.998	0.996	0.999	31,136.11	0.000
PIC	1.000	1.000	1.000	33,898.25	0.000
FM-AP	1.000	1.000	1.000	13,630.25	0.000
FM-T	1.000	1.000	1.000	8093.8	0.000
Sella turcica	1.000	1.000	1.000	10,672.43	0.000
Clivus	1.000	1.000	1.000	-	0.000
ACP	1.000	1.000	1.000	-	0.000
PCP	1.000	1.000	1.000	12,780.68	0.000
FO-APT-R	1.000	1.000	1.000	6457.25	0.000
FO-APT-L	1.000	1.000	1.000	4593.39	0.000
Cadaver skull					
OC-AP-R	1.000	1.000	1.000	64,438.03	0.000
OC-T-R	0.990	0.974	0.996	98.35	0.000
OC-AP-L	1.000	1.000	1.000	5607.08	0.000
OC-T-L	1.000	1.000	1.000	-	0.000
AIC	1.000	1.000	1.000	33,755.67	0.000
PIC	1.000	1.000	1.000	34,208.40	0.000
FM-AP	1.000	1.000	1.000	17,706.93	0.000
FM-T	1.000	1.000	1.000	63,144.55	0.000
Sella turcica	1.000	1.000	1.000	-	0.000
Clivus	1.000	0.999	1.000	4501.09	0.000
ACP	1.000	0.999	1.000	4626.31	0.000
PCP	1.000	0.999	1.000	3860.46	0.000
FO-APT-R	1.000	1.000	1.000	6733.68	0.000
FO-APT-L	1.000	1.000	1.000	36,549.9	0.000
3D skull					
OC-AP-R	0.906	0.763	0.963	10.647	0.000
OC-T-R	1.000	1.000	1.000	-	0.000
OC-AP-L	1.000	1.000	1.000	21,667.13	0.000
OC-T-L	1.000	1.000	1.000	-	0.000
AIC	1.000	1.000	1.000	7530.25	0.000
PIC	1.000	1.000	1.000	25,413.28	0.000
FM-AP	1.000	1.000	1.000	41,555.98	0.000
FM-TR	1.000	1.000	1.000	10,909.93	0.000
SELLA TURCICA	1.000	1.000	1.000	-	0.000
Clivus	0.999	0.998	1.000	1111.69	0.000
ACP	1.000	1.000	1.000	27,071.08	0.000
PCP	1.000	1.000	1.000	9592.75	0.000
FO-APT-R	1.000	1.000	1.000	5958.18	0.000
FO-APT-L	1.000	1.000	1.000	14,065.93	0.000

CI: Confidence interval, CT: Computed tomography, OC: Occipital condyles, FM: Foramen magnum, AP: Anteroposterior, T: Transverse diameter, R: Right, L: Left, AIC: Anterior intercondylar distance, PIC: Posterior intercondylar distance, ACP: Anterior clinoid process, PCP: Posterior clinoid process, FO: Foramen ovale, APT: Apex of petrous part of temporal bone, 3D: Three dimensional

Supplementary Table 2: Measurement of dimension error in terms of absolute and relative difference

Parameter	Mean±SD			Absolute difference (skull)-mm	Absolute difference (CT)-mm	Relative difference (skull) (%)	Relative difference (CT) (%)
	Cadaver skull	CT	3D skull				
OC-AP-R	20.327	20.38	20.558	0.231	0.178	1.13642	0.873405
OC-T-R	12.47	12.572	12.426	−0.044	−0.146	−0.35285	−1.16131
OC-AP-L	21.739	21.58	21.663	−0.076	0.083	−0.3496	0.384615
OC-T-L	13.293	12.839	12.997	−0.296	0.158	−2.22674	1.230625
AIC	19.158	19.025	19.33	0.172	0.305	0.897797	1.603154
PIC	41.333	41	41.7	0.367	0.7	0.88791	1.707317
FM-AP	33.463	33.42	33.612	0.149	0.192	0.445268	0.574506
FM-T	27.72	27.962	28.455	0.735	0.493	2.651515	1.763107
Sella turcica	10.123	10.41	10.225	0.102	−0.185	1.007606	−1.77714
Clivus	42.002	42.13	42.49	0.488	0.36	1.161849	0.854498
ACP	25.176	25.335	25.718	0.542	0.383	2.152844	1.511743
PCP	15.581	15.765	15.48	−0.101	−0.285	−0.64823	−1.8078
FO-APT-R	9.345	8.94	9.315	−0.03	0.165	−0.32103	1.803279
FO-APT-L	9.39	9.455	9.375	−0.015	−0.08	−0.15974	−0.84611

The interobserver reliability between two independent observers were measured for each of the 14 parameters separately in each group, viz, dry skull, CT, and 3D model group. This is summarized in Supplementary Table 2 and as evident from it, all parameters had high interobserver reliability in all three groups for each of the 14 parameters that were measured (P<0.000). OC: Occipital condyles, FM: Foramen magnum, AP: Anteroposterior, T: Transverse diameter, R: Right, L: Left, AIC: Anterior intercondylar distance, PIC: Posterior intercondylar distance, ACP: Anterior clinoid process, PCP: Posterior clinoid process, FO: Foramen ovale, APT: Apex of petrous part of temporal bone, CT: Computed tomography, SD: Standard deviation, 3D: Three dimensional

Original Article

Gender Prediction with the Parameters Obtained from Pelvis Computed Tomography Images and Machine Learning Algorithms

Yusuf Secgin, Zulal Oner[1], Muhammed Kamil Turan[2], Serkan Oner[3]

Department of Anatomy, Faculty of Medicine, Karabük University, Karabük, [1]Department of Anatomy, Faculty of Medicine, İzmir Bakırçay University, İzmir, [2]Department of Medical Biology, Faculty of Medicine, Karabük University, Karabük, [3]Department of Radiology, Faculty of Medicine, İzmir Bakırçay University, İzmir, Turkey

Abstract

Introduction: In the skeletal system, the most dimorphic bones employed for postmortem gender prediction include the bones in the pelvic skeleton. Bone measurements are usually conducted with cadaver bones. Computed tomography (CT) is an increasingly popular method due to its ease of use, reconstruction opportunities, and lower impact of age bias and provides a modern data source. Even when parameters obtained with different or same bones are missing, machine learning (ML) algorithms allow the use of statistical methods to predict gender. This study was carried out in order to obtain high accuracy in estimating gender with the pelvis skeleton by integrating ML algorithms, which are used extensively in the field of engineering, in the field of health. **Material and Methods:** In the present study, pelvic CT images of 300 healthy individuals (150 females, 150 males) between the ages of 25 and 50 (the mean female age = 40, the mean male age = 37) were transformed into orthogonal images, and landmarks were placed on promontory, iliac crest, sacroiliac joint, anterior superior iliac spine, anterior inferior iliac spine, terminal line, obturator foramen, greater trochanter, lesser trochanter, femoral head, femoral neck, body of femur, ischial tuberosity, acetabulum, and pubic symphysis, and coordinates of these regions were obtained. Four groups were formed based on various angle and length combinations obtained from these coordinates. These four groups were analyzed with ML algorithms such as Logistic Regression, Linear Discriminant Analysis (LDA), Random Forest, Extra Trees Classifier, and ADA Boost Classifier. **Results:** In the analysis, it was determined that the highest accuracy was 0.96 (sensitivity 0.95, specificity 0.97, Matthew's Correlation Coefficient 0.93) with LDA. **Discussion and Conclusion:** The use of length and angle measurements obtained from the pelvis showed that the LDA model was effective in estimating gender.

Keywords: *Computed tomography, gender prediction, machine learning algorithms, pelvis*

Introduction

Gender prediction is the foundation of forensic science and anthropology. Gender prediction is the first step in identity determination, including factors such as age, height, weight, etc.[1] Gender could be predicted with osteometry, odontometrics, and DNA analysis. DNA analysis is expensive and not commonly available and requires qualified staff. Furthermore, osteometry is a reliable, preferred, inexpensive, and highly accessible method that provides fast results, and does not require qualified staff.[2]

Almost all parts of the human skeleton have been studied for gender prediction, and it was observed that the most dimorphic region was the pelvic skeleton and cranium.[3,4] Certain studies reported that the pelvic skeleton was more dimorphic than the cranium.[5] One of the key factors that led to the determination of the pelvis skeleton as the most dimorphic region was the impact of sex hormones (estrogen and androgen) on the human skeleton. Sex hormones affect the pelvic skeleton the most. Because estrogen leads a female pelvis suitable for birth, androgen leads to one that could support the muscle mass and tonus in men.[3]

Multidetector computed tomography (MDCT) is a modern imaging method that could distinct bone tissue and other tissues. Thin section images lead to the determination of 3-dimensional image direction and the image could be positioned vertically. This feature allows the determination of a more realistic coordinate, angle, and length.[2] Computed tomography (CT) is preferred in postmortem cases with

How to cite this article: Secgin Y, Oner Z, Turan MK, Oner S. Gender prediction with the parameters obtained from pelvis computed tomography images and machine learning algorithms. J Anat Soc India 2022;XX:XX-XX.

Article Info

Received: 30 December 2020
Revised: 06 June 2022
Accepted: 09 June 2022
Available online: ***

Address for correspondence:
Dr. Zulal Oner, Department of Anatomy, Faculty of Medicine, İzmir Bakırçay University, İzmir, Turkey.
E-mail: zulal.oner@bakircay.edu.tr

Access this article online

Website: www.jasi.org.in
DOI: 10.4103/jasi.jasi_280_20
Quick Response Code:

soft tissue loss or partial bone deformities since it allows easy, fast, and low-cost reconstruction.[6]

There are three machine learning (ML) algorithm types. The first is the controlled type that models the correlations between the inputs and outputs, the second lass is the uncontrolled type that can provide outputs based on previously unknown data, and the third is the amplified type that matches the inputs with the desired outputs.[7] The present study aimed to obtain accurate results based on various pelvic skeleton parameters with ML algorithms that offer new horizons in the field of medicine.

Material and Methods

This section includes details on image sample sources, image transformation to the orthogonal plane, the collection of the parameters, and employed ML algorithms.

Image samples

The present study was approved by the ethics committee decision no: 6/23. In the present retrospective study, pelvic CT images of 300 randomly selected individuals (150 females, 150 males), who were admitted to the hospital with various indications and without pelvic skeleton fracture or any related pathology were employed. The mean female participant age was 40 and the mean male participant age was 37. The Anderson-Darling normality test was used to determine whether the participant age exhibited normal distribution, and it was determined that the participant age did not exhibit a normal distribution. A significant difference was found between participant age with the Mann–Whitney U-test ($P \leq 0.001$).

Multidetector computed tomography protocol

The supine pelvic CT images were taken with a 16-row MDCT scanner (Aquilion 16; Toshiba Medical Systems, Otawara, Japan) with a section thickness of 5 mm. Scanning protocol values were as follows: tube voltage: 120 kV, gantry rotation: 0.75 s, and pitch: 1.0 mm.

Image Analysis

The pelvic CT images were recorded on Horos Medical Image Viewer 3.0 (United States) software in Digital Imaging and Communications in Medicine format. Three dimensional Curved Multiplanar Reconstruction was conducted on the recorded images to obtain 3-planar images (coronal, sagittal, transversal). All images were transformed into an orthogonal plane by matching the coronal, sagittal, and transversal image series and the promontory plane. All sections transformed into the orthogonal plane were superimposed with Horos software to obtain a single image [Figure 1].

Landmarks were placed on orthogonal pelvic CT image promontory, iliac crest, sacroiliac joint, anterior superior iliac spine, anterior inferior iliac spine, terminal line, obturator foramen (for), greater trochanter, lesser trochanter, femoral head, femoral neck, body of femur, ischial tuberosity, acetabulum, and pubic symphysis to obtain the coordinates for these anatomic locations [Figure 2].

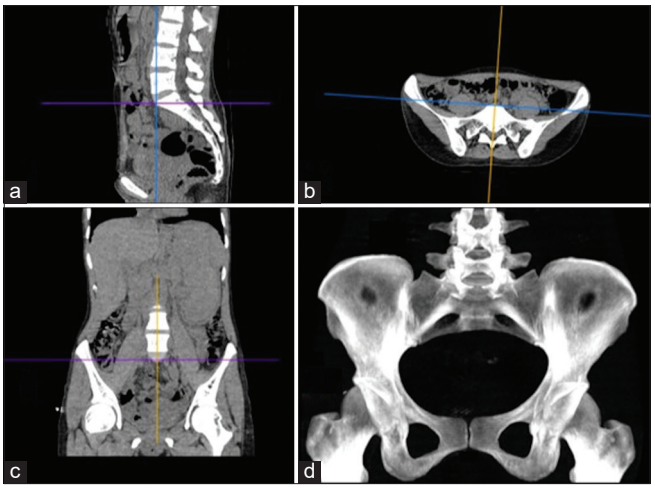

Figure 1: (a) The transversal image in orthogonal form, (b) The sagittal image in orthogonal form, (c) Coronal image in the orthogonal form (d) Superposed image

These coordinates were transferred to a graphics software developed by Karabük University faculty members in Medical Biology, Anatomy, Radiology departments called Sekazu (Version 3.0, Karabük, Turkey) which could calculate mathematical concepts such as length, angle, and area automatically and could analyze gender prediction with ML algorithm.

Four groups were formed based on the mathematical units such as length and angle and the transferred coordinates. The determining lengths and angles are presented in Table 1.

Various ML algorithms (Linear Discriminant Analysis [LDA], Random Forest [RF], Logistic Regression [LR], Extra Trees Classifier [ETC], ADA Boost Classifier [ADA]) were applied to the above-mentioned mathematical elements and the groups with an accuracy (ACC) of 90% or over were selected. The ACC of the groups that were not selected was between 80 and 90%. The 4 groups created based on the determined angles and lengths are presented in Table 2.

Machine learning algorithms

The RF algorithm, which is fast and load resistant, was introduced by Brierman in 2001 and is a community learning algorithm that collects the decisions of several independent multivariate trees.[8]

The LR algorithm is employed to reveal the unique effect of one or more independent variables on the result. Due to its ability to predict the outcome and to reveal the unique effect of each data on the result, it is preferred in medical research.[9]

Table 1: Mathematical elements based on the coordinates

Abbreviation	Parameter
Length 1	Right iliac crest – Left iliac crest
Length 2	Right iliac crest – Promontory
Length 3	Left iliac crest – Promontory
Length 4	Pubic symphysis superior – Promontory
Length 5	Pubic symphysis inferior – Promontory
Length 6	Right terminal line – Promontory
Length 7	Left terminal line – Promontory
Length 8	Right sacroiliac joint – Left terminal line
Length 9	Left sacroiliac joint – Right terminal line
Length 10	Right ASIS – Left ASIS
Length 11	Right AIIS – Left AIIS
Length 12	Right terminal line – Left terminal line
Length 13	Right greater trochanter – Left greater trochanter
Length 14	Right lesser trochanter – Left lesser trochanter
Length 15	Right ischial tuberosity – Left ischial tuberosity
Length 16	Right acetabulum superior – Right acetabulum inferior
Length 17	Left acetabulum superior – Left acetabulum inferior
Length 18	Right sacroiliac joint – Left sacroiliac joint
Length 19	Right femoral head – Left femoral head
Length 20	Right obturator foramen superior – Left obturator foramen superior
Length 21	Right obturator foramen inferior – Left obturator foramen inferior
Length 22	Right obturator foramen superior – Right obturator foramen inferior
Length 23	Left obturator foramen superior – Left obturator foramen inferior
Length 24	Pubic symphysis superior – Pubic symphysis inferior
Length 25	Right acetabulum superior – Left acetabulum superior
Length 26	Right acetabulum inferior – Left acetabulum inferior
Length 27	Right sacroiliac joint – Pubic symphysis superior
Length 28	Right sacroiliac joint – Pubic symphysis inferior
Length 29	Left sacroiliac joint – Pubic symphysis superior
Length 30	Left sacroiliac joint – Pubic symphysis inferior
Length 31	Right femoral neck – Left femoral neck
Length 32	Right body of femur – Left body of femur
Length 33	Promontory – Right femoral head
Length 34	Promontory – Left femoral head
Angle 35	Right iliac crest – Promontory – Left iliac crest
Angle 36	Right terminal line – Promontory – Left terminal line
Angle 37	Right ischial tuberosity – Pubic symphysis inferior – Left ischial tuberosity
Angle 38	Right femoral head – Right femoral neck – Right body of femur
Angle 39	Left femoral head – Left femoral neck – Left body of femur
Angle 40	Right obturator foramen superior – Promontory – Left obturator foramen
Angle 41	Right terminal line – Pubic symphysis superior – Left terminal line
Angle 42	Right femoral head – Promontory – Left femoral head

ASIS: Anterior superior iliac spine, AIIS: Anterior inferior iliac spine

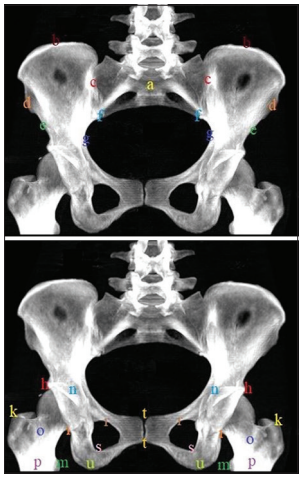

Figure 2: (a) promontory, (b) iliac crest, (c) sacroiliac joint, (d) anterior superior iliac spine, (e) anterior inferior iliac spine, (f) sacroiliac joint lower end, (g) terminal line, (h) acetabulum upper end, (i) acetabulum lower end, (k) greater trochanter, (n) femoral head, (o) femoral neck, (p) body of femur, (r) obturator foramen upper end, (s) obturator foramen lower end, (u) ischial tuberosity, (t) pubic symphysis, (m) lesser trochanter

The LDA is an analysis method commonly used by anthropologists, which could discriminate various classes, is easy to access and implement, and could categorize new classes based on the input data.[10,11]

Although the ETC algorithm is similar to RF, it is a proven method when compared to RF due to stronger variance. There are two important differences between ETC and RF; it employs all data in the training series, and the nodes are randomly divided.[12]

ADA is a high-result method that provides strong classifier algorithms by integrating weak classifier algorithms that are proven to yield stronger results.[13]

The results were obtained by applying ML algorithms to the 4 groups.

Performance criteria

These included accuracy (Acc), sensitivity (Sen), specificity (Spe), F1, and Matthews Correlation Coefficient (Mcc) obtained with the confusion matrix.

$$\text{Acc} = \frac{\text{TP}}{\text{TP} + \text{FN} + \text{FP} + \text{TN}}$$

$$\text{Sen} = \frac{\text{TP}}{\text{TP} + \text{FN}}$$

$$Spe = \frac{TN}{TN + FP}$$

$$Mcc = \frac{TP \times TN - FP \times FN}{\sqrt{(TP + FP) \times (TP + FN) \times (TN + FP) \times (TN + FN)}}$$

$$F1 = 2\frac{Specificity \times Sensitivity}{Specificity + Sensitivity}$$

Equation 1. (TP: True positive, TN: True negative, FP: False positive, FN; False negative).

Results

In the present study, 5 ML algorithms were applied separately to 4 groups, and Acc, Spe, Sen, Mcc were obtained [Tables 3-6]. The highest Acc was 0.96 determined with the LDA algorithm applied to the first group. The mean Acc obtained with 5 ML algorithms applied to the four groups was 0.91. The highest Sen was 0.96 with the ADA algorithm applied to the first and second groups. The mean Sen obtained with 5 ML algorithms applied to the four groups was 0.91. The highest Spe was 0.97 obtained with the LDA algorithm applied to the first and second groups. The mean Spe obtained with 5 ML algorithms applied to four groups was 0.91. The highest Mcc was 0.97 obtained with the LDA algorithm applied to the first group. The mean Mcc obtained with 5 ML algorithms applied to four groups was 0.91.

Discussion

Gender prediction determined with all or certain sections of the skeletal system is the first step in anthropological studies. Employment of the entire skeletal system often provides clear and accurate results; however, it is possible to achieve accurate results with a section of the skeletal system.[14] In the present study, a gender prediction test was conducted with an ML algorithm on CT images of 150 female and 150 male subjects without a pelvic skeleton pathology. The highest Acc was 0.96 with the LDA algorithm applied to the 1st group, and the highest Mcc was 0.97 with the LDA algorithm applied to the 1st group.

One of the key differences in the present study was the determination of the desired combinations of angles and lengths by placing landmarks on the pelvic skeleton. Thus, landmarks were placed on 35 anatomical locations on the pelvic skeleton and 34 lengths and 8 angles were obtained. In the literature review, it was observed that the highest number of parameters or angles and lengths were employed in the present study. d'Oliveira Coelho and Curate employed subpubic angle, pelvic height, and bispiniatic width, Pretorius *et al*. employed sciatic notch, Savall *et al*. employed 17 anatomical points on the os coxae, Blake *et al*. employed 10 anatomical locations on the pubis, Bonczarowska *et al*. employed various anatomical points on the ilium in gender prediction.[15-19] The present

Table 2: The groups developed to apply the algorithms

Groups	Parameters
Group 1	Angle 35 – 42, Length 2 – 7, Length 10 – 17, Length 19 – 23, Length 31 – 34
Group 2	Angle 35 – 42, Length 2 – 7, Length 10 – 17, Length 19 – 23, Length 26 – 29, Length 31 – 34
Group 3	Length 1 – 34
Group 4	Angle 35 – 42

Table 3: Group accuracy rates

Machine learning algorithm	Group 1	Group 2	Group 3	Group 4
LDA	0.96	0.95	0.93	0.92
LR	0.89	0.89	0.92	0.90
ADA	0.94	0.94	0.86	0.92
RF	0.92	0.89	0.87	0.90
ETC	0.90	0.93	0.88	0.91

LDA: Linear discriminant analysis, LR: Logistic regression, RF: Random forest, ETC: Extra trees classifier, ADA: ADA boost classifier

Table 4: Group sensitivity rates

Machine learning algorithm	Group 1	Group 2	Group 3	Group 4
LDA	0.95	0.93	0.91	0.89
LR	0.87	0.87	0.89	0.87
ADA	0.96	0.96	0.85	0.89
RF	0.93	0.89	0.87	0.94
ETC	0.94	0.96	0.87	0.91

LDA: Linear discriminant analysis, LR: Logistic regression, RF: Random forest, ETC: Extra trees classifier, ADA: ADA boost classifier

Table 5: Group spesificity rates

Machine learning algorithm	Group 1	Group 2	Group 3	Group 4
LDA	0.97	0.97	0.95	0.95
LR	0.91	0.91	0.95	0.84
ADA	0.93	0.93	0.88	0.95
RF	0.90	0.88	0.87	0.86
ETC	0.86	0.91	0.88	0.94

LDA: Linear discriminant analysis, LR: Logistic regression, RF: Random forest, ETC: Extra trees classifier, ADA: ADA boost classifier

Table 6: Group Matthew's correlation coefficient rates

Machine learning algorithm	Group 1	Group 2	Group 3	Group 4
LDA	0.97	0.96	0.93	0.92
LR	0.89	0.89	0.92	0.90
ADA	0.94	0.94	0.87	0.92
RF	0.92	0.89	0.87	0.90
ETC	0.80	0.93	0.88	0.90

LDA: Linear discriminant analysis, LR: Logistic regression, RF: Random forest, ETC: Extra trees classifier, ADA: ADA boost classifier

study employed the pelvis skeleton as a whole based on the lengths and angles obtained with the landmarks and contributed to the literature with a holistic approach.

In the present study, osteometry measurements were conducted on CT images instead of the measurements with conventional osteometry devices (calipers, odontometers, digital distance meters) employed for gender prediction. CT was preferred since it is a sensitive, modern method that is not affected by orientation and allows images to be transformed into the orthogonal form and reconstructed. CT imaging allowed the reconstruction of each bone section, providing an advantage in the measurement of missing and damaged sections.[2,10]

The literature review demonstrated that orthogonalization was used in a few studies. In their study on the sternum, Oner *et al*. orthogonalized the sternum based on the T4 vertebra. In the present study, the images were superimposed and orthogonalized based on the promontory point on the pelvis skeleton. Thus, the images were not affected by orientation, and accurate and clear findings were obtained.[2]

Instead of conventional simple and advanced statistical methods, ML algorithms with higher reliability and accuracy were preferred. The literature review demonstrated that d'Oliveira Coelho and Curate reported 0.86 Acc for the pelvic skeleton with the RF algorithm.[17] In the present study, the RF algorithm revealed 0.92 Acc in the first group. In a study conducted on French, American, Thai, and Portuguese cranium bones, Santos *et al*. reported an Acc of 0.80 with LDA and LR algorithms.[20] In their study conducted on femoris, Curate *et al*. reported 0.85.5–92.5 Acc with LDA and 0.84–91 with LR.[11] In a study conducted on tarsal bones from the Coimbra skeleton collection, Navega *et al*. reported 0.86 Acc with LDA and LR.[21] In the present study, it was determined that Acc was 0.96 with the LDA algorithm in the first group, and 0.92 with the LR algorithm in the third group. In a study conducted on maxilla Akkoç *et al*. reported 0.90 Acc with RF algorithm.[22] In the present study, 0.92 Acc was determined with the RF algorithm in the first group. Based on previous study findings in the literature, this demonstrated that the pelvic skeleton was more dimorphic when compared to other bones.[3,4]

The literature review revealed that the research samples employed in gender prediction with ML algorithms were smaller than the present study. The sample size was 40 in Akkoç *et al*., 194 in Bonczarowska *et al*., 113 in Savall *et al*., and 256 in d'Oliveira Coelho and Curate.[16,17,19,22] The higher sample size in the present study and the employment of the ML algorithm significantly improved the performance criteria.

Mcc is a performance criterion that varies between −1 and +1. An Mcc of-1 indicates that all the classes are inversely predicted, an Mcc of 0 indicates that the results are random, and an Mcc of + 1 indicates that there is no error in the prediction. In the present study, an alternative Mcc was used to analyze Acc, Spe, and Sen, meaning that the reliability and accuracy were tested by various methods and reliable results were obtained in the study.[14]

The literature review demonstrated that gender prediction was never conducted with ETC and ADA algorithms before. In the present study, 0.93 Acc was obtained with the ETC algorithm in the second group, and 0.94 Acc was obtained with the ADA algorithm in the first and second groups. Thus, the present study employed an ML algorithm that was never used before, and it was demonstrated that it provided better results when compared to frequently used ML algorithms and other algorithms.

The measurements were performed on a specific population sample. For this reason, it may be more valuable to present data specific to each population. The fact that the measurements are repeated at different times and the images are brought to the orthogonal plane minimizes measurement errors. In our study, attention has been paid to these features to eliminate measurement errors. This can also be considered the strong side of our work.

Conclusion

According to the literature, high accuracy was obtained as a result of gender estimation with traditional osteometric measurements and basic statistics with modern imaging technologies and software-based ML algorithms. As seen in this study, the obtained accuracy rate increased up to 0.96. We believe that increasing the number of parameters will further increase the accuracy rate.

Financial support and sponsorship

Nil.

Conflicts of interest

There are no conflicts of interest.

References

1. Colman KL, van der Merwe AE, Stull KE, Dobbe JG, Streekstra GJ, van Rijn RR, *et al.* The accuracy of 3D virtual bone models of the pelvis for morphological sex estimation. Int J Legal Med 2019;133:1853-60.
2. Oner Z, Turan MK, Oner S, Secgin Y, Sahin B. Sex estimation using sternum part lenghts by means of artificial neural networks. Forensic Sci Int 2019;301:6-11.
3. Best KC, Garvin HM, Cabo LL. An investigation into the relationship between human cranial and pelvic sexual dimorphism. J Forensic Sci 2018;63:990-1000.
4. Spradley MK, Jantz RL. Sex estimation in forensic anthropology: Skull versus postcranial elements. J Forensic Sci 2011;56:289-96.
5. Pickering RB, Bachman DC. The Use of Forensic Anthropology. England: CRC Press; 1997.
6. Ali Z, Cox C, Stock MK, Zandee vanRilland EE, Rubio A, Fowler DR. Estimating sex using metric analysis of the

scapula by postmortem computed tomography. J Forensic Sci 2018;63:1346-9.
7. Krems RV. Bayesian machine learning for quantum molecular dynamics. Phys Chem Chem Phys 2019;21:13392-410.
8. Park S, Park H, Im J, Yoo C, Rhee J, Lee B, *et al.* Delineation of high resolution climate regions over the Korean Peninsula using machine learning approaches. PLoS One 2019;14:e0223362.
9. Stoltzfus JC. Logistic regression: A brief primer. Acad Emerg Med 2011;18:1099-104.
10. Djorojevic M, Roldán C, García-Parra P, Alemán I, Botella M. Morphometric sex estimation from 3D computed tomography os coxae model and its validation in skeletal remains. Int J Legal Med 2014;128:879-88.
11. Curate F, Umbelino C, Perinha A, Nogueira C, Silva AM, Cunha E. Sex determination from the femur in Portuguese populations with classical and machine-learning classifiers. J Forensic Leg Med 2017;52:75-81.
12. Désir C, Petitjean C, Heutte L, Salaün M, Thiberville L. Classification of endomicroscopic images of the lung based on random subwindows and extra-trees. IEEE Trans Biomed Eng 2012;59:2677-83.
13. Gu W, Xie X, He Y, Zhang Z. Drug-target protein interaction prediction based on AdaBoost algorithm. Sheng Wu Yi Xue Gong Cheng Xue Za Zhi 2018;35:935-42.
14. Turan MK, Oner Z, Secgin Y, Oner S. A trial on artificial neural networks in predicting sex through bone length measurements on the first and fifth phalanges and metatarsals. Comput Biol Med 2019;115:103490.
15. Blake KA, Hartnett-McCann K. Metric assessment of the pubic bone using known and novel data points for sex estimation. J Forensic Sci 2018;63:1472-8.
16. Bonczarowska JH, Bonicelli A, Papadomanolakis A, Kranioti EF. The posterior portion of the ilium as a sex indicator: A validation study. Forensic Sci Int 2019;294:216.e1-6.
17. d'Oliveira Coelho J, Curate F. CADOES: An interactive machine-learning approach for sex estimation with the pelvis. Forensic Sci Int 2019;302:109873.
18. Pretorius E, Steyn M, Scholtz Y. Investigation into the usability of geometric morphometric analysis in assessment of sexual dimorphism. Am J Phys Anthropol 2006;129:64-70.
19. Savall F, Faruch-Bilfeld M, Dedouit F, Sans N, Rousseau H, Rougé D, *et al.* Metric sex determination of the human coxal bone on a virtual sample using decision trees. J Forensic Sci 2015;60:1395-400.
20. Santos F, Guyomarc'h P, Bruzek J. Statistical sex determination from craniometrics: Comparison of linear discriminant analysis, logistic regression, and support vector machines. Forensic Sci Int 2014;245:204.e1-8.
21. Navega D, Vicente R, Vieira DN, Ross AH, Cunha E. Sex estimation from the tarsal bones in a Portuguese sample: A machine learning approach. Int J Legal Med 2015;129:651-9.
22. Akkoç B, Arslan A, Kök H. Automatic gender determination from 3D digital maxillary tooth plaster models based on the random forest algorithm and discrete cosine transform. Comput Methods Programs Biomed 2017;143:59-65.

Original Article

Description of an Atypical Vascular Arch in the Renal Parenchyma

Alberto Garcia Barrios, Ana Isabel Cisneros Gimeno, Jesus Obon Nogue, Jaime Whyte Orozco

Department of Human Anatomy and Histology, Medical and Genetic Research Group (GIIS099) IIS Aragón, Zaragoza, Spain

Abstract

Introduction: Variability in renal vascularization occurs with a frequency of around 30%. During the routine dissection of one cadaver without renal pathology, we revealed the presence of one. **Material and Methods:** Dissection of a cadaver carried out in the practicing room of School of Medicine. **Results:** During the routine dissection of one cadaver without renal pathology, we revealed the presence of an early bifurcation of the renal artery on the left side, and the presence of two polar arteries – superior and inferior -, the latter presenting an anterior and posterior vascular arch to the renal pelvis in the parenchyma, which anastomoses the pre- and retro-pyelic branches of the renal artery with the pre- and retro-pyelic branches of the inferior accessory polar artery. In addition, the presence of an accessory polar artery was observed in the right kidney. **Discussion and Conclusion:** For vascular surgeons, knowledge of this anatomical variation is of real clinical relevance in cases such as fenestrated endografting in order to preserve the function of the entire kidney.

Keywords: *Inferior polar artery, intrarenal vascular arch, renal artery, variations*

Introduction

In classical anatomical terminology, standard renal vascularization is generally described as a single renal artery originating bilaterally and laterally from the abdominal aortic artery at the level of lumbar vertebrae L1 and L2, approximately 1 cm below the exit from the superior mesenteric artery.[1-3] In general, at a variable distance from the renal hilum, it splits into two terminal branches, the prepyelic artery (PA) and the retro-pyelic artery (RP), which in turn will split into segmental branches. However, this vascular pattern may present anatomical variations with a variable incidence depending on the ethnic origin, ranging from 4% to 61.5% (with an average of 20%), and on the number of accessory arteries, between 3% and 30% unilaterally, and 10% bilaterally, and the study method (computerized tomography/dissection).[1,2,4-8]

These variations have been classified as hilar, when they go to the renal hilum, and polar, when they go to the renal poles, and the latter, in turn, as solitary, pedicular, false supernumerary, and true supernumerary.[9]

The inferior polar artery generally comes from the aorta, in its superior or inferior portion, from the renal artery, and less frequently from the suprarenal artery, common iliac, or superior mesenteric artery. The incidence of this inferior polar artery coming from the abdominal aorta varies between 1 and 9.7%.[10]

In this case, we present a rare anatomical variation that involves the presence of accessory polar arteries in the right kidney, and more prominently, the presence of an anterior (PA) and posterior (RP-pyelic) vascular arch to the renal pelvis in the renal parenchyma, between the branches of the main renal artery and the branches of the inferior polar artery.

Material and Methods

During the routine dissection of one cadaver without renal pathology, carried out for university teaching, given by the department of human anatomy and histology, the presence of two anatomical variants related to the arterial supply of the kidney was observed: On the one hand, an early division of the segmental branches in the left kidney, and on the other hand, the presence of two polar arteries – superior and inferior, in the right kidney. For a better visualization of the structures found, specific silicone was used

How to cite this article: García A, Cisneros A, Obón J, Whyte J. Description of an atypical vascular arch in the renal parenchyma. J Anat Soc India 2022;XX:XX-XX.

Article Info

Received: 01 May 2021
Revised: 23 February 2022
Accepted: 17 March 2022
Available online: ***

Address for correspondence:
Dr. Ana Isabel Cisneros Gimeno, Domingo Miral, S/N, School of Medicine, Unversity of Zaragoza, Zaragoza 50009, Spain.
E-mail: aicisner@unizar.es

Access this article online

Website: www.jasi.org.in
DOI: 10.4103/jasi.jasi_83_21
Quick Response Code:

Figure 1: Green silicone injected into arteries

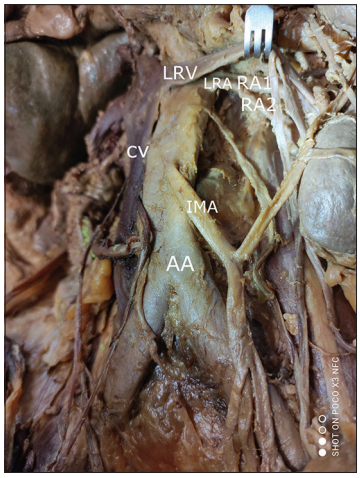

Figure 2: Early bifurcation of the left renal artery. AA: Aorta artery; IMA: Inferior Mesenteric Artery; CV: Cava Vein; LRV: Left Renal Vein; LRA: Left Renal Artery; RA1: Prepyelic segmentary Artery; RA2: Retro-pyelic segmentary Artery

(Green color: 3M ESPE ExpressTM. Vinyl Polysiloxane Impression Material. Regular Set-Light-Body-Hydrophilic. ISO 4823 Type 3.50 ml.Base Paste/Catalyst Paste. 7302. Made in Germany by 3M ESPE AG, D-82229 Seefeld), administered through an arterial line, through the exit point of the inferior polar branch, from the side of the right aorta [Figure 1].

Results

The arteries were designated as AR (renal artery), AR1 (pre-PA), and AR2 (RP-PA) in the left kidney [Figure 2 and Diagram 1], showing the early bifurcation of the renal artery before reaching the hilum area, and in the right one as R1 (renal artery), R2 (superior polar artery), and R3, respectively [Figure 3a and Diagram 2a]. The inferior right polar artery also showed a similar segmentation to that of the main renal artery in the vicinity of the hilum, from which two branches emerged that ran in front of and behind the ureter and renal pelvis in that distal location [Figure 3b and Diagram 2b].

Dissection of the left renal artery showed early branching of the anterior and posterior lobar branches to the renal pelvis [Figure 2].

Instead, dissection of the arteries and renal parenchyma in the right kidney revealed the presence of two anatomical variations: First, the presence of two accessory polar arteries, one superior and one inferior, in the direction of the superior and inferior renal poles, respectively, and on the other, the presence of two communicating vascular arches, not previously described in the literature consulted, one being anterior and the other posterior to the renal pelvis, between the branches coming from the main renal artery, penetrating the renal sinus, and ascending branches

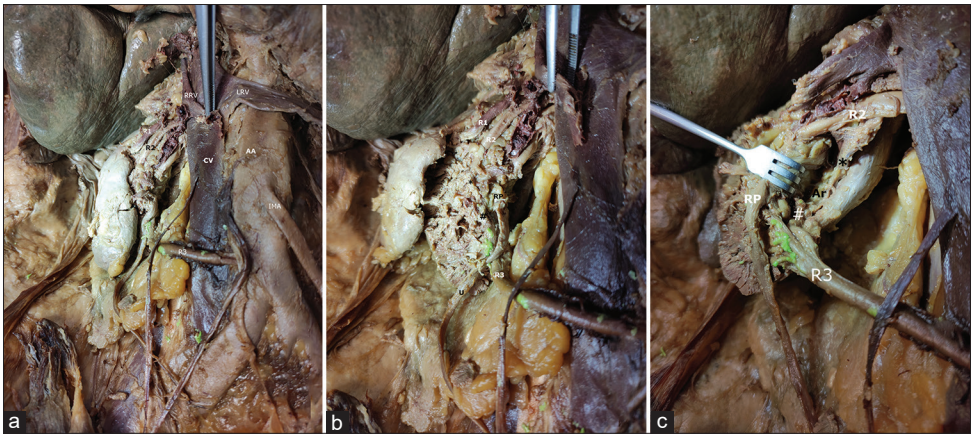

Figure 3: (a) Presence of polar superior, renal, and polar inferior arteries. AA: Aorta artery; IMA: Inferior Mesenteric Artery; CV: Cava Vein; LRV: Left Renal Vein; R1: Right superior polar artery; R2: Renal artery; R3: Inferior polar artery. (b) Presence of pre and retropyelic bifurcation of the inferior polar arteries with description of anastomosis between the prepyelic branches of the main renal artery and the inferior polar artery. R1: Right superior polar artery; R2: Renal artery; R3: Inferior polar artery; U: Ureter; RP: Renal Pelvis; *: Prepyelic branch of the renal artery; # Prepyelic branch of the inferior polar artery. (c) Presence of pre- and retropyelic bifurcation of the inferior polar arteries with description of anastomosis between the prepyelic branches of the main renal artery and the inferior polar artery. R2: Renal artery; R3: Inferior polar artery; U: Ureter; RP: Renal Pelvis *: Retro-pyelic branch of the renal artery; #Retro-pyelic branch of the inferior polar artery; Ar: Vascular Arch between prepyelic branches

of the bifurcation of the lower polar artery [Figure 3b, c and Diagram 2b, c].

Discussion

Anatomical variants related to renal vascularization appear relatively frequently (around 30%), due to the permanence of some of the caudal and cranial mesonephric arteries, which in normal conditions should degenerate, and the complex development of renal formation in the embryonic period.[11,12] Among the anatomical variants, most frequently described by dissection studies is the presence of superior or inferior polar numerary arteries, mainly unilaterally, as described in our case.[13,14]

According to the literature consulted, both in studies of dissection of cadavers and image diagnosis, there is talk of the irrigation of the renal territory being terminal, and even of the presence of two independent vascular territories: One anterior and one posterior, irrigated, respectively, by the PA and RP-pyelic arteries, without the presence of anastomosis between some areas and others. However, in our case, the findings do not correspond to the previous description, due to the presence of a vascular arch that allows anastomosis between the PA and RP-pyelic branches of the renal artery in the right kidney, with similar distribution (anterior and posterior to the pelvis) of the branches derived from the inferior polar artery on the same side.

The knowledge of the renal anatomy and its possible variations is necessary to avoid medical-surgical problems, and its fortuitous presence should raise the need for complete studies, at the vascular level, before any surgical procedure.

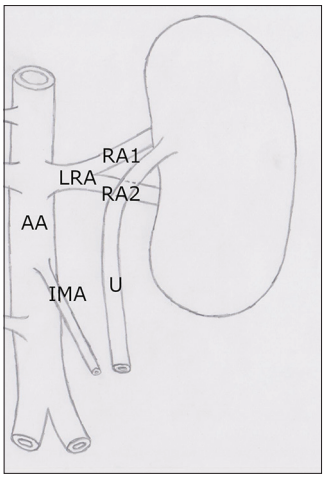

Diagram 1: Early bifurcation of the left renal artery. AA: Aorta artery; IMA: Inferior Mesenteric Artery; CV: Cava Vein; LRV: Left Renal Vein; LRA: Left Renal Artery; RA1: Prepyelic segmentary Artery; RA2: Retro-pyelic segmentary Artery

Conclusion

Vascular surgeons describe that this anatomic variation has a true clinical utility. The connection between both arteries makes it possible to perfuse the whole kidney even if one of them is occluded. This fact makes it possible to embolize one of the arteries without impairing the renal function. In the case of an aortic aneurysm, knowing this fact could be key for the surgical planning. When planning a fenestrated endograft, it is very difficult to deal with double renal arteries, as there is seldom space to stent both of them. In patients with this variation, it is possible to embolize one and revascularize the other, thus preserving the function of the whole kidney.

Financial support and sponsorship

Nil.

Conflicts of interest

There are no conflicts of interest.

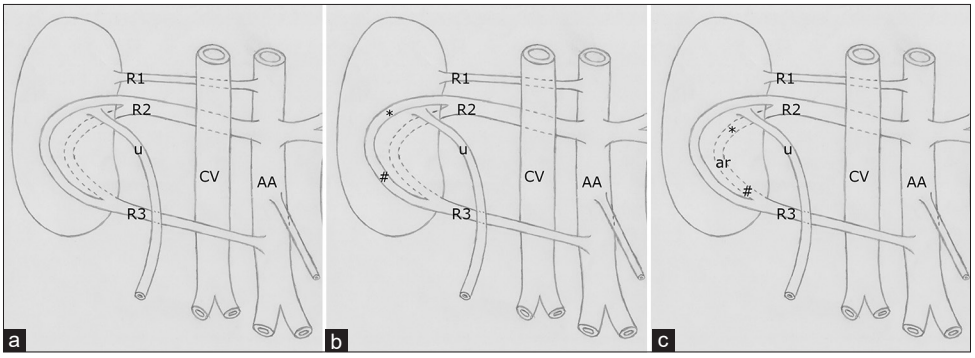

Diagram 2: (a) Presence of polar superior, renal, and polar inferior arteries. AA: Aorta artery; IMA: Inferior Mesenteric Artery; CV: Cava Vein; LRV: Left Renal Vein; R1: Right superior polar artery; R2: Renal artery; R3: Inferior polar artery. (b) Presence of pre and retropyelic bifurcation of the inferior polar arteries with description of anastomosis between the prepyelic branches of the main renal artery and the inferior polar artery. R1: Right superior polar artery; R2: Renal artery; R3: Inferior polar artery; U: Ureter; RP: Renal Pelvis; *: Prepyelic branch of the renal artery; # Prepyelic branch of the inferior polar artery. (c) Presence of pre- and retropyelic bifurcation of the inferior polar arteries with description of anastomosis between the prepyelic branches of the main renal artery and the inferior polar artery. R2: Renal artery; R3: Inferior polar artery; U: Ureter; RP: Renal Pelvis *: Retro-pyelic branch of the renal artery; # Retro-pyelic branch of the inferior polar artery; Ar: Vascular Arch between prepyelic branches

References

1. Gulas E, Wysiadecki G, Cecot T, Majos A, Stefańczyk L, Topol M, *et al.* Accessory (multiple) renal arteries – Differences in frequency according to population, visualizing techniques and stage of morphological development. Vascular 2016;24:531-7.
2. Gulas E, Wysiadecki G, Szymański J, Majos A, Stefańczyk L, Topol M, *et al.* Morphological and clinical aspects of the occurrence of accessory (multiple) renal arteries. Arch Med Sci 2018;14:442-53.
3. Koplay M, Onbas O, Alper F, Gulcan E, Kantarci M. Multiple renal arteries: Variations demonstrated by multidetector computed tomography angiography. Med Princ Pract 2010;19:412-4.
4. Urban BA, Ratner LE, Fishman EK. Three-dimensional volume-rendered CT angiography of the renal arteries and veins: Normal anatomy, variants, and clinical applications. Radiographics 2001;21:373-86.
5. Cho Y, Yoon SP. Bilateral inferior renal polar arteries with a high origin from the abdominal aorta. Folia Morphol (Warsz) 2021;80:215-8.
6. Rao M, Bhat SM, Venkataramana V, Deepthinath R, Bolla SR. Bilateral prehilar multiple branching of renal arteries: A case report and literature review. Kathmandu Univ Med J (KUMJ) 2006;4:345-8.
7. Aristotle S, Sundarapandian R, Felicia C. Anatomical study of variations in the blood supply of kidneys. J Clin Diagn Res 2013;7:1555-7.
8. Saldarriaga TB, Pinto SA, Ballesteros LE. Morphological expression of the renal artery: A direct anatomical study in a Colombian half-caste population. Int J Morphol 2008;26:31-8.
9. Zăhoi DE, Sztika D, Dăescu E. Morphological variability of arterial sources of the renal polar parenchyma and its clinical importance. Rom J Morphol Embryol 2015;56:1403-9.
10. Gesase AP. Rare origin of supernumerary renal vessels supplying the lower pole of the left kidney. Ann Anat 2007;189:53-8.
11. Mazengenya P. Multiple variations of the renal and testicular vessels: Possible embryological basis and clinical importance. Surg Radiol Anat 2016;38:729-33.
12. Nayak BS. Multiple variations of the right renal vessels. Singapore Med J 2008;49:e153-5.
13. Budhiraja V, Rastogi R, Anjankar V, Babu CS, Goel P. Supernumerary renal arteries and their embryological and clinical correlation: A cadaveric study from north India. ISRN Anat 2013;2013:405712.
14. Talovic E. Kulenovic A. Voljevica A. Kapur E. Review of the supernumerary renal arteries by dissection method. Acta Med Acad 2007;36:59-69.

Original Article

Relationship between Digit Ratio of 2D:4D and The Physical Health among College Students of Han Ethnicity in Southern Fujian

Tongjun Chen[1,2], Jianmei Xiang[3], Shaokang Teng[1,2], Zhongqing Huang [1,2], Xiaoliang Li[1], Liping Huang[1,2], Huihua Chen[1,2], Baoying Luo[1,2]

[1]Department of Basic Medicine and Department of Clinical Medicine, Zhangzhou Health Vocational College, [2]Fujian Collaborative Innovation Center for Translation Medical Testing and Application Technology, [3]Department of Rehabilitation Medicine, Zhangzhou Municipal Hospital of Fujian Province, Zhangzhou, Fujian Province, China

Abstract

Introduction: Studying the association between finger length ratios of 2D:4D and the physical health among college students of Han ethnicity in Southern Fujian can provide an indirect macrobiology reference index for early predictions of physical health status. **Material and Methods:** A total of 835 students in Southern Fujian were selected as test subjects through a stratified cluster sampling method. The 2D:4D ratio was recorded using physical measurement methods. The body mass index (BMI), vital capacity, 50-m run, and sit-and-reach test results were collected and analyzed based on the National Student's Health Standards. **Results:** Among male Han college students in Southern Fujian, the left 2D:4D ratio was negatively correlated with the vital capacity and sit-and-reach test results, while the right 2D:4D ratio was negatively correlated with the vital capacity, 50-m run, and sit-and-reach test results, as well as the comprehensive evaluation result of physical health. Among female Han college students in Southern Fujian, the left 2D:4D ratio was positively correlated with BMI and negatively correlated with the vital capacity, 50-m run, and 800-m run results, as well as the comprehensive evaluation result of physical health. The right 2D:4D ratio was negatively correlated with the vital capacity, 50-m run, 800-m run, and sit-and-reach test results, as well as the comprehensive evaluation results of physical health. The comprehensive evaluation results of physical health were statistically significant differences among low, medium, and high bilateral 2D:4D groups of female students, with poorer results in the high 2D:4D group than that of the medium and low 2D:4D groups. **Discussion and Conclusion:** The bilateral 2D:4D ratio of female and right 2D:4D ratio of male Han college students in Southern Fujian has a correlation with the comprehensive evaluation of physical health, which can serve as one of the reference indexes for adolescents' early health education, physical health monitoring, dietary intervention, and athlete selection.

Keywords: *College students, digit ratio, Han ethnic group, Southern Fujian, the physical health*

Introduction

The *Student's Physique and Health Standard* was introduced in 2002 in China. After further exploration and a summary of experience, the *National Student Physical Health Standard (Revised in 2014)* (hereinafter referred to as "*The Standard*") was issued by the Ministry of Education, to assess students' physical health from their body shape, function, and fitness. This lays a good foundation for providing reference standards on the development of students' physical health.

Digit ratio refers to the ratio of finger lengths. The length of the thumb to the little finger (1–5) is expressed as 1D-5D; however, it is generally difficult to determine the length of the thumb, so 2D:3D, 2D:4D, 2D:5D, 3D:4D, 3D:5D and 4D:5D are usually used, of which the second finger–to fourth finger length ratio (2D:4D) is most commonly used. Digit ratio is determined by the HOX gene[1] and is affected by intrauterine sex hormones during embryonic development,[2] with a positive correlation with maternal intrauterine testosterone and a negative correlation with estrogen. Human right-hand 2D:4D is negatively correlated with the testosterone/estradiol ratio in amniotic fluid.[3] Digit ratio remains unchanged during individual growth, so it can serve as a marker for perinatal sex hormone levels. In addition to digit ratio, body mass index (BMI), exercise skills, and exercise capacity are also associated with perinatal sex hormone levels.[4-6] Scholars found that prenatal sex hormone levels have a certain impact on the flexibility and muscle strength of adolescent females.[7] A lower 2D:4D

How to cite this article: Chen T, Jianmei X, Shaokang T, Zhongqing H, Xiaoliang L, Liping H, *et al*. Relationship Between digit ratio of 2D:4D and the physical health among college students of Han ethnicity in Southern Fujian. J Anat Soc India 2022;XX:XX-XX.

Article Info

Received: 19 November 2021
Revised: 29 January 2022
Accepted: 21 June 2022
Available online: ***

Address for correspondence:
Prof. Tongjun Chen, Zhangzhou Health Vocational College, Zhangzhou, Fujian Province, China.
Fujian Collaborative Innovation Center for Translation Medical Testing and Application Technology, Zhangzhou, Fujian Province, China.
E-mail: 11895750@qq.com

Access this article online

Website: www.jasi.org.in
DOI: 10.4103/jasi.jasi_189_21
Quick Response Code:

often corresponds to a better physical ability and greater exercise performance.[8] especially in athletes involving in aerobic exercise[5] including rowing athletes,[9] elite tennis players,[10] and swimmers.[11] Perinatal sex hormone levels are also related to body size and the distribution of substances in the body.[12] Digit ratio (2D:4D) is associated with individual development and physical function[13,14] but the relationship differs among ethnic groups in different regions.[15] Therefore, the relationship between digit ratio and physical health, assessed by BMI, cardiopulmonary function, and exercise capacity, deserves further attention and research. In the present study, the correlation between 2D:4D and physical health, and the possibility of an indirect macrobiological index for early prediction of physical health were explored among Han college students in Southern Fujian Province of China.

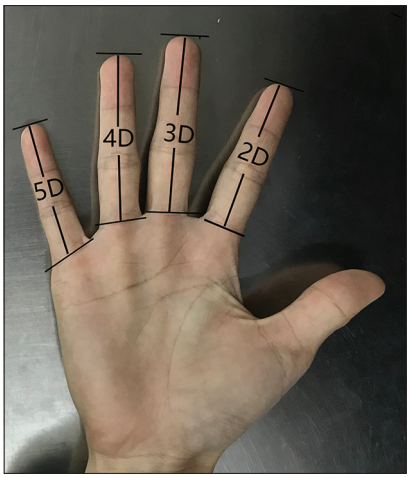

Figure 1: The schematic diagram of each digit length

Material and Methods

Material

Eight hundred and thirty-five participants (303 males and 532 females) aged 17–21-year-old were selected from undergraduate classes of 2018 and 2019 attending Zhangzhou Health Vocational College in Fujian Province. The participants were chosen through stratified random cluster sampling from September 2018 to January 2020. The inclusion criteria include: Han people in Southern Fujian (Zhangzhou, Xiamen and Quanzhou) within 3 generations; no major somatopsychic illness; no dyskinesia, no injured or deformed fingers, having never received special physical training, and with a mother that did not take any hormone drugs during pregnancy. This study was reviewed and approved by the Ethics Department of the college, and informed consent was obtained from all students.

Methods

According to the *Anthropometric Manual* authored by Shao XQ,[16] the finger length of subjects was measured through the indirect method, specifically as follows: The photos of both palms were taken using a digital camera at a fixed shooting distance. Then, the measuring point of each finger was marked using the image analysis software on a computer, and the photos were printed in color [Figure 1]. Finally, the straight-line distance between the midpoint of the palmar flexural fold of the proximal phalanx and the midpoint of the fingertip was measured using an electronic digimatic caliper (Guanglu Measuring Instrument Co., Ltd., China, 0–150 mm, precision: 0.01 mm).

A total of eight indexes were measured for each subject according to the requirements and regulations in *The Standard*,[17] including body shape indexes (height [cm] and weight [kg]), body function indexes (vital capacity [mL]), and body fitness indexes (speed fitness test: 50-m run [s], flexibility fitness test: Sit-and-reach (cm), lower limb explosive strength test: Standing broad jump [cm], strength fitness test: Chin-up for males [times] and 1 min crunches for females [times], endurance fitness test: 1000-m run for males [s] and 800-m run for females [s]). The vital capacity was measured in a standing position using a spirometer. Each subject repeated the test twice with an interval of 30 s. The sit-and-reach test was measured using a sit and reach box (brand, city). The subject sat with legs stretched and feet 10–15 cm apart on the test board. They were instructed to bend forward and push the cursor as far as they could. The test was repeated twice. The higher of the two was used in the analysis. The standing broad jump test measures the distance of the double leg jump in centimeters. The 1 min crunches test measures how many crunches the subject can do in a minute. The testing position was supine with foot on the plinth, hips and knees at 90°, and fingers crossed behind the head. A tester held the subject's ankle for fixation. A successful attempt is counted when the subject completing the sitting-up with the elbow touching the knees while keeping the hands behind or around the head. The 50-m run test and 1000-m (800-m) run test were measured in seconds using a stopwatch. Height and weight were measured and BMI was calculated as weight (kg)/height $(m)^2$. The test results were assessed according to *The Standard*.

Quality control

Two testers received standardized training before the start of the study. Intrarater and interrater reliabilities were assessed using correlation coefficient and reached 0.94 or higher in all tests using in this study.

Statistical procedures

A database was set up using EpiData 3.1 (EpiData Association; Odense, Denmark) software. SPSS 22.0 (IBM Corp. Armonk, NY, USA) software was utilized for all statistical analyses. Descriptive analysis was expressed as mean ± standard deviation ($\chi \pm s$). Reliability and correlation were analyzed using Pearson correlation analysis and variance tests. ANOVA and *post hoc* analyses

were used to compare the differences among the three groups. The significance level was set at $\alpha = 0.05$.

Results

Among Han male college students in Southern Fujian, the left 2D:4D was negatively correlated with vital capacity and sit-and-reach results, but had no correlations with other indexes. The right 2D:4D was negatively correlated with vital capacity, 50-m run, sit-and-reach results, and the total score of physical health, but had no correlations with other indexes [Table 1].

Among Han female college students in Southern Fujian, the left 2D:4D was positively correlated with BMI, and negatively correlated with vital capacity, 50-m run, 800-m run, and the total score of physical health. The right 2D:4D was negatively correlated with vital capacity, 50-m run, 800-m run, sit-and-reach results, and the total score of physical health [Table 2].

Using the 25th and 75th percentile of bilateral 2D:4D of Han college students in Southern Fujian as cutoff scores, all subjects were divided into low, mid, and high 2D:4D groups. It was found that the chin-up results had statistically significant differences among male right-hand low, mid, and high 2D:4D groups. The *post hoc* analysis revealed that the low 2D:4D group is significantly different from the mid and high 2D:4D groups [Table 3].

The BMI, vital capacity, 50-m run and 800-m run results, and the total score were statistically significant differences among female left-hand low, mid, and high 2D:4D groups. The *post hoc* analysis revealed that the high 2D:4D group is different from the mid and low 2D:4D groups. The 800-m run results had a statistically significant difference between mid and low 2D:4D groups. There were statistically significant differences in BMI, vital capacity, 50-m run, 800-m run, standing broad jump and sit-and-reach results, and the total score among female right-hand low, mid, and high 2D:4D groups. The vital capacity, 50-m run and sit-and-reach results and the total score all had statistically significant differences in the high 2D:4D group compared with those in the mid and low 2D:4D groups. Moreover, there was a statistically significant difference in BMI between high and low 2D:4D groups, and also in standing board jump results between high and mid 2D:4D groups [Table 4].

Table 1: The correlation analysis between finger length ratio of second finger–to fourth finger length ratio and the physical health related indexes of College Students of Han male ethnic in southern Fujian (*r*)

Items (*n*=303)	Left 2D:4D		Right 2D:4D	
	r	*P*	*r*	*P*
BMI	−0.049	0.394	0.062	0.281
Vital capacity	−0.152	0.008*	−0.187	0.001*
50-m run	−0.014	0.809	−0.158	0.006*
1000-m run	−0.041	0.479	−0.077	0.179
Standing broad jump	−0.039	0.495	−0.058	0.317
Sit-and-reach	−0.152	0.008*	−0.197	0.001*
Chin-up	0.062	0.278	−0.085	0.138
Total score	−0.092	0.108	−0.164	0.004*

*P<0.05. 2D:4D: Second finger–to fourth finger length ratio, BMI: Body mass index

Table 2: The correlation analysis between finger length ratio of second finger–to fourth finger length ratio and the physical health related indexes of College Students of Han female ethnic in southern Fujian (*r*)

Items (*n*=532)	Left 2D:4D		Right 2D:4D	
	r	*P*	*r*	*P*
BMI	0.138	0.001*	0.065	0.137
Vital capacity	−0.134	0.002*	−0.218	<0.001*
50-m run	−0.133	0.002*	−0.096	0.027*
800-m run	−0.178	<0.001*	−0.231	<0.001*
Standing broad jump	−0.024	0.588	−0.051	0.243
Sit-and-reach	0.014	0.747	−0.014	0.001*
Crunches	0.074	0.090	0.080	0.065
Total score	−0.158	<0.001*	−0.263	<0.001*

*P<0.05. 2D:4D: Second finger–to fourth finger length ratio, BMI: Body mass index

Discussion

In October 2016, the *2030 Planning Outline of Healthy China* was issued by the Central Committee of the Communist Party of China and the State Council of the PRC.[18] As stipulated in Section 4 of Chapter 6, adolescents are listed as the target population for the implementation of the physical health plan, and it is also required that the interest of adolescents in physical exercise be developed through the implementation of the youth sports promotion program, with an excellence rate of more than 25% in *The Standard* as a quantifiable goal. China has decided to enhance the physical health of students as an approach to achieve the goal of healthy China. *The Standard* comprehensively assesses the students' physical health from body shape, function, and fitness. Body shape indexes are an important basis reflecting the growth and development speed and nutritional status of the human body.[19] BMI displays the relation between adults' weight and height, which is recommended by the WHO as a preferred index for assessing overweight and obesity and their change trends and can also be used to measure the fat distribution in the human body.[20]

In the present study, the BMI was significantly higher among female students in the left-hand high 2D:4D group than that of the mid and low 2D:4D groups, and it was also significantly higher in the right-hand high 2D:4D group than that of the low 2D:4D group. Fink *et al*.[21] found that BMI positively correlates with left hand 2D:4D in males. In females, the reversed relationship was found but it was not statistically significant. Muller *et al*.[22] found that 2D:4D is

Table 3: Differences in physical health-related indexes in bilateral low, medium and high second finger–to fourth finger length ratio groups among College Students of Han male ethnic in southern Fujian ($\bar{X}$±S)

Items (*n*=303)	Left 2D:4D					Right 2D:4D				
	Low 2D:4D (*n*=76)	Mid 2D:4D (*n*=151)	High 2D:4D (*n*=76)	*F*	*P*	Low 2D:4D (*n*=76)	Mid 2D:4D (*n*=151)	High 2D:4D (*n*=76)	*F*	*P*
BMI	21.44±3.47	21.37±3.48	21.41±3.90	0.09	0.992	21.27±2.87	21.65±3.77	21.04±3.81	0.814	0.444
Vital capacity	58.42±21.48	63.77±23.04	57.72±22.34	2.45	0.088	61.09±24.21	62.22±20.48	58.14±24.89	0.82	0.440
50-m run	79.45±14.89	78.83±15.32	79.05±15.02	0.04	0.959	79.32±12.46	79.40±15.76	78.05±16.22	0.22	0.805
1000-m run	67.24±10.97	66.73±10.30	68.68±10.93	0.86	0.424	67.17±10.67	66.99±10.90	68.22±10.10	0.35	0.704
Standing board jump	67.82±16.80	68.80±18.49	68.82±19.42	0.83	0.920	68.02±16.60	68.75±18.86	68.71±18.88	0.04	0.958
Sit-and-reach	70.53±11.90	71.29±12.15	73.63±9.87	1.55	0.214	72.25±12.30	71.03±11.38	72.43±11.31	0.49	0.612
Chin-up	39.49±25.06	43.90±42.28	42.28±23.56	0.89	0.410	36.03±23.50	43.62±23.02†	46.30±23.40†	4.14	0.017*
Total score	70.80±8.92	70.35±9.78	71.84±9.67	0.62	0.537	70.56±9.34	70.64±9.76	71.50±9.35	0.25	0.780

*P<0.05, †P<0.05 versus low 2D:4D. 2D:4D: Second finger–to fourth finger length ratio, BMI: Body mass index

Table 4: Differences in physical health-related indexes in bilateral low, medium and high second finger–to fourth finger length ratio groups among College Students of Han female ethnic in southern Fujian ($\bar{X}$±S)

Items (*n*=532)	Left 2D:4D					Right 2D:4D				
	Low 2D:4D (*n*=133)	Mid 2D:4D (*n*=266)	High 2D:4D (*n*=133)	*F*	*P*	Low 2D:4D (*n*=133)	Mid 2D:4D (*n*=266)	High 2D:4D (*n*=133)	*F*	*P*
BMI	19.33±2.55	19.76±2.50	20.43±3.69†,‡	5.09	0.006*	19.29±2.45	19.88±3.00	20.23±2.97†	3.71	0.025*
Vital capacity	63.86±18.99	62.59±20.22	57.82±23.55†,‡	3.36	0.035*	65.19±19.06	64.53±17.77	52.99±25.78†,‡	13.67	<0.001*
50-m run	70.61±7.96	70.50±12.13	66.54±15.57†,‡	5.32	0.005*	69.60±10.25	71.04±9.68	66.49±17.50†,‡	6.14	0.002*
1000-m run	71.83±9.88	68.50±11.58†	65.50±14.62†,‡	9.21	<0.001*	71.23±9.81	69.79±11.15	63.52±14.80†,‡	16.79	<0.001*
Standing board jump	69.26±12.88	70.01±12.48	70.10±13.33	0.19	0.828	70.47±12.31	70.60±13.42	67.71±11.73‡	2.50	0.083
Sit-and-reach	70.52±17.13	71.86±12.39	72.68±12.41	0.85	0.430	72.72±13.03	72.89±13.75	68.42±13.93†,‡	5.24	0.006*
Chin-up	63.54±13.31	65.11±10.67	65.65±15.83	0.83	0.436	64.39±10.17	65.68±11.98	63.35±16.22	1.55	0.213
Total score	72.06±6.40	71.31±7.53	69.05±9.03†,‡	5.75	0.003*	72.34±6.08	72.23±6.35	66.93±10.09†,‡	25.93	<0.001*

*P<0.05, †P<0.05 versus low 2D:4D, ‡P<0.05 versus mid 2D:4D. 2D:4D: Second finger–to fourth finger length ratio, BMI: Body mass index

not strongly associated with adult anthropometric measures. BMI is greatly affected by gender, ethnicity, living habits, age, and regional dietary rules. Therefore, the correlation results between 2D:4D and BMI in different regions, ethnicities, and genders are not consistent. It is well known that BMI reflects the overall body fat content, whereas the waist circumference and waist-to-hip ratio reflect the abdominal fat content. All three can reflect body fat content, but each has certain limitations. If an index, such as the 2D:4D can be used to represent all three measures then it can provide a useful alternative for estimating body composition.

Body function refers to the functional capability of organs and systems in the body. Vital capacity, i.e., maximum lung capacity in one-time ventilation, is an important index for assessing respiratory function. In this study, both male and female bilateral 2D:4D had a negative correlation with vital capacity, and vital capacity in the female bilateral high 2D:4D group was significantly lower than that of the mid and low 2D:4D groups. However, vital capacity was measured in a one-time ventilation test and closely related to height and weight, thus failing to fully reflect the elastic state of lung tissues and the patency degree of the airway,[23] so it had certain limitations. Therefore, vital capacity/weight ratio will be considered for future analysis, to display the differences in body function and physical activity more objectively and analyze their correlations with digit ratio (2D:4D) more scientifically and reasonably.

Body fitness is a general term for the speed, strength, endurance, and flexibility of the human body in muscle activities. Scholars in China also found the correlation between 2D:4D and human body fitness in research on the digit ratio of university students in Jinzhou and Guangdong youthsm,[24,25] but the results are not consistent. In the present study, it was found that male bilateral 2D:4D was negatively correlated with the sit-and-reach results among Han college students in southern Fujian, indicating that males with lower right 2D:4D had better performance in the 50-m run. This result is consistent with the result from Manning and Hill on 241 boys.[5] Right 2D:4D had no correlation with the chin-up results, but the low 2D:4D group performed worse than those in the mid and high 2D:4D groups. Besides, this study found that females with higher right 2D:4D have poorer body flexibility. In addition, females with a lower bilateral 2D:4D finger length ratio had better endurance and speed. The result is consistent with those of Pasanen *et al*.[26] He studied the correlation between 2D:4D and sports performance of 114 boys and 175 girls and found that their sports performance

was negatively correlated with the female bilateral 2D:4D and male right 2D:4D. However, the result differs from the result from Lombardo *et al*.[27] in which digit ratio and physical skills and fitness were negatively correlated on the right side of male, but not in female. We speculate that the difference may be due to the elite status of young athletes and the small sample size in the study by Lombardo *et al*. Whether the strength test results are associated with 2D:4D remains to be further analyzed after collecting more data from different types of strength tests in the future.

Through the comprehensive assessment of physical health based on *The Standard*, it was found that the higher female bilateral 2D:4D and male right 2D:4D indicated a lower total score of physical health, and the total score was significantly lower in the female high 2D:4D group than that of the mid and low 2D:4D groups. Experiments with rodents show that the length of 2D is positively influenced by prenatal exposure to estrogen, whereas the length of 4D is positively influenced by prenatal testosterone exposure.[28-30] In humans, 2D:4D is established by the end of the first trimester.[31] Prenatal testosterone exposure may also affect subsequent athletic behavior and performance.[32-34] Athletic prowess in both males and females, especially their performance on distance running,[35-37] is associated with smaller 2D:4D.[38,39] The relationship between 2D:4D and athletic prowess may be mediated by the effects of prenatal testosterone exposure on the cardiovascular system.[39] Multiple lines of evidence suggest that prenatal testosterone exposure influences not only sports performance but also sports interest and motivation.[34,40] It can be speculated that higher levels of androgen in individuals and mothers during embryonic development have a greater impact on the body function and fitness of females and males.

Conclusion

It was found that female bilateral 2D:4D and male right 2D:4D can serve as one of the macrobiological indexes indirectly predicting the physical health of college students, which offers a basis for early health education, physical health monitoring, lifestyle (diet) intervention, and athlete selection among adolescents. Body fitness is comprehensively assessed using a variety of parameters and affected by genetics, nutritional status and lifestyle. In this study, young Han college students in Southern Fujian were used as the subjects, thus reducing the errors caused by living environment, habits, human body development, and hormone levels *in vivo* to a certain extent. Other influencing factors, however, were not collected and analyzed, so further research is needed in future.

Financial support and sponsorship

Nil.

Conflicts of interest

There are no conflicts of interest.

References

1. Luo TX, Huang CX. Research progress on human body deformity caused by HOX gene alteration. Foreign Med Sci (Section of Genetics) 2005;28:105-8.
2. Manning JT, Callow M, Bundred PE. Finger and toe ratios in humans and mice: Implications for the aetiology of diseases influenced by HOX genes. Med Hypotheses 2003;60:340-3.
3. Lutchmaya S, Baron-Cohen S, Raggatt P, Knickmeyer R, Manning JT. 2nd to 4th digit ratios, fetal testosterone and estradiol. Early Hum Dev 2004;77:23-8.
4. Manning JT, Morris L, Caswell N. Endurance running and digit ratio (2D:4D): Implications for fetal testosterone effects on running speed and vascular health. Am J Hum Biol 2007;19:416-21.
5. Manning JT, Hill MR. Digit ratio (2D:4D) and Spring Speed in boys. Am J Hum Biol 2009;21:210-3.
6. Tester N, Campbell A. Porting achievement: What is the contribution of digit ratio? J Pers 2007;75:663-77.
7. Marek K, Raja C, Zofia I, Sławomir K. Is digit ratio (2D:4D) associated with the choice for the uniformed versus a civil study course by the Polish youth? Anthropol Rev 2019;82:177-90.
8. Agha-Alinejad H, Farzad B, Akbari M, Moffit DM, Dakhili A. Digit ratios and motor and health-related fitness in pre-adolescent females. Ann Hum Biol 2019;46:225-30.
9. Hull MJ, Schranz NK, Manning JT, Tomkinson GR. Relationships between digit ratio (2D:4D) and female competitive rowing performance. Am J Hum Biol 2015;27:157-63.
10. Hsu CC, Su B, Kan NW, Lai SL, Fong TH, Chi CP, *et al.* Elite collegiate tennis athletes have lower 2D:4D ratios than those of nonathlete controls. J Strength Cond Res 2015;29:822-5.
11. Sudhakar HH, Veena UB, Tejaswi RN. Digit ratio (2D:4D) and performance in Indian swimmers. Indian J Physiol Pharmacol 2013;57:72-6.
12. Abbott DH, Dumesic DA, Franks S. Developmental origin of polycystic ovary syndrome – A hypothesis. J Endocrinol 2002;174:1-5.
13. Ertuğrul B, Özener B, Pawłowski B. Prenatal exposure to oestrogens estimated by digit ratio (2d/4d) and breast size in young nulliparous women. Ann Hum Biol 2020;47:81-4.
14. Manning JT, Cook C, Crewther B. Digit ratio (2D:4D) and testosterone supplementations. Early Hum Dev 2019;139:104843.
15. Manning JT, Barley L, Walton J, Lewis-Jones DI, Trivers RL, Singh D, *et al.* The 2nd: 4th digit ratio, sexual dimorphism, population differences, and reproductive success. Evidence for sexually antagonistic genes? Evol Hum Behav 2000;21:163-83.
16. Shao XQ. Anthropometric Manual. Shang Hai, China: Shanghai, Shanghai Cishu Publishing House; 1985.
17. Ministry of Education of the People's Republic of China. Notice of the Ministry of Education on the National Student Physical Fitness Standard 2014. Available from: http://www.moe.gov.cn/s78/A17/twys_left/moe_938/moe_792/s3273/201407/t20140708_171692.html.; [Last accessed on 2022 Jul 07].
18. The Central Committee of the Communist Party of China, 2030 Planning Outline of Healthy China. Available from: http://www.otcmoh.org.cn/info/183.html; 2016. [Last accessed on 2022 Jul 07].
19. Kong DG, Gao H. Comparative study of body shape, body composition and bone density of urban and rural primary school students in Handan. Chin J School Health 2017;38:704-7.
20. Lu H, Wang L, Zhang C, Pei LG, Sheng YJ, Geng Z, *et al.* Relationships between digit ratio (2D:4D) and body mass index, waist-to-hip ratio in college students of Ningxia Han. Chin J

Anat 2016;39:720-3.
21. Fink B, Neave N, Manning JT. Second to fourth digit ratio, body mass index, waist-to-hip ratio, and waist-to-chest ratio: Their relationships in heterosexual men and women. Ann Hum Biol 2003;30:728-38.
22. Muller DC, Manning JT, Hopper JL, English DR, Giles GG, Severi G. No strong association between second to fourth digit ratio (2D:4D) and adult anthropometric measures with emphasis on adiposity. Ann Hum Biol 2013;40:201-4.
23. Wang XZ, Luo HB, Leng ZW. Two-step cluster analysis of physical fitness of medical college students. Chin J Sch Health 2020;41:922-8.
24. Qu QY, Xiao YJ, Wen YF. Ren JZ, Xi HJ. Relationship between the digit ratio and physical fitness test of university students in Jinzhou. Chin J Anat 2019;42:64-7.
25. Wu YH, Zhang L, Wu YM, Wu YZ, Wang ZM, Wu JR, *et al.* Correlation between the digit ratio and physical fitness of Guangdong youths. Chin J Anat 2019;42:60-3.
26. Pasanen BE, Tomkinson JM, Dufner TJ, Park CW, Fitzgerald JS, Tomkinson GR. The relationship between digit ratio (2D:4D) and muscular fitness: A systematic review and meta-analysis. Am J Hum Biol 2022;34:e23657.
27. Lombardo MP, Otieno S. The associations between digit ratio, aerobic fitness, physical skills, and overall physical fitness of elite youth distance runners. Am J Hum Biol 2021;33:e23448.
28. Talarovicova A, Krskova L, Blazekova. Testosterone enhancement during pregnancy influ-ences the 2D:4D ratio and open field motor activity of rat siblings in adulthood. Horm Behav 2009;55:235-9.
29. Zheng Z, Cohn MJ. Developmental basis of sexually dimorphic digit ratios. Proc Natl Acad Sci U S A 2011;108:16289-94.
30. Auger J, Le Denmat D, Berges R, Doridot L, Salmon B, Canivenc-Lavier MC, *et al.* Environmental levels of oestrogenic and antiandrogenic compounds feminize digit ratios in male rats and their unexposed male progeny. Proc Biol Sci 2013;280:20131532.
31. Malas MA, Dogan S, Evcil EH, Desdicioglu K. Fetal development of the hand, digits and digit ratio (2D:4D). Early Hum Dev 2006;82:469-75.
32. Manning JT, Bundred PE, Taylor R. The Ratio of 2nd and 4th Digit Length: A Prenatal Correlate of Ability in Sport. Kinanthropometry VIII London: Roudledge; 2003. p. 165-74.
33. Golby J, Meggs J. Exploring the organizational effect of prenatal testosterone upon the sporting brain. J Sports Sci Med 2011;10:445-51.
34. Reed S, Meggs J. Examining the effect of prenatal testosterone and aggression on sportingchoice and sporting longevity. Pers Individ Diff 2017;116:11-5.
35. Hill R, Simpson B, Millet G, Manning J, Kilduff L. Right-left digit ratio (2D:4D) and maximal oxygen uptake. J Sports Sci 2012;30:129-34.
36. Paul SN, Kato BS, Hunkin JL, Vivekanandan S, Spector TD. The big finger: The second to fourth digit ratio is a predictor of sporting ability in women. Br J Sports Med 2006;40:981-3.
37. Trivers R, Hopp R, Manning J. A longitudinal study of digit ratio (2D:4D) and its relationships with adult running speed in Jamaicans. Hum Biol 2013;85:623-6.
38. Hönekopp J, T Manning J, Müller C. Digit ratio (2D:4D) and physical fitness in males and females: Evidence for effects of prenatal androgens on sexually selected traits. Horm Behav 2006;49:545-9.
39. Manning JT, Taylor RP. Second to fourth digit ratio and male ability in sport: Implications for sex-ual selection in humans. Evol Hum Behav 2001;22:61-9.
40. Deaner RO, Balish SM, Lombardo MP. Sex differences in sports interest and motivation: Anevolutionary perspective. Evol Behav Sci 2016;10:73-97.

Original Article

Variations of the Circle of Willis Determined via Magnetic Resonance Angiography: A Single-Center Analysis of the Serbian Population

Mimoza Đevukaj[1], Igor Nosek[1,2], Miloš Vuković[1,2], Duško Kozić[1,2]

[1]Department of Radiology, Faculty of Medicine, University of Novi Sad, [2]Center for Imaging Diagnostics, Oncology Institute of Vojvodina, Novi Sad, Serbia

Abstract

Introduction: The circle of Willis (CoW) represents the collateral pathway between large brain-feeding arteries, the knowledge of which is important in interventional and neurosurgical procedures, in the diagnosis and planning of procedures in acute stroke and subarachnoid hemorrhage. **Aim:** The study aims to determine the prevalence of variations of the CoW in patients from Serbia via magnetic resonance angiography (MRA). **Material and Methods:** The study was conducted as a retrospective study at the Center for Imaging Diagnostics, Oncology Institute of Vojvodina. Magnetic resonance imaging was analyzed in 665 patients of both sexes (471 females and 194 males), who underwent MRA during 2018 and 2019. **Results:** Complete CoW was found in 48.42% of cases, mostly in females (68.01%). Partially complete CoW and incomplete CoW were encountered in 38.05% and 13.55% of patients, mostly in females (73.52% and 73.33%). Anterior circulation variations were seen in 27.41% of cases, higher in females (63.83%), most commonly A1 anterior cerebral artery hypoplasia (9.32%). Posterior circulation variations were seen in 46.36% of cases, higher in females (79.25%), most commonly posterior communicating (PCom) artery hypoplasia (25.56%). Combined variations were seen in 26.24% of patients, with higher prevalence in females (73.33%). The prevalence of variations of posterior circulation between male and female patients was statistically significant (P = 0.007) and was higher in females. **Discussion and Conclusion:** This study showed that the most common variations were that of the posterior circulation, most commonly PCom artery hypoplasia. Complete CoW was found in <50% of cases (48.42%).

Keywords: *Circle of Willis, magnetic resonance angiography, three-dimensional time-of-flight magnetic resonance angiography, variations*

Introduction

The circle of Willis (CoW) represents the collateral pathway between large brain-feeding arteries, the knowledge of which is important in interventional and neurosurgical procedures, in the diagnosis and planning of procedures in acute stroke and subarachnoid hemorrhage.[1,2] The two main segments are the anterior collateral (A segment, which includes the internal carotid arteries and their branches) and the posterior collateral (P segment, which includes the posterior cerebral arteries and both posterior communicating [PCom] arteries). Variations of the CoW can be detected using various methods, including noninvasive, noncontrast magnetic resonance angiography (MRA), such as three-dimensional (3D) time-of-flight (TOF) MRA.

Material and Methods

The study was conducted as a retrospective study at the Center for imaging Diagnostics, Oncology Institute of Vojvodina, Sremska Kamenica, Serbia. Magnetic resonance imaging scans of 665 patients of both sexes, acquired during 2018 and 2019, were evaluated. The only inclusion criterion was that 3D TOF MRA was performed during the scan. The exclusion criterion was the presence of vascular pathology that could cause misinterpretation. The research was approved by the Ethics Committee of the Oncology Institute of Vojvodina.

To evaluate the morphology of the CoW [Figure 1], 3D TOF MRA was used. Acquisition was performed using two clinical scanners: 1.5T (Siemens Aera, Erlangen, Germany) and 3T (Siemens Trio Tim, Erlangen, Germany). The patients were in the supine position during acquisition. The standard protocol of the

How to cite this article: Đevukaj M, Nosek I, Vuković M, Kozić D. Variations of the circle of Willis determined via magnetic resonance angiography: A single-center analysis of the Serbian population. J Anat Soc India 2022;XX:XX-XX.

Article Info

Received: 01 May 2020
Revised: 23 November 2021
Accepted: 03 April 2022
Available online: ***

Address for correspondence:
Dr. Igor Nosek,
Hajduk Veljkova 3, Novi Sad 21000, Serbia.
E-mail: igor.nosek@mf.uns.ac.rs

Access this article online

Website: www.jasi.org.in
DOI: 10.4103/JASI.JASI_78_20
Quick Response Code:

Center for Imaging Diagnostics was utilized, with the following parameters:

a. 3T: Repetition Time and Time to Echo (TR/TE) 22/3,86 ms; flip angle 18°, voxel size 0.8 mm × 0.5 mm × 0.7 mm; field of view (FOV) 210 mm, slice thickness 0.65 mm. Total protocol duration: 6 min, 8 s
b. 1.5T: TR/TE 25/7 ms; flip angle 25°, voxel size 0.6 mm × 0.6 mm × 0.6 mm; FOV 207 mm, slice thickness 0.6 mm. Total protocol duration: 6 min, 53 s.

Patients were divided into three groups: those with variations of the anterior collateral segment, and those with variations of the posterior collateral segments, and those with no apparent variations. Anterior segment variations included azygos anterior cerebral artery (ACA) [Figure 2], ACA trifurcation, ACA fenestration, hypoplasia of the A1 segment of ACA, aplasia of the A1 segment of ACA [Figure 3], and anterior communicating (ACom) artery hypoplasia and aplasia. The variations of the posterior segment included hypoplasia and aplasia of the posterior cerebral artery (PCA) [Figure 4], as well as hypoplasia and aplasia of the PCom artery [Figure 5].

Further divisions were made based on the potential collateral pathway formation, where three further groups were made: complete, partially complete, and incomplete CoW. Complete CoW group consisted of patients who did not have variations in either the anterior or posterior segments. Partially complete CoW group consisted of patients with a variation in either the anterior or posterior segments, while the incomplete CoW group consisted of patients with variations in both anterior and posterior segments. Complete COW was assumed in patients who had azygos ACA, ACA trifurcation, ACA fenestration, and A1 ACA hypoplasia, as well as hypoplasia of the P1 segment of PCA and PCom. The presence of variations was assessed visually. Hypoplasia of a given segment or artery was noted when the contralateral segment or artery was of significantly greater caliber. Aplasia was noted in cases where the given segment or artery were not detectable on the acquired scans.

Results

A total of 665 patients were included in the study, of which there were 471 females and 194 males. The study included

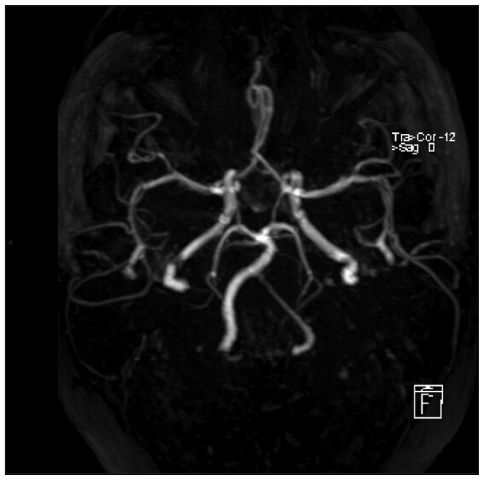

Figure 1: Normal, complete circle of Willis

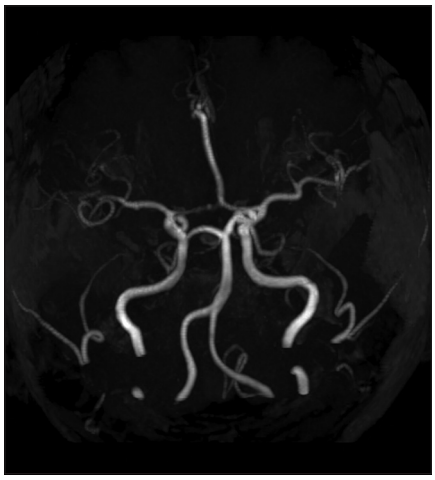

Figure 2: Azygos anterior cerebral artery

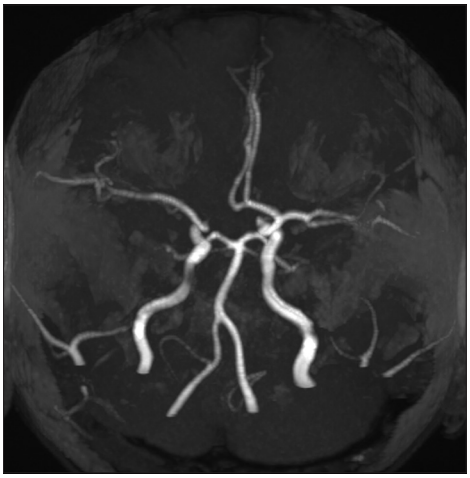

Figure 3: Aplasia of the A1 segment of the right anterior cerebral artery

Figure 4: Aplasia of the P1 segment of the right posterior cerebral artery

patients from 2 to 85 years old (51.986 ± 2 standard deviation).

Variations of the CoW were detected in 252 female patients (out of 471) and 91 male patients [out of 194, Figure 6]. The incidence of variations did not significantly differ between genders ($P = 0.122$).

The complete CoW was detected in 322 patients (48.42%), of which 103 (31.99%) were male and 219 (68.01%) were female. Partially complete CoW was detected in 253 patients (38.05%), 67 (26.48%) of which were male and 186 (73.52%) female. Incomplete CoW was detected in 90 (13.53%) patients, 24 (26.67%) males and 66 (73.33%) females, as seen in Figure 7.

Anterior collateral segment variations

Variations of the anterior collateral segment were detected in 94 (27.41%) patients. This group consisted of 34 (36.17%) male and 60 (63.83%) female patients, as shown in Figure 8. The difference in incidence of anterior circulation variations between men and women was not significant ($P = 0.107$).

The most common type of anterior collateral segment variation was hypoplasia of the A1 segment of the ACA (prevalence of 9.32%), which was more common in female patients (59.68% vs. 40.32%). The least common type of anterior collateral segment variation was azygos ACA (prevalence of 0.9%), which was only detected in female patients. The prevalence of different anterior collateral segment variations is observed in Table 1.

Posterior collateral segment variations

The most common posterior collateral segment variation was hypoplasia of the PCom artery, with a prevalence of 25.56%, and was more frequently observed in female patients (74.71%), than in male (25.29%). The least common variation was aplasia of the posterior cerebral artery, with a prevalence of 2.26%, which was also more common in female patients (80%). The prevalence of different posterior collateral segment variations is observed in Table 2.

Simultaneous anterior and posterior collateral segment variations were detected in 90 (26.24%) patients, of

Figure 5: Aplasia of the right posterior communicating artery

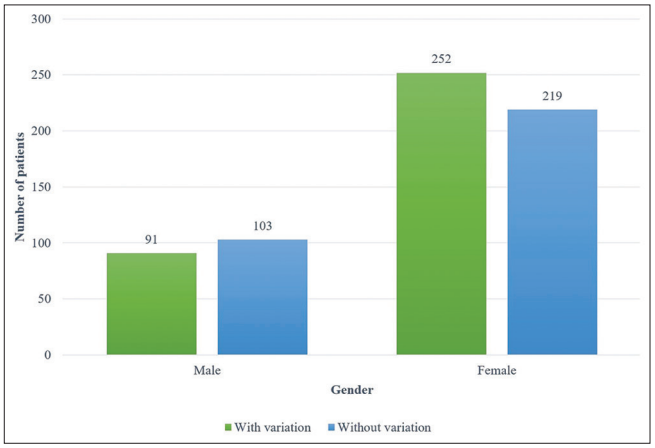

Figure 6: The number of male and female patients with and without the presence of a variation of CoW, COW: Circle of Willis

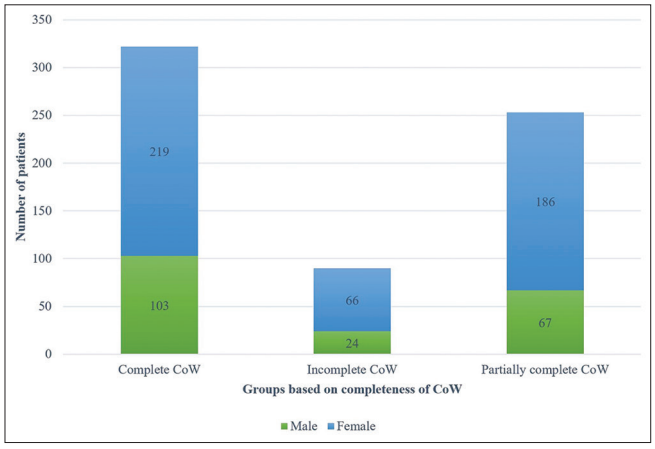

Figure 7: The distribution of patients concerning gender and completeness of CoW, COW: Circle of Willis

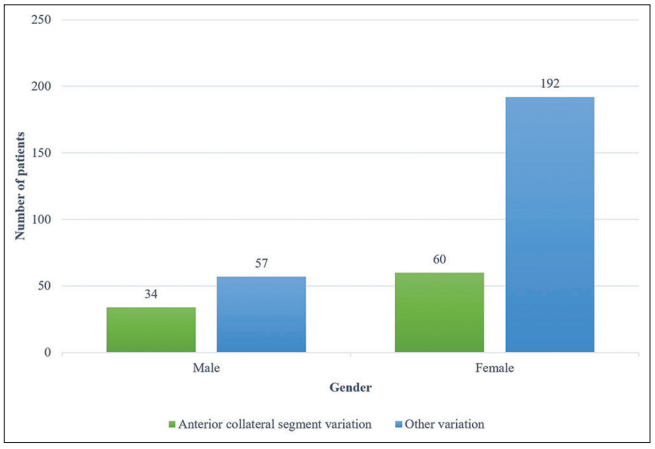

Figure 8: Anterior collateral segment versus other variation, divided by gender

Table 1: The number of patients and prevalence of anterior collateral segment variations

Types	Azygos ACA (%)	ACA trifurcation (%)	ACA fenestration (%)	ACom Aplasia (%)	A1 ACA hypoplasia (%)	A1 ACA aplasia (%)
Male	0 (0.00)	16 (8.25)	1 (0.52)	13 (6.70)	25 (12.89)	8 (4.12)
Female	6 (1.27)	29 (6.16)	7 (1.49)	41 (8.70)	37 (7.86)	12 (2.55)
Total	6 (0.90)	45 (6.77)	8 (1.20)	54 (8.12)	62 (9.32)	20 (3.01)

ACA: Anterior cerebral artery, ACom: Anterior communicating artery

Table 2: The number of patients and prevalence of posterior collateral segment variations

Types	PCA hypoplasia (%)	PCA aplasia (%)	PCom hypoplasia (%)	PCom aplasia (%)
Male	20 (10.31)	3 (1.55)	43 (22.16)	7 (3.61)
Female	64 (13.59)	12 (2.55)	127 (26.96)	25 (5.31)
Total	84 (12.63)	15 (2.26)	170 (25.56)	32 (4.81)

PCA: Posterior cerebral artery, PCom: Posterior communicating artery

which 24 (26.67%) were male and 66 (73.33%) were female [Figure 9]. The difference in incidence of simultaneous variations was not significantly different between genders (P = 0.574).

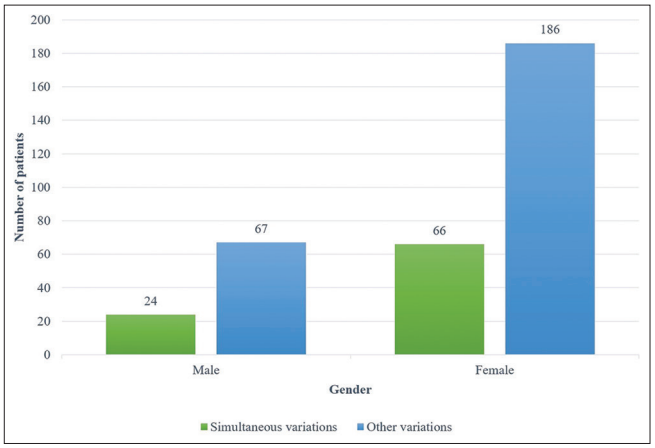

Figure 9: Simultaneous anterior and posterior segment variations, divided by gender

Discussion

The CoW is the main arterial collateral pathway which provides blood supply to the brain.[3] Collateral blood supply enables adequate perfusion of the brain in the vascular territory of affected arteries in patients who have reduced blood flow through the basilar or internal carotid arteries.[4] Knowledge of the variations of the CoW is important in interventional and neurosurgical procedures, as well as in diagnosis and planning in acute stroke and subarachnoid hemorrhage.[1-6]

Various modalities have been used to detect CoW variations, including CT angiography, as well as MRA, which was utilized in this study. The most sensitive, noninvasive method for detecting variations of the COW was shown to be MRA, except in the case of the PCom artery.[5-8]

The evaluation of the CoW in this study showed that 48.42% of the patients had a complete CoW, which was more prevalent in women (68.01%). A study conducted by Kapoor *et al*. showed similar results, where the prevalence of the complete CoW was 45.2% and also higher in women (prevalence of 53.2%).[9] Other studies have shown that the prevalence of complete CoW was far lower, detected in 27% and 28% of patients, respectively.[7] On the other hand, other studies have found complete CoW in 89.7% of patients.[10] The great disparity in prevalence of complete CoW among these different studies could be related to the number of patients included in each study, the demographic differences between patient groups, as well as the modality used to detect variations.

The prevalence of partially complete CoW was 38.05%, again more common in women (73.52%), which is in accordance with results published in other studies, where the prevalence of partially complete CoW was detected in around 38% of cases.[4,7] Incomplete CoW was found in 13.53% of patients, which other studies have linked to migraine in certain patients, as well as an increased risk of stroke.[3,11,12]

Variations of the anterior collateral segment were detected in 27.41% of cases, opposed to 34% in a study conducted by Zaki *et al*.[7] The most common type of variation of this segment was hypoplasia of the A1 segment of the ACA, which is in contrast to numerous other studies that have shown that the most common anterior collateral segment variation was the hypoplasia or aplasia of the ACom artery.[4,7,13]

Variations of the posterior collateral segment were detected in 46.36% of patients, more commonly in women (79.25%). A study conducted by Zaki *et al*. concluded that the prevalence of posterior collateral segment variations was 38%. However, these variations were more prevalent in men (64%).[7] Variations of the posterior collateral segment were the most common type of variation, as was reported by other studies.[7,14] The most common type of variation was hypoplasia of the PCom artery (25.56%, more common in women 74.71%). This type of variation was also the most common posterior collateral segment variation in the study by Zaki *et al*., yet it was more prevalent in men – 75%.[7] This type of variation has been linked with increased risk of stroke.[7,15]

Conclusion

The results of this study show that the complete Circle of Willis was present in only 48.42% of patients. The prevalence

of variations of the circle of Willis was 51.58% in total, without statistically significant difference between men and women (46.90% vs 53.50%, *P*=0.122). The most common variations of the Circle of Willis were that of the posterior collateral segment, with the most prevalent variation being AcomP hypoplasia. Collateral blood supply enables adequate perfusion of the brain in the vascular territory of affected arteries in patients who have reduced blood flow through the basilar, or internal carotid arteries. Knowledge of the variations of the circle of Willis is important in interventional and neurosurgical procedures, as well as in diagnosis and planning in acute stroke, and subarachnoid hemorrhage.

Financial support and sponsorship

Nil.

Conflicts of interest

There are no conflicts of interest.

References

1. Hoksbergen AW, Majoie CB, Hulsmans FJ, Legemate DA. Assessment of the collateral function of the circle of Willis: Three-dimensional time-of-flight MR angiography compared with transcranial color-coded duplex sonography. AJNR Am J Neuroradiol 2003;24:456-62.
2. Hoksbergen AW, Legemate DA, Csiba L, Csáti G, Síró P, Fülesdi B. Absent collateral function of the circle of Willis as risk factor for ischemic stroke. Cerebrovasc Dis 2003;16:191-8.
3. Manojlović V. Significance of carotid endarterectomy in asymptomatic patients with incomplete collateralisation within circle of Willis [dissertation]. Novi Sad (Serbia): University of Novi Sad; 2015.
4. Maaly MA, Ismail AA. Three dimensional magnetic resonance angiography of the circle of Willis: Anatomical variations in general Egyptian population. Egypt J Radiol Nucl Med 2011;42:405-12.
5. Shatri J, Cerkezi S, Ademi V, Reci V, Bexheti S. Anatomical variations and dimensions of arteries in the anterior part of the circle of Willis. Folia Morphol (Warsz) 2019;78:259-66.
6. Yeniçeri IÖ, Çullu N, Deveer M, Yeniçeri EN. Circle of Willis variations and artery diameter measurements in the Turkish population. Folia Morphol (Warsz) 2017;76:420-5.
7. Zaki SM, Shaaban MH, Abd Al Galeel WA, El Husseiny AA. Configuration of the circle of Willis and its two parts among Egyptian: A magnetic resonance angiographic study. Folia Morphol (Warsz) 2019;78:703-9.
8. Ghazali RM, Shuaib IL. Comparison between 3D TOF magnetic resonance angiography and intraarterial digital subtraction angiography in imaging the circle of Willis. Malays J Med Sci 2003;10:37-42.
9. Kapoor K, Singh B, Dewan LI. Variations in the configuration of the circle of Willis. Anat Sci Int 2008;83:96-106.
10. Tanaka H, Fujita N, Enoki T, Matsumoto K, Watanabe Y, Murase K, *et al*. Relationship between variations in the circle of Willis and flow rates in internal carotid and basilar arteries determined by means of magnetic resonance imaging with semiautomated lumen segmentation: Reference data from 125 healthy volunteers. AJNR Am J Neuroradiol 2006;27:1770-5.
11. van Seeters T, Hendrikse J, Biessels GJ, Velthuis BK, Mali WP, Kappelle LJ, *et al*. Completeness of the circle of Willis and risk of ischemic stroke in patients without cerebrovascular disease. Neuroradiol 2015;57:1247-51.
12. Henry BM, Roy J, Ramakrishnan PK, Vikse J, Tomaszewski KA, Walocha JA. Association of migraine headaches with anatomical variations of the circle of Willis: Evidence from a meta-analysis. Neurol Neurochir Pol 2015;49:272-7.
13. Ravikanth R, Philip B. Magnetic resonance angiography determined variations in the circle of Willis: Analysis of a large series from a single center. Ci Ji Yi Xue Za Zhi 2019;31:52-9.
14. Karatas A, Yilmaz H, Coban G, Koker M, Uz A. The anatomy of circulus arteriosus cerebri (Circle of Willis): A study in turkish population. Turk Neurosurg 2016;26:54-61.
15. Chuang YM, Liu CY, Pan PJ, Lin CP. Posterior communicating artery hypoplasia as a risk factor for acute ischemic stroke in the absence of carotid artery occlusion. J Clin Neurosci 2008;15:1376-81.

Original Article

The Normal Vermiform Appendixin Adults: Its Anatomical Location, Visualization, and Diameter at Computed Tomography

Abstract

Introduction: The anatomic location of the appendiceal tip is not certain and it may extend to the retrocecal, pelvic, subcecal, paracecal, postileal, or preileal positions. Its positional variations may alter the degree of inflammation and lead to further illness diagnoses such as colitis, ureteric colic, or pelvic inflammatory disease. Increase in appendiceal diameter is very important regarding the diagnosis of appendicitis. Therefore, the determination of cut-off values for normal appendiceal diameter in computed tomography (CT) would aid in ruling out appendicitis in suspected cases. We aimed in this study to evaluate the frequency of visualization and determine the location and diameter of the normal appendix on CT. **Material and Methods:** We scanned 1842 abdominal CT that were performed in our hospital for any reason, retrospectively. A total of 597 patients were excluded with various indications. **Results:** Lower-upper abdominal CT examinations of a total of 1245 patients were evaluated, and the appendix could be visualized in 984 patients (79%). The appendiceal diameter was ranged between 2.7 mm and 10 mm and it was >6 mm in 19% of the patients. The most common location of the appendiceal tip was pelvic in 318 (32%) appendices. The appendiceal tip was subcecal in 222 (23%), retrocecal in 180 (18%), postileal in 180 (18%), preileal in 54 (6%), and paracaecal in 30 (3%) appendices. **Discussion and Conclusion:** This study showed that the most frequent location of the normal appendix is pelvic type both in women and men.

Keywords: *Computed tomography, location, variation, vermiform appendix*

Aysegul Altunkas, Fatma Aktas, Zafer Ozmen, Eda Albayrak, Osman Demir[1]

Departments of Radiology and [1]Statistics, Faculty of Medicine, Gaziosmanpasa University, Tokat, Turkey

Introduction

The vermiform appendix is a tube-shaped muscular organ localized to the right lower abdominal quadrant, which contains an abundance of microscopic lymphoid tissue.[1] Its length varies from 2 to 20 cm and is 9 cm on average. It stems from the posteromedial wall of the cecum 2 cm below the ileocecal junction, or closer to it.[2] Appendix is connected to a peritoneal fold called the mesoappendix, which carries its own arterial structures, and the length of this mesenteric structure differs according to sex and age.[3] The inadequacy of mesoappendix to supply the tip of the organ may lead to early perforation of this part in case of inflammation.

The vermiform appendix is the only organ in the human body that has an indefinite anatomical position. Its ultimate location is influenced by the changes occurring in the cecum during its growth and development.[4] Since anterior and lateral walls of the cecum grow faster during its development, the orifice of the vermiform appendix is often localized at the posteromedial side of the cecum. The tip of the appendix may be found in any one of the following positions retrocecal, pelvic, subcecal, paracecal, postileal or preileal.[5]

Localization of the appendix has been a topic of interest, not only because of its developmental significance but also because of its pathological and surgical importance. Location of vermiform appendix is important in terms of diagnosis and prognosis of appendicitis, and the surgical approach to it. Variations in its position may alter the degree of inflammation, and clinical presentation of appendicitis as well. Indeed, retrocecal appendicitis may mimic colitis; postileal appendicitis may mimic ureteric colic, pelvic inflammatory disease, and ovarian cyst torsion; and subhepatic appendicitis may mimic hepatitis and biliary colic. Misdiagnosis rates are 10%–33% in various age groups.[6] Thus, awareness of the positional variations of appendix may prevent misdiagnosis.

How to cite this article: Altunkas A, Aktas F, Ozmen Z, Albayrak E, Demır O. The normal vermıform appendıxın adults: ıts anatomıcal locatıon, vısualızatıon, and dıameter at computed tomography. J Anat Soc India 2022;XX:XX-XX.

Article Info

Received: 20 September 2019
Accepted: 21 December 2021
Available online: ***

Address for correspondence:
Prof. Aysegul Altunkas, Department of Radiology, Faculty of Medicine, Gaziosmanpasa University, Tokat, Turkey.
E-mail: aaltunkas@hotmail.com

Access this article online

Website: www.jasi.org.in
DOI: 10.4103/JASI.JASI_135_19
Quick Response Code:

Various studies have shown differences between populations in terms of appendix position.[7] These studies have often been conducted on either autopsied bodies or cadavers or by evaluating patients undergoing surgical operation. A careful review of the studies related to the localization of the appendix reveals some methodological errors. Following death, all muscles in the body, including the smooth muscles of the intestines display some changes such as primary flaccidity, rigor mortis, and secondary flaccidity.[8] Furthermore, the formaldehyde that is used for cadaveric fixation has a shrinking and distorting effect on tissues.[9] Considering the effects of these postmortem changes and formaldehyde fixation on the internal organs, data from the autopsy and cadaveric studies related to localization of appendix have limited credibility. On the other hand, surgical studies have usually determined appendix localization in patients undergoing appendectomy. Since appendix is swollen (edematous) in patients with appendicitis, and therefore, can be displaced with gravity, it is obvious that surgical studies cannot provide accurate data on normal appendix position. For this reason, it is very important to establish the normal position of appendix in living and healthy individuals intraabdominal via radiological studies.

Demonstration of the normal appendix in computed tomography (CT) would aid to rule out the diagnosis of appendicitis in suspicious cases.[10] For this reason, studies that evaluate normal appendix with radiological examinations have great clinical significance. While there are many studies that were conducted to establish CT criteria for appendicitis, studies that evaluate normal appendix with CT images are few and show contradicting results. Apart from the study by Lee *et al*.,[11] these studies were generally conducted on small sample sizes. Therefore, we have designed our study to include the largest number of participants. In addition, apart from the studies by Picken *et al*.[12] and Lee *et al*., the classification of appendix locations in all other radiological studies do not allow comparison with the classical classification system commonly used in anatomical, autopsy, and surgical studies.

The aims of our study were: (1) to evaluate the frequency of visualization of the normal appendix on CT, (2) to determine the location and diameter of the normal appendix, (3) to assess whether gender, age, or administration of contrast material (IV, IV + oral) before CT examination had any influence on these parameters.

Material and Methods

Study population and design

This research received approval from our institution's Clinical Research Ethics Committee. In our study, which has a retrospective study design, we scanned 1842 abdominal CT examinations that were performed in our hospital from January 2014 to January 2015 for any reason [Figure 1]. Pediatric patients and patients with appendicitis or any other intraabdominal pathology (ascites, abscess, postoperative early period, etc.) were not included in the analysis. After exclusion of 597 patients, lower-upper abdominal CT examinations of 1245 patients were evaluated, and appendix could be visualized in 984 patients (417 female, 567 male; age range: 18–89 years; mean age: 51 ± 16 years). For those patients, whose appendix could not be visualized, patient record system was investigated to determine whether these patients had a previous appendectomy operation. If there was no information available on the system, patients were phoned to retrieve this information. Thus, a total of 984 patients whose appendix could be visualized were accepted as having normal appendix, and appendiceal diameter and localization were evaluated in these patients.

Computed tomography examination and image analysis

All evaluations were performed with spiral CT (LightSpeed Ultra; GE, Milwaukee, United States), using a section thickness of 5 mm, intersection gap of 5 mm, and pitch of 0.875:1. In all scans, 120 kVp and 100 mA values were selected. The scans were performed in the supine position, starting from a level above the liver to the end of the urinary bladder, while patients holding their breath. In some patients, intravenous (IV) and oral contrast agents were administered. Oral contrast agent (1000–1500 mL; 2% barium suspension) was given approximately 1 h before the scan. IV contrast agent (120 mL; nonionic contrast substance) was administered as IV bolus injection, with a rate of 2 mL/s. Of all the examinations included in the study, 38% (390) were without contrast administration, 32% (322) were with IV contrast administration, and 30% (295) were with IV + oral contrast administration. None of the patients received rectal contrast administration. While axial images were the source images, multiplanar reformat images were also used.

Picture Archiving Communication Systems network was used for localizing appendix and measuring its thickness.

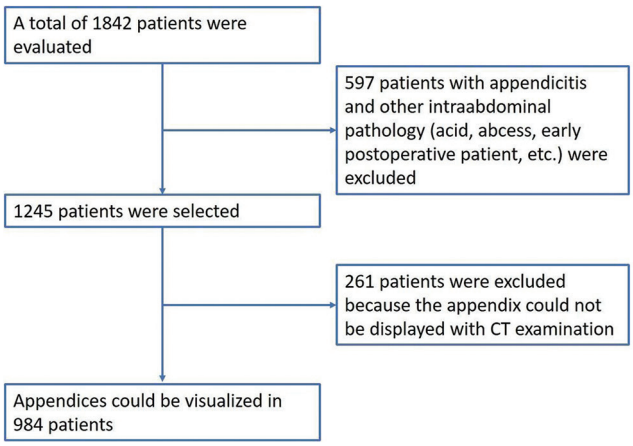

Figure 1: The study flowchart

CT scans were retrospectively evaluated by two radiologists with more than 10 years of experience in abdominal imaging. For patients, whose appendix could be visualized, appendix thickness and location were noted. In the absence of intraluminal content in appendix, appendiceal thickness was measured as the double wall thickness. In the presence of intraluminal content, measurement was performed from one wall to the other (maximum full-thickness) [Figure 2]. Appendix localization was classified based on the position of the tip of the appendix. Accordingly, appendix was classified as "retrocecal" if the tip of appendix was localized posterior to the cecum, "subcecal" if the was localized inferior to the cecum, "paracecal" if the tip was localized lateral to the cecum, "pelvic" if the tip extended to the pelvis, "postileal" if the tip was localized posterior to the ileum, and "preileal" if the tip was localized anterior to the cecum.

Statistical analysis

Statistical analyses were performed using the SPSS package program (IBM-SPSS 20, Chicago). Data were expressed as mean ± standard deviation. The association of visualization and localization frequency of appendix with sex and contrast administration was analyzed with Chi-square test. Comparisons between different sexes and contrast and noncontrast groups in terms of appendiceal diameter were made with Student's *t*-test. $P < 0.05$ was accepted as statistically significant.

Results

The appendix was visualized in 79% (984/1245) of the patients. This rate was 76% (417/551) in females and 82% (567/694) in males, and there was no significant difference between the different sexes in terms of visualization rate of appendix ($P = 0.712$). In addition, appendix visualization rate did not show a significant difference in comparison to noncontrast, IV contrast and IV + oral contrast CT scans ($P = 0.227$).

Mean appendiceal diameter was 5.28 ± 0.99 mm (ranged between 2.7 and 10 mm) [Table 1 and Figure 3]. Appendiceal diameter was >6 mm in 19% of the patients (female: 18%; male: 20%) [Figure 4]. Mean appendiceal diameter was 5.24 ± 1.01 mm in females and 5.31 ± 0.97 mm in males. Appendiceal diameter did not show a significant difference between different sexes or groups based on contrast administration ($P = 0.147$ and $P = 0.212$, respectively).

Table 1: Diameter of the normal appendix on computed tomography

	Mean±SD	Minimal	Maximal
Male (*n*=567)	5.31±0.97	2.7	10
Female (*n*=417)	5.24±1.01	2.9	8,9
Total (*n*=984)	5.28±0.99	2.7	10

SD: Standard deviation

In all patients, the most common location of the appendiceal tip was pelvic in 318 (32%) of 984 appendices. The appendiceal tip was subcecal in 222 (23%), retrocecal in 180 (18%), postileal in 180 (18%), preileal in 54 (6%) and paracaecal in 30 (3%) appendices [Table 2], [Figures 5 and 6]. Location of appendix did not show significant difference between sexes, or groups based on contrast administration ($P = 0.349$ and $P = 0.285$, respectively). The differences between the relative frequency of the male and female subgroups for different appendix locations were as follows: pelvic (male: 29%

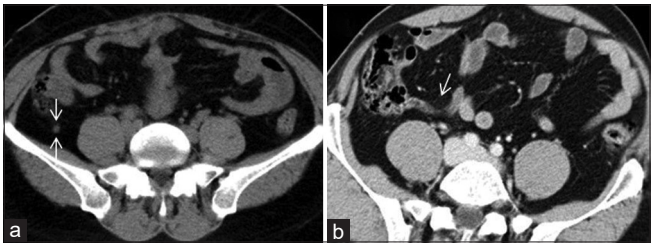

Figure 2: (a) The appendiceal diameter (arrow) was determined by measuring the double wall thickness, since the intraluminal content was not recognizable. (b) If content was recognizable, the maximum full thickness (arrow) was measured and it was accepted as diameter

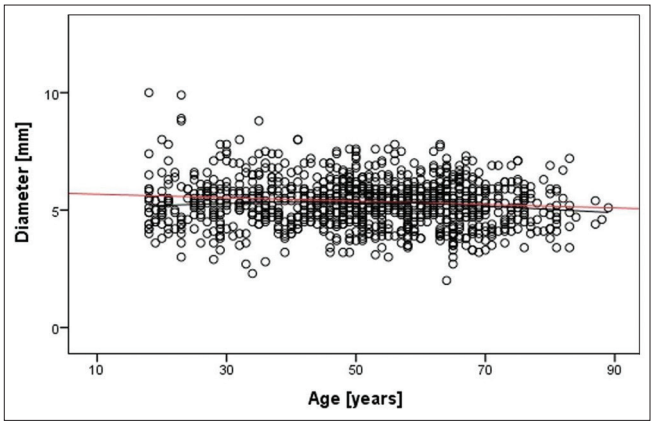

Figure 3: Scatter diagram showing statistically significant but low-degree negative correlation between the age of the subject and the diameter ($r = 0.129$, $P = 0.002$)

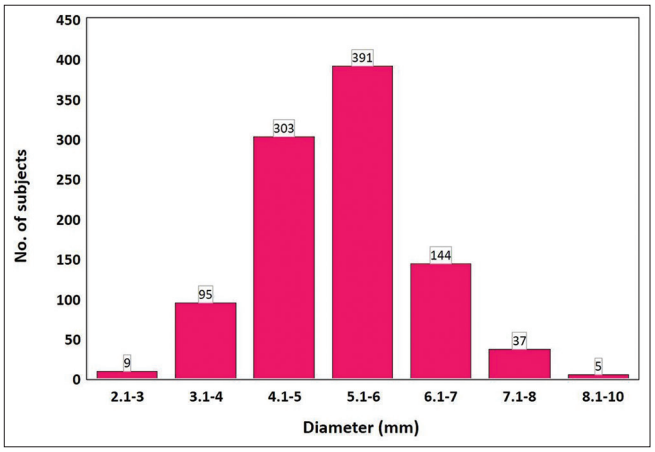

Figure 4: Frequency distribution of the diameter of the normal appendix

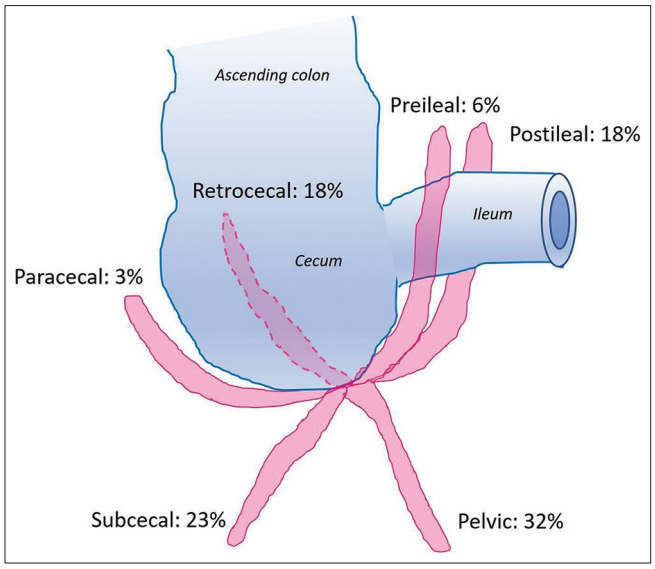

Figure 5: Locations and relative frequencies of the normal appendix

Table 2: Location of the appendiceal tip according to gender

	All subjects	Male	Female	*P**
Pelvic	318 (32)	165 (29)	153 (37)	0.325
Subcecal	222 (23)	136 (24)	86 (20)	0.655
Retrocecal	180 (18)	114 (20)	66 (16)	0.505
Postileal	180 (18)	103 (18)	77 (18)	1.000
Preileal	54 (6)	35 (6)	19 (5)	0.808
Paracecal	30 (3)	14 (3)	16 (4)	0.537
Total	984 (100)	567 (100)	417 (100)	

*Between the male and female

vs. female: 37%, $P = 0.325$); subcecal (male: 24% vs. female: 20%, $P = 0.655$); retrocecal (male: 20% vs. female: 16%, $P = 0.505$); postileal (male: 18% vs. female: 18%, $P = 1.000$); preileal (male: 6% vs. female: 5%, $P = 0.808$); and paracaecal (male; 3% vs. female; 4%, $P = 0.537$) [Table 2].

Discussion

CT is currently the main imaging method used to assess patients with acute appendicitis. Only 60% of appendicitis cases have clinical manifestations, and pelvic pathologies can mimic acute appendicitis; therefore, if the diagnosis is based on clinical findings alone, it is likely to get quite high negative appendectomy rates, reaching rates around 20% especially in women.[13-16] Utilization of CT examinations for diagnosis of appendicitis has made ruling out the other causes of acute abdomen easier and significantly reduced the negative appendectomy rates.[17]

Diagnostic CT criteria for acute appendicitis include appendiceal diameter over 6 mm, demonstration of calcified appendicolith, and observation of periappendiceal inflammatory changes.[18] In their study, Jacobs *et al*.[19] reported that, in their CT scans, 22% of patients

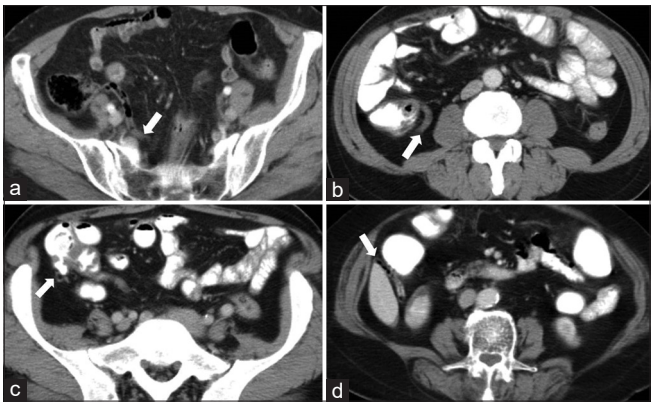

Figure 6: Computed tomography scans of different locations of the appendiceal tip. Axial image shows an appendix extends into the pelvis (a), paracecal (b) and posteriorof the terminal ileum (c). Axial image demonstrates a retrocecal appendix is located posterior to the cecum (d)

with appendicitis did not show stranding sign that is formed by periappendiceal inflammatory changes and the surrounding fat tissue. Moreover, "periappendiceal fat stranding" in CT can be observed in 3%–7% of normal individuals.[20] In addition to these, appendicolith is not only observed in appendicitis cases but can also be detected in 2%–8% of normal individuals.[21-23] Therefore, measurement of appendiceal diameter is very important regarding the diagnosis of appendicitis, and previous studies have shown that increase in appendiceal diameter is the most sensitive and specific diagnostic criteria.[24] However, the established cut-off values for normal appendiceal diameter are based on the diagnostic criteria determined by ultrasonography (USG) studies.[25-27]

During USG examination, the lumen is often obliterated due to the compression exerted on the anterior abdominal wall. For this reason, many researchers believe that USG criteria cannot be adapted to CT images. In our study, appendiceal diameter was measured as the maximum outer diameter, and 19% of the study participants had appendiceal diameters over 6 mm. Other studies that evaluated appendix with CT also reported that 17%–59% of healthy individuals had appendiceal diameter over 6 mm.[28,29] Due to these high rates observed in normal individuals, the researchers noted that it was necessary to raise the upper limit of normal appendiceal diameter from 6 mm to 10 mm.[30,31] Consistent with this proposal, normal appendiceal diameter was not over 10 mm in any of our cases. Furthermore, only 5 cases (0.5%) in our study had an appendiceal diameter over 8 mm. Our findings indicate that in case the appendiceal diameter is measured using the maximal outer diameter method in CT examination, a cut-off measurement value of 8 mm can be used conveniently for discriminating between normal appendix and appendicitis. Nonetheless, since 0.5% of normal individuals have appendiceal diameter above 8 mm, relying on appendiceal size measurement alone without consideration of clinical and laboratory findings

for the diagnosis of appendicitis may lead to misdiagnosis and wrong treatment.

Demonstration of normal appendices in CT would aid in ruling out appendicitis in suspected cases. This is especially the case for patients who are suspected to have appendicitis but in fact have another abdominopelvic pathology as the cause of patient's symptoms. In these patients, the picture is further complicated if this alternative etiology does not reveal any signs in CT. In such complicated cases, demonstration of normal appendix in CT would direct the physician away from the diagnosis of appendicitis, and guide him/her for further examination aimed at the alternative etiology. Therefore, it is very important to have knowledge about the appearance, location, size, visualization rate, and other characteristics of the normal appendix in CT scan.[32] A review of the studies related to the visualization rate of the normal appendix in CT shows us that this rate has displayed a profound increase in parallel with the advances in CT technology over the years. Normal appendix can be visualized in the rates of 40%–50% with conventional CT,[33,34] 70%–80% with spiral CT[35,36] and up to 90%–95% with multidetector CT (MDCT).[37] In our study, appendix could be visualized in 79% of normal individuals without appendicitis, which is a consistent finding with the previous spiral CT studies.

Oral and/or IV contrast administration is frequently used in CT examination to aid in the visualization of normal appendix and diagnosis of appendicitis.[38] It was believed that oral contrast administration would opacify the appendiceal lumen and IV contrast agent would make the appendiceal wall more recognizable so that it would be easier to visualize appendix, particularly in normal individuals. However, results from the related studies do not support this view. In our study, we found that contrast administration in spiral CT did not cause a change in visualization rate of the normal appendix. Similarly, studies using either conventional or MDCT did not find any effect of IV or oral contrast administration on visualization rate of appendix. There are several disadvantages to oral contrast administration. It causes delayed transit times of up to 4 h; the appendiceal lumen can be filled only in a portion of patients; and its tolerability is low because it requires a large volume such as 1400 mL, and it causes nausea. On the other hand, IV contrast administration can lead to adverse effects (e.g., allergic reactions) at a rate of 0.5%–4%, and brings an additional cost as well.[39,40] For this reason, there is a tendency toward the use of noncontrast CT scan today.

The increased image quality provided by MDCT technology renders contrast administration less and less preferable.[41] A review of studies on contrast and noncontrast (unenhanced) MDCT examinations shows that visualization rates are similar with both, which supports this view. Although MDCT is becoming increasingly available, spiral CT is still used commonly, and it is still the most frequently used CT in many countries.[42] Therefore, it is very important to determine whether contrast administration is necessary with spiral CT for visualization of normal appendix, and thus, ruling out the diagnosis of appendicitis. Considering the uncontrollable factors (patient characteristics, scanning protocol, radiologist's experience, etc.) in our study, further studies are necessary to confirm our results regarding contrast administration.

In our study, we did not find a significant difference between male and female sex in terms of visualization rate of the normal appendix. Negative appendectomy rates are reported to be twice as higher in women than in men (23% vs. 12%) because gynecological pathologies can mimic acute appendicitis. Therefore, visualization of the normal appendix is particularly important in women for ruling our appendicitis. Among previous studies related to visualization of the normal appendix, only four studies have examined the difference between female and male sex. Similar to our results, three of them did not find any difference between the sexes, whereas one study reported lower visualization rate in women.[43,44] Our study includes a larger sample size, which is considered as a strength of our study, increasing the credibility of our results. In light of our findings, CT examination in women for ruling out the diagnosis of appendicitis is as effective as in men.

If we categorize the previous studies examining the appendix location as anatomical (cadaveric), radiological, surgical, autopsy, and mixed studies, we see that retrocecal position was the most frequent location in all the anatomical studies [Tables 3 and 4]. Anatomical studies use cadavers that are prepared in formalin (PF-Cadavers), and formaldehyde has shrinking and distorting effects on tissues; therefore, appendix position may be altered in these studies. Because of this bias, the credibility of the results from anatomical studies has dwindled. Similar to the effect of formaldehyde, due to the postmortem changes (primary flaccidity, rigor mortis, and secondary flaccidity) encountered in autopsy studies and edematous changes secondary to appendicitis encountered in the surgical studies, it is difficult to generalize the results of these studies to the general population, i.e., appendix in a healthy human.

Our literature review yielded totally four mixed type studies evaluating PF-Cadavers, autopsied bodies, and operated patients together [Table 4]. Although these mixed-type studies presented no information on the percentage of PF-Cadavers among the total number of subjects evaluated, a bias caused by formaldehyde use is also apparent in these studies, as the most frequent appendix position was retrocecal.[45-47] Among the mixed type of studies, the study by Wakeley[48] stands out with its large sample size, which

Table 3: Major locations of the vermiform appendix reported in autopsy and cadaveric studies

Author(s)	Year	Country	Number of subjects	Type of study	Major location (%)
Solanke[7]	1970	Nigeria	203	Autopsy	Retrocecal (38)
Delić *et al*.[55]	2002	Bosnia and Herzegovina	50	Autopsy	Retrocecal (38)
Ndoye *et al*.[56]	2005	Senegal	80	Autopsy	Pelvic (50)
Clegg-Lamptey *et al*.[57]	2006	Ghana	1,358	Autopsy	Retrocecal (67)
Rahman *et al*.[58]	2006	Bangladesh	100	Autopsy	Pelvic (47)
Paul *et al*.[59]	2009	Bangladesh	60	Autopsy	Retrocecal (65)
Tofighi *et al*.[60]	2013	Iran	400	Autopsy	Pelvic (56)
Bakar *et al*.[61]	2013	Bangladesh	56	Autopsy	Retrocecal (54)
Ghorbani *et al*.[62]	2014	Iran	200	Autopsy	Pelvic (55)
El-Amin *et al*.[63]	2015	Sudan	60	Autopsy	Retrocecal (60)
de Souza *et al*.[64]	2015	Brazil	377	Autopsy	Retrocecal (44)
Ajmani and Ajmani[65]	1983	India	100	PF-Cadaveric	Retrocecal (58)
Gómez *et al*.[66]	2009	Colombia	100	PF-Cadaveric	Retrocecal (41)
Banerjee *et al*.[67]	2012	India	25	PF-Cadaveric	Retrocecal (68)
Setty and Katikireddi[68]	2013	India	40	PF-Cadaveric	Retrocecal (50)
Sinha and Kumar[69]	2014	India	50	PF-Cadaveric	Retrocecal (62)
Mwachaka *et al*.[70]	2014	Kenya	48	PF-Cadaveric	Retrocecal (27)
Salwe *et al*.[71]	2014	India	60	PF-Cadaveric	Retrocecal (57)
Patel and Naik[72]	2016	India	50	PF-Cadaveric	Retrocecal (64)
Vidya and Kuberappa[73]	2016	India	28	PF-Cadaveric	Retrocecal (71)

PF: prepared in formalin

Table 4: Major locations of the vermiform appendix reported in surgical, mixed, and radiologic studies

Author(s)	Year	Country	Number of subjects	Type of study	Major location (%)
O'Connor and Reed[74]	1994	United States	129	Surgical	Retrocecal (33)
Varshney *et al*.[75]	1996	United Kingdom	600	Surgical	Pelvic (53)
Golalipur *et al*.[5]	2003	Iran	117	Surgical	Pelvic (33)
Denjalić *et al*.[76]	2009	Bosnia and Herzegovina	65	Surgical	Pelvic (58)
Verdugo and Olave[77]	2010	Chile	65	Surgical	Retrocecal (47)
Ashindoitiang and Ibrahim[78]	2012	Nigeria	80	Surgical	Pelvic (41)
Casado *et al*.[79]	2014	Cuba	236	Surgical	Pelvic (54)
Swargam *et al*.[80]	2015	India	50	Surgical	Retrocecal (44)
Gladstone and Wakeley[45]	1924	United Kingdom	3,000	Autopsy + EC + surgical	Retrocecal (69)
Wakeley[48]	1933	United Kingdom	10,000	Autopsy + EC + surgical	Retrocecal (65)
Iqbal *et al*.[46]	2012	Pakistan	500	Autopsy + EC + surgical	Retrocecal (57)
Manisha *et al*.[47]	2013	India	200	Autopsy + EC	Retrocecal (56)
Picken *et al*.[12]	1993	United Kingdom	79	Radiologic	Postileal (48)
Benjaminov *et al*.[18]	2002	Canada	187	Radiologic	Paracolic (62)
Bursali *et al*.[30]	2005	Turkey	137	Radiologic	Paracolic (64)
Turkoglu *et al*.[23]	2012	Turkey	491	Radiologic	Pelvic (47)
Willekens *et al*.[10]	2014	Belgium	186	Radiologic	Pelvic (66)
Lee *et al*.[11]	2014	Korea	615	Radiologic	Subcecal (43)
Current study	2017	Turkey	984	Radiologic	Pelvic (32)

EC: Endoscopic

included 10,000 individuals. The results of this study have been used as reference in many textbooks, and thus, it became a common opinion that the appendix is usually found in retrocecal position. However, their results become less credible when we consider the effects of cadaveric fixation and postmortem changes occurring in the body. This view is further supported by the fact that none of the radiological studies, including ours, have found retrocecal position as the most frequent location as proposed by Wakeley.

Radiological studies related to the localization of appendix have often used USG, MRI and CT. Retrocecal appendix cannot be evaluated with USG, and excess abdominal fat mass hampers evaluation with USG, which are the main limitations to the utilization of USG.[49] MRI is not a commonly used method due cost-effective reasons, therefore studies that examine appendix position in adults with MRI are quite few. For these reasons, studies on the localization of appendix have often used CT. We also

preferred CT in the present study, and based on the position of the appendiceal tip, we found the most frequent appendix location as pelvic position (32%). Similarly, Turkoglu *et al*. and Willekens *et al*. also found pelvic position as the most frequent location, in the rates of 47% and 66% respectively. Unlike these studies, there are some other CT studies which reported the most frequent appendix position as paracolic, subcecal, or postileal [Table 4].

Methodological differences like the type of the CT used (classical, helical, or multidetector), section thickness and intersection gap, patient groups included in the study, the age range of participants, and whether contrast is administered or not make it difficult to compare our results with the other CT studies. Another factor that complicates the comparison between the studies is that different classification criteria were used for the localization of appendix. While some researchers used their own new classification systems, others preferred to use a modified classification. This makes it impossible to make comparisons between radiological studies and other types of studies in terms of position frequency. Only three CT studies including the present one used a classical classification system that has been commonly used in anatomical and autopsy studies. The most frequent appendix positions found in these three studies were retroileal in the study by Pickenet *et al*., subcecal in the study by Lee *et al*., and pelvic position in our study.

The main reasons why appendix can be observed in so much various positions in CT images can be listed as (1) variations in mesoappendix and in cecum position, (2) the effect of appendiculoovarian ligament, (3) the level of peritoneal reflection line at the posterior surface of the cecum, (4) interindividual variations in appendiceal length, (5) presence of fetal type of appendix, (6) variations in origin of the appendiceal ostium, and (7) the fact that appendix can develop while adhered to the cecum or posterior abdominal wall. For example, pelvic-type appendix occurs more likely when cecum is positioned more inferiorly than normal (close to iliac vessels) or when the appendix has a long mesoappendix. In addition, if the mesoappendix originates from the anterior side instead of the posterior side of cecum, backward movements of the appendix would cause excess tension in the mesoappendix, which would prevent appendix from having a retrocecal position. Furthermore, if the peritoneal reflection line at the posterior side of the cecum is positioned too low, formation of retrocecal fossa would be prevented, and this would result in appendix not having a retrocecal position. To have a better understanding of the appendix position, further studies planned in a multi-center setting that will take all these factors into consideration and use a similar classification system are necessary.

Some authors suggested that appendix can move freely around the cecum with a "free-floating" motion, and therefore it does not stay in a fixed position in any individual.[50] It has also been proposed that appendix may move to different positions throughout the day or at different times in each person, influenced by the fullness state of cecum and changes in body position.[51-53] In our review of the literature, we did not encounter any study on this subject. Therefore, further studies evaluating CT images of the same person scanned at different times may clarify this topic.

The main limitation of the present study is the lack of surgical-pathological evidence for the normal appendix. However, since excision of appendices of normal individuals would not be ethically approved, patient history and CT findings were taken into consideration for accepting the appendix as normal. Another limitation is that anamnesis related to previous appendectomy operations was obtained from patients. In some patients who underwent pelvic operation due to another cause, it is possible that the normal appendix has been excised and the patient was unaware of it. In addition, ignorance of congenital absence of appendix is another limitation of our study. Nonetheless, the incidence rate of appendiceal agenesis has been reported as 1 in 100,000 (0.001%) in laparotomies performed for appendicitis, and as 6 in 100,000 (0.006%) in autopsies; therefore, this is not likely to cause a significant impact on our results.[54]

Conclusion

We found the most frequent location of the normal appendix as pelvic type both in women and men. In addition, noncontrast CT was as successful as contrast CT for visualizing the normal appendix, and appendiceal diameter in CT was above the cut-off value of 6 mm in nearly one-fifth of the patients with normal appendix. Therefore, we believe it would be appropriate to raise this cut-off value of the normal appendiceal diameter to 8 mm for evaluation of appendix with CT.

Financial support and sponsorship

Nil.

Conflicts of interest

There are no conflicts of interest.

References

1. Williams P. Gray's Anatomy. 38th ed. New York: Churchill Livingstone; 1995.
2. Zinner MJ, Schwartz SI, Ellis HM. Maingot's Abdominal Operations. 10th ed. Philadelphia: Appleton and Lange; 1997.
3. Snell RS. Clinical Anatomy. 7th ed. Baltimore: Lippincot William and Wilkins; 2004.
4. Moore KL, Persaud TV. Essentials of Embryology and Birth Defects. 5th ed. Philadelphia: Saunders Company; 1998.
5. Golalipur MJ, Arya B, Azarhoosh R, Jahanshahi M. Anatomical variations of vermiform appendix in South East Caspian sea [Gorgoan – Iran]. J Anat Soc India 2003;52:141-3.

6. Karpelowsky JS, Bickler S, Rode H. Appendicitis – Pitfalls and medicolegal implications. S Afr Med J 2006;96:866-72.
7. Solanke TF. The position, length, and content of the vermiform appendix in Nigerians. Br J Surg 1970;57:100-2.
8. Chadha PV. Handbook of Forensic Medicine and Toxicology. 5th ed. New Delhi; Jaypee Brothers Medical Publishers; 2004.
9. Fox CH, Johnson FB, Whiting J, Roller PP. Formaldehyde fixation. J Histochem Cytochem 1985;33:845-53.
10. Willekens I, Peeters E, De Maeseneer M, de Mey J. The normal appendix on CT: Does size matter? PLoS One 2014;9:e96476.
11. Lee SL, Ku YM, Choi BG, Byun JY. *In vivo* location of the vermiform appendix in multidetector CT. J Korean Soc Radiol 2014;70:283-9.
12. Picken G, Ellis H, Dixon AK. The normal vermiform appendix at computed tomography: Visualization and anatomical location. Clin Anat 1993;6:9-14.
13. Flum DR, Morris A, Koepsell T, Dellinger EP. Has misdiagnosis of appendicitis decreased over time? A population-based analysis. JAMA 2001;286:1748-53.
14. Hale DA, Molloy M, Pearl RH, Schutt DC, Jaques DP. Appendectomy: A contemporary appraisal. Ann Surg 1997;225:252-61.
15. van Breda Vriesman AC, Kole BJ, Puylaert JB. Effect of ultrasonography and optional computed tomography on the outcome of appendectomy. Eur Radiol 2003;13:2278-82.
16. Wiersma F, Srámek A, Holscher HC. US features of the normal appendix and surrounding area in children. Radiology 2005;235:1018-22.
17. Balthazar EJ, Rofsky NM, Zucker R. Appendicitis: The impact of computed tomography imaging on negative appendectomy and perforation rates. Am J Gastroenterol 1998;93:768-71.
18. Benjaminov O, Atri M, Hamilton P, Rappaport D. Frequency of visualization and thickness of normal appendix at nonenhanced helical CT. Radiology 2002;225:400-6.
19. Jacobs JE, Birnbaum BA, Macari M, Megibow AJ, Israel G, Maki DD, *et al.* Acute appendicitis: Comparison of helical CT diagnosis focused technique with oral contrast material versus nonfocused technique with oral and intravenous contrast material. Radiology 2001;220:683-90.
20. Johnson PT, Eng J, Moore CJ, Horton KM, Fishman EK. Multidetector-row CT of the appendix in healthy adults. Emerg Radiol 2006;12:248-53.
21. Charoensak A, Pongpornsup S, Suthikeeree W. Wall thickness and outer diameter of the normal appendix in adults using 64 slices multidetector CT. J Med Assoc Thai 2010;93:1437-42.
22. Jan YT, Yang FS, Huang JK. Visualization rate and pattern of normal appendix on multidetector computed tomography by using multiplanar reformation display. J Comput Assist Tomogr 2005;29:446-51.
23. Turkoglu H, Onur MR, Poyraz AK, Kocakoc E. Evaluation of normal appendix vermiformis in adults with multidetector computed tomography. Clin Imaging 2012;36:758-62.
24. Webb EM, Wang ZJ, Coakley FV, Poder L, Westphalen AC, Yeh BM. The equivocal appendix at CT: Prevalence in a control population. Emerg Radiol 2010;17:57-61.
25. Jeffrey RB Jr., Laing FC, Townsend RR. Acute appendicitis: Sonographic criteria based on 250 cases. Radiology 1988;167:327-9.
26. Rioux M. Sonographic detection of the normal and abnormal appendix. AJR Am J Roentgenol 1992;158:773-8.
27. Simonovský V. Sonographic detection of normal and abnormal appendix. Clin Radiol 1999;54:533-9.
28. Mahafza WS. Evaluation of normal appendix in adult jordanians using non-enhanced dual source 64-slice MDCT. J Med J 2015;49:193-203.
29. Tamburrini S, Brunetti A, Brown M, Sirlin CB, Casola G. CT appearance of the normal appendix in adults. Eur Radiol 2005;15:2096-103.
30. Bursali A, Araç M, Oner AY, Celik H, Ekşioğlu S, Gümüş T. Evaluation of the normal appendix at low-dose non-enhanced spiral CT. Diagn Interv Radiol 2005;11:45-50.
31. Rao PM, Rhea JT, Novelline RA, McCabe CJ, Lawrason JN, Berger DL, *et al.* Helical CT technique for the diagnosis of appendicitis: Prospective evaluation of a focused appendix CT examination. Radiology 1997;202:139-44.
32. Kim HC, Yang DM, Jin W. Identification of the normal appendix in healthy adults by 64-slice MDCT: The value of adding coronal reformation images. Br J Radiol 2008;81:859-64.
33. Grosskreutz S, Goff WB, Balsara Z, Burkhard TK. CT of the normal appendix. J Comput Assist Tomogr1991;15:575-7.
34. Scatarige JC, DiSantis DJ, Allen HA 3rd, Miller M. CT demonstration of the appendix in asymptomatic adults. Gastrointest Radiol 1989;14:271-3.
35. Karabulut N, Boyaci N, Yagci B, Herek D, Kiroglu Y. Computed tomography evaluation of the normal appendix: Comparison of low-dose and standard-dose unenhanced helical computed tomography. J Comput Assist Tomogr 2007;31:732-40.
36. Lane MJ, Liu DM, Huynh MD, Jeffrey RB Jr., Mindelzun RE, Katz DS. Suspected acute appendicitis: Nonenhanced helical CT in 300 consecutive patients. Radiology 1999;213:341-6.
37. Keyzer C, Pargov S, Tack D, Creteur V, Bohy P, De Maertelaer V, *et al.* Normal appendix in adults: Reproducibility of detection with unenhanced and contrast-enhanced MDCT. AJR Am J Roentgenol 2008;191:507-14.
38. Pinto Leite N, Pereira JM, Cunha R, Pinto P, Sirlin C. CT evaluation of appendicitis and its complications: İmaging techniques and key diagnostic findings. AJR Am J Roentgenol 2005;185:406-17.
39. Hershko DD, Sroka G, Bahouth H, Ghersin E, Mahajna A, Krausz MM. The role of selective computed tomography in the diagnosis and management of suspected acute appendicitis. Am Surg 2002;68:1003-7.
40. Mun S, Ernst RD, Chen K, Oto A, Shah S, Mileski WJ. Rapid CT diagnosis of acute appendicitis with IV contrast material. Emerg Radiol 2006;12:99-102.
41. Yaqoob J, Idris M, Alam MS, Kashif N. Can outer-to-outer diameter be used alone in diagnosing appendicitis on 128-slice MDCT? World J Radiol 2014;6:913-8.
42. Daga BV, Shah VR, Daga SV. Radiodiagnosis, Nuclear Medicine, Radiotherapy and Radiation Oncology. New Delhi: Jaypee Brothers Medical Publisher; 2013.
43. Ansari MA, Kumar M, Subedi K. Visualization of normal appendix in multidetector computed tomography. J Inst Med 2015;37:103-7.
44. Joo SM, Lee KH, Kim YH, Kim SY, Kim K, Kim KJ, *et al.* Detection of the normal appendix with low-dose unenhanced CT: Use of the sliding slab averaging technique. Radiology 2009;251:780-7.
45. Gladstone RJ, Wakeley CP. The relative frequency of the various positions of the vermiform appendix: As ascertained by an analysis of 3000 cases: With an account of its development. Br J Surg 1924;11:503-20.
46. Iqbal T, Amanullah A, Nawaz R. Pattern and positions of vermiform appendix in people of Bannu district. Gomal J Med Sci 2012;10:100-3.
47. Manisha C, Divyesh K, Sanjay K, Jitendra P, Ritesh S, Ashok N.

A study of morphology of vermifrom appendix in 200 cases. Int J Med Res Heath Sci 2013;2:780-5.
48. Wakeley CP. The position of the vermiform appendix as ascertained by an analysis of 10,000 cases. J Anat 1933;67:277-83.
49. Hörmann M, Puig S, Prokesch SR, Partik B, Helbich TH. MR imaging of the normal appendix in children. Eur Radiol 2002;12:2313-6.
50. Nayak BS. Why the tip of vermiform appendix has variable position? Med Hypotheses 2010;75:682-3.
51. De Garis CF. Topography and development of the cecum-appendıx. Ann Surg 1941;113:540-8.
52. Kelly HA. The Vermiform Appendix and its Disease. Philadelphia: W.B. Saunders and Company; 1905.
53. Maisel H. The position of the human vermiform appendix in fetal and adult age groups. Anat Rec 1960,136:385-91.
54. Collins DC. Agenesis of the vermiform appendix. Am J Surg 1951;82:689-96.
55. Delić J, Savković A, Isaković E. Variations in the position and point of origin of the vermiform appendix. Med Arh 2002;56:5-8.
56. Ndoye JM, Ndiaye A, Ndiaye A, Dia A, Fall B, Diop M, *et al.* Topographie et morphométriecadavériques de l'appendicevermiculaire. Morphologie 2005;89:59-63.
57. Clegg-Lamptey JN, Armah H, Naaeder SB, Adu-Aryee NA. Position and susceptibility to inflammation of vermiform appendix in Accra, Ghana. East Afr Med J 2006;83:670-3.
58. Rahman MM, Khalil M, Rahman H, Mannan S, Sultana SZ, Ahmed S. Anatomical positions of vermiform appendix in Bangladeshi people. J Bangladesh Soc Physiol 2006;1:5-9.
59. Paul UK, Naushaba H, Begum T, Alam J. Position of vermiform appendix: A postmortem study. Bangladesh J Anat 2009;7:34-6.
60. Tofighi H, Taghadosi-Nejad F, Abbaspour A, Rahmani M, Mohammadi M, Moghadam MD, *et al.* The anatomical position of appendix in Iranian cadavers. Int J Med Toxicol Forensic Med 2013;3:126-30.
61. Bakar SM, Shamim M, Alam GM, Sarwar M. Negative correlation between age of subjects and length of the appendix in Bangladeshi males. Arch Med Sci 2013;9:55-67.
62. Ghorbani A, Forouzesh M, Kazemifar AM. Variation in anatomical position of vermiform appendix among Iranian population: An old ıssue which has not lost ıts ımportance. Anat Res Int 2014;2014:313575.
63. El-Amin EI, Ahmed GY, Ahmed WA, Khalid EK, Sakran ME. Lengths and positions of the vermiform appendix among Sudanese Cadavers. Med Sci 2015;2:222-7.
64. de Souza SC, da Costa SR, de Souza IG. Vermiform appendix: Positions and length – A study of 377 cases and literature review. J Coloproctol 2015;35:212-6.
65. Ajmani ML, Ajmani K. The position, length and arterial supply of vermiform appendix. Anat Anz 1983;153:369-74.
66. Corzo EG, Forero PL, Amaya L, Bohórquez D, Bohórquez S. Anatomical position and length of caecal appendix in a mixtured population from Bucaramanga. de MedUNAB 2009; 12:116-20.
67. Banerjee A, Kumar IA, Tapadar A, Pranay M. Morphological variations in the anatomy of caecum and appendix-A cadaveric study. Nat J Clin Anat 2012;1:30-5.
68. Setty SN, Katikireddi RS. Morphometric study of human cadaveric caecum and vermiform appendix. Int J Health Sci Res 2013;3:48-55.
69. Sinha SK, Kumar V. Observation on anatomical variations of vermiform appendix in Kosi region of Bihar – A cadaveric study. J Evid Based Med Healthcare 2014;1:564-8.
70. Mwachaka P, El-Busaidy H, Sinkeet S, Ogeng'o J. Variations in the position and length of the vermiform appendix in a black Kenyan population. ISRN Anat 2014;2014:871048.
71. Salwe NA, Kulkarni PG, Sinha RS. Study of Morphological variations of vermiform appendix and caecum in cadavers of western Maharashtra region. Int J Adv Physiol Allied Sci 2014;2:31-41.
72. Patel S, Anshuman N. Anatomical variations in the positions of the vermiform appendix. IOSR J Dent Med Sci 2016;15:106-9.
73. Vidya CS, Kuberapp V. Anatomical variations of caecum and appendix: A cadveric study in Mysore based population. Indian J Clin Anat Physiol 2016;3:265-8.
74. O'Connor CE, Reed WP. *In vivo* location of the human vermiform appendix. Clin Anat 1994;7:139-42.
75. Varshney S, Johnson CD, Rangnekar GV. The retrocaecal appendix appears to be less prone to infection. Br J Surg 1996;83:223-4.
76. Denjalić A, Delić J, Delić-Custendil S, Muminagić S. Variations in position and place of formation of appendix vermiformis found in the course of open appendectomy. Med Arh 2009;63:100-1.
77. Verdugo R, Olave E. Anatomic and biometric features of the vermiform appendix in chilean children operated by acute appendicitis. Int J Morphol 2010;28:615-22.
78. Ashindoitiang JA, Ibrahim NA. Anatomical variations of appendix in patients with acute appendicitis among two major tribes in Lagos Nigeria. Int J Med Med Sci 2012;2:72-6.
79. Casado MP, Ferrer MC, Labrada GD. Morphometric variants of the cecal appendix in a living person. Rev Méd Electrón 2014;36:49-59.
80. Swargam N, Malvadi AK, Madan S. A study of anatomical variations in the caeco-appendicular position. Sch J App Med Sci 2015;3:1376-9.

Review Article

An Anatomical Description of the Obturator Region with Clinical Aspects

Lidija Kocbek Šaherl, Mateja Rakuša

Faculty of Medicine, Institute of Anatomy, Histology and Embryology, University of Maribor, Taborska Ulica 8, SI-2000 Maribor, Slovenia

Abstract

Structures surrounding the obturator foramen, the obturator internus and obturator externus muscles and regional neurovascular bundle, the obturator artery, vein, and nerve, pass through from the lesser pelvis into the medial compartment of the thigh and build up the obturator region. The region is demanding and complex both in terms of anatomical and clinical points of view. This article aims to write an overview of the obturator region about normal and variant anatomy and relate its various parts to their importance in clinical practice. The connections between various anatomical structures, concerning their different critical sites in the obturator region, as well as a thorough overview essential for clinicians, especially surgeons, are discussed.

Keywords: *Obturator artery, obturator canal, obturator foramen, obturator muscles, obturator nerve, obturator vein*

Introduction

The pelvis is considered an important anatomical region. Surgical procedures in the pelvis are more challenging because of the large number of organs and their close relationship with major blood vessels and nerves.[1-3] Clear awareness of the vascular[4,5] and nerve anatomy,[6] as well as the presence of any anomalous vessels in the obturator region, is critical because of the significant source of bleeding during surgical interventions in this region.[4,7] Awareness of variations in the vascular anatomy of the pelvis is also essential due to the rapid development of modern minimally invasive techniques like transobturator procedures in urogenital interventions.[8,9] In addition, surgery, hemorrhage, or tumor compression around the length of the obturator nerve may damage the obturator nerve and cause obturator neuropathy.[6,10]

Anatomical description of the obturator area, the obturator foramen as the anatomical landmark for the obturator neurovasculature, localization of the obturator artery, obturator venous system, and collateral pathways are being discussed for educational purposes.

Material and Methods

In preparing the article and reviewing the literature, we searched in PubMed, Google Scholar, Springer, Elsevier (ScienceDirect), and books. The following keywords were used to search the databases: obturator foramen, obturator canal, obturator artery, obturator vein, obturator nerve, and obturator muscle.

The obturator region

The obturator area includes the structures that cover the hip joint on its medial side. These are mainly the obturator externus muscle and the muscle group of the hip adductors, forming rings around the obturator foramen and their corresponding regional nerves and vessels, coming through the obturator canal from the pelvis.[11,12] Superior border of the obturator region represents the superior pubic ramus, the lateral is the hip joint and the shaft of the femur, the medial the pubic arch, the perineum, and the gracilis muscle, and the inferior border is the attachment of the adductor magnus muscle on the adductor tubercle of the femur.[13]

Obturator foramen and obturator canal and importance of nerovascular interactions

The obturator foramen is the largest opening in the body located in the hip bone between the ischium and pubis,[14] situated on the anterolateral pelvic wall, below and anterior to the acetabulum.[15,16] It is surrounded by a thin and nonuniform margin limited superiorly by the superior

How to cite this article: Šaherl LK, Rakuša M. An anatomical description of the obturator region with clinical aspects. J Anat Soc India 2022;XX:XX-XX.

Article Info

Received: 14 July 2020
Revised: 09 December 2021
Accepted: 18 April 2022
Available online: ***

Address for correspondence:
Dr. Lidija Kocbek Šaherl, Faculty of Medicine, Institute of Anatomy, Histology and Embryology, University of Maribor, Taborska Ulica 8, SI-2000 Maribor, Slovenia. E-mail: lidija.kocbek-saherl@um.si

Access this article online

Website: www.jasi.org.in
DOI: 10.4103/JASI.JASI_134_20
Quick Response Code:

pubic ramus, with the obturator groove that is transformed into a canal by an obturator membrane attached to this margin, anteromedially by the pubic body, inferiorly by the inferior pubic ramus and the ischial ramus, posterolaterally by the ischial body [Figure 1].[15] In the male, the foramen is large and oval[14,15] with the main axis passing obliquely from upward and forward to backward.[17] Despite the great variation in females,[18,19] the foramen is smaller and almost triangular.[14,15,20] In the female bony pelvis, the obturator foramen area is proportional to height and is racially independent.[19] Obturator foramen can be in rare cases duplicated or even triplicated.[19,21] In the latter case, the obturator foramen was oval and had two additional openings. A bone plate that could potentially compress the nerves and vessels and cause neurological and vascular complications closed the obturator canal. The incidence of numerous openings related to the obturator foramen could also affect the obturator externus and obturator internus muscle function by changing biomechanics.[21] The obturator foramen is almost completely closed by an obturator membrane, except in the superior lateral part.[14,16,21] Obturator membrane is composed of fibers, which are intertwined, and mostly transverse in their course.[14] The fibers are continuous with the periosteum of the surrounding bones and with tendinous attachments of the obturator muscles.[16] The uppermost part of the membrane attaches to two tubercles, the posterior obturator tubercle located on the medial margin of the ischium and in front of the acetabular notch, and the anterior obturator tubercle caudal to the middle third of the obturator crest of the superior ramus of the pubis.[14] In the superior lateral part of the obturator foramen, the obturator membrane transforms the obturator groove into the canal through the obturator artery, vein and nerve pass out of the pelvis surrounded by a fat cushion [Figure 1].[11,16,21] The neurovascular bundle that passes through the obturator canal is located at its cranial and ventral margins.[20] The obturator canal is an oblique tunnel 2–3 cm long and 1 cm wide, oriented downwards and medial, that connects the pelvis to the medial compartment of the thigh. The superior and lateral border of the obturator canal is formed by the wall of the obturator groove of the pubic bone and the inferior border represents the free margin of the obturator membrane and the internal and external obturator muscles. The parietal pelvic fascia covers the inner opening of the canal. The outer opening lies medial to the femoral vein and the deep aspect of the pectineus muscle.[16] Due to the deficiency of the obturator canal, the obturator hernia can occur when a fat, intestinal loop, or rarely the urinary bladder can protrude through the obturator foramen, particularly in geriatric, emaciated, multiparous women with associated medical problems.[13] Factors that contribute to the occurrence of the obturator hernia include loss of the adipose body within the obturator canal, wider pelvis, and more triangular obturator canal with a larger transverse diameter in women and other predisposing factors that increase the intraabdominal pressure.[16] In the obturator canal, the hernia sac can have three potential routes [Figure 2]. When the sac emerges through the external opening of the canal and follows the anterior division of the obturator nerve, it is found in front of the external obturator muscle and under the pectineus muscle. The sac can continue the route between the middle and superior fibers of the obturator externus muscle following the posterior division of the obturator nerve and is then located behind the adductor brevis muscle. If herniated content compresses and affects either or both divisions of the obturator nerve, a typical hip–knee pain (Howship-Romberg sign) or loss of thigh adductor reflex and simultaneous positive patellar reflex (Hannington-Kiff sign) are present.[11,13]

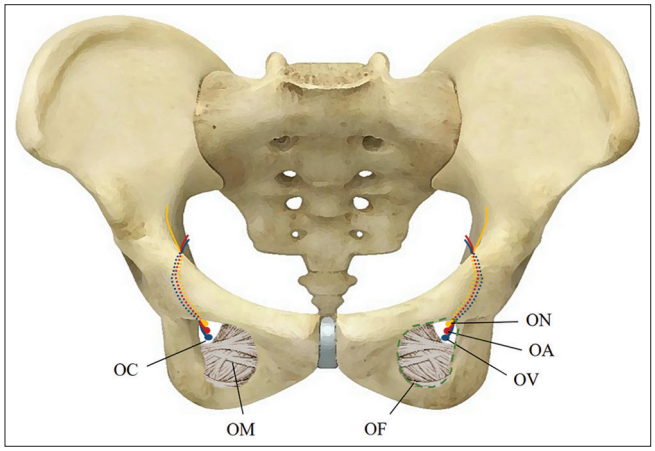

Figure 1: Obturator foramen and obturator neurovascular bundle. OA: Obturator artery, OC: Obturator canal, OF: Obturator foramen, OM: Obturator membrane, ON: Obturator nerve, OV: Obturator vein

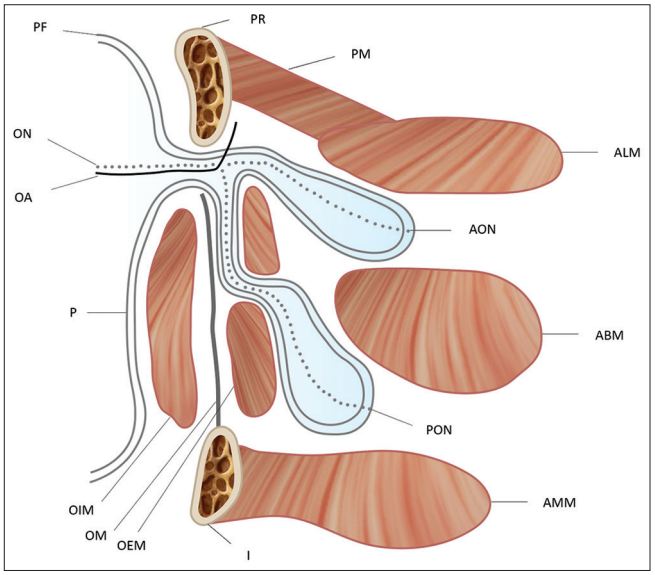

Figure 2: Types of obturator hernia. PR: Pubic ramus, I: Ischium, OEM: Obturator externus muscle, OIM: Obturator internus muscle, OM: Obturator membrane, ALM: Adductor longus muscle, ABM: Adductor brevis muscle, AMM: Adductor magnus muscle, PM: Pectineus muscle, PF: Pelvic fascia, P: Peritoneum, ON: Obturator nerve, AON: Anterior division of obturator nerve, PON: Posterior division of obturator nerve, OA: Obturator artery[11]

The sac can lie also between the obturator muscles and membrane.[22] The vessels are in most individuals found lateral to the sac.[16] Within the foramen, the structures of the neurovascular bundle are mainly located on the superolateral aspect[19] with a central triangular avascular area between the anterior and posterior obturator artery.[20] There are no data about how the size and shape of the obturator foramen influence the position of the obturator vessels and nerves although women with smaller obturator foramen are more likely to suffer nerve and vascular damage since trocars for transobturator mid-urethral slings and prolapse repair kits that are used have fixed sizes and angles.[19] The neurovascular bundle situated in the obturator canal is protected when the sutures for paravaginal defect repair are placed deep enough to cover the obturator internus or obturator membrane that is 1–1.5 cm below the inferior margin of the superior pubic ramus.[23] For the obturator bypass as an alternative technique in cases of vascular prosthesis infection, mycotic aneurysms, traumatic ulcer, irradiation ulcer, excessively scarred tissue in the femoral region, the tunnel through the obturator foramen has to be precise to avoid damage to the obturator artery, vein, and nerve.[24,25] Therefore, the bypass has to course inferior to the neurovascular bundle and superior to the fibers of the obturator internus muscle.[26] The topographical relationships between the obturator artery, vein, and nerve in the lateral pelvic wall are summarized in Table 1.[7,27-29] Because the obturator nerve is quite permanent from the origin to the obturator canal, it represents a significant landmark in pelvic lymph node dissection in urologic and gynecologic surgery.[29] Despite the invariable location of the obturator nerve, the obturator artery and particularly the obturator vein is among the obturator neurovascular bundle the most variable due to their variable origins.[23,29] The obturator vein can extend from the ischial spine to the obturator canal. The sutures for paravaginal defect repair are, therefore, safely placed in front of the line connecting the ischial spine to the entrance of the obturator canal.[23]

Obturator internus and obturator externus muscles: Anatomy and function with clinical aspects

The obturator internus muscle lies within the lesser pelvis and behind the hip joint. The muscle is attached to the inferior rami of the pubis and ischium, to the inner surface of the hip bone, and the pelvic surface of the obturator membrane.[14] The muscle thickness varies between 4.5 mm and 7 mm.[23] The muscle ends in four to five tendinous bands that leave the pelvis through the lesser sciatic foramen. The bands combine into a single tendon that turns sharply laterally from the lesser pelvis, travels horizontally across the capsule of the hip joint, and before inserting to the greater trochanter of the femur, it receives the attachments of the gemelli muscles [Figure 3].[14,30] The muscle is covered on its medial side by the obturator membrane that forms in its central part a tendinous arch for the attachment of the pelvic diaphragm. The pelvic diaphragm splits the muscle into a superior pelvic part and an inferior perineal part.[30] The distance of the obturator internus muscle from the mid urethra is determined by the pubic arch angle. New generations of slings for the prolapse and anti-incontinence operations enable mesh enclosure to the obturator internus muscle to avoid transobturator or retropubic trocar passage.[19] The muscle rotates the thigh laterally and assists in holding the head of the femur in the acetabulum. Innervation for the obturator internus ensures the first, second, and third sacral nerves.[14] The irritation of obturator internus muscle and inflammation in the lower pelvis (appendicitis, pelvic abscess or hemorrhage, injury to muscles of pelvic floor) during flexion or internal rotation of the hip, causing hypogastric abdominal pain, is known as the obturator sign or Cope's obturator test.[31]

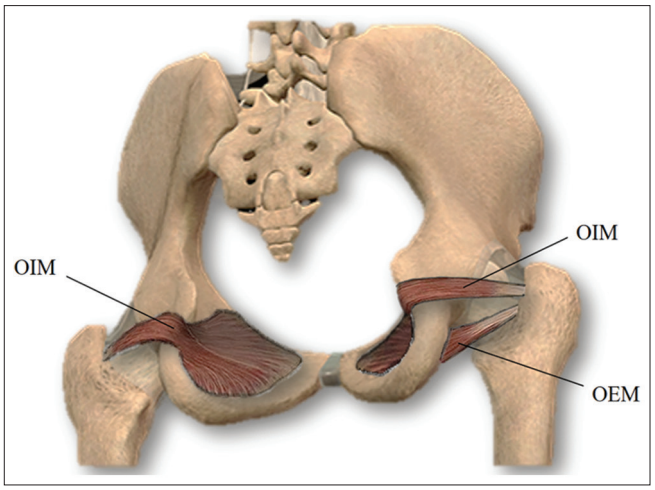

Figure 3: Obturator muscles. OEM: Obturator externus muscle, OIM: Obturator internus muscle

The obturator externus muscle is a triangular-shaped flat muscle that surrounds and covers the external surface of the anterior pelvic wall. The muscle originates from the pubic ramus and the inferior ramus of the ischium, from the obturator membrane and the tendinous arch that creates the obturator canal.[14] At the femoral neck level, the muscle forms a musculotendinous junction. The fibers of the cylindrical tendon pass laterally along the inferior margin of the acetabulum and run over the lower part of the hip joint capsule acting as a sling below the neck of the femur. The tendon attaches to the trochanteric fossa [Figure 3].[14,32]

The basic function of the muscle is external rotation of the femur with the hip in a neutral position and flexed at 90°. The additional action is adduction with the hip in flexion. The obturator externus muscle helps to stabilize the hip joint due to the course of the muscle and its fibers which strengthen the posterior capsule.[32] The influence of the obturator externus muscle on the hip joint has to be taken into consideration since hip pain is associated with primary pyomyositis[33] and abscess of the obturator externus muscle[34] and even with obturator externus hematoma in hemophilia

Table 1: Origin and topographic variations of the obturator artery, vein, and nerve in the lateral pelvic wall

	OA	OV (draining into)	ON (topographic variations)	
Origin of anatomical structures	The common trunk of the internal iliac artery		ON-OA-OV	Lateral pelvic wall
	Anterior division of internal iliac artery (normal)		ON-OV-OA OA-ON-OV	Without any topographic variation
	The posterior division of the internal iliac artery		ON-OA ON-OV OA-OV	Twisted around each other in the lateral pelvic wall
	Separate branch		ON-OA-OV	Presence of two or three OVs and the presence of two OAs
	With superior gluteal artery		OV above ON	Lateral pelvic wall
	With iliolumbar artery		OA and OV	Absent from the lateral pelvic wall
	External iliac artery	External iliac vein	ON and OV	Without OA in the lateral pelvic wall
	Separate branch	Venous anastomosis between OV and external iliac vein	ON and OA	Without OV in the lateral pelvic wall
	With inferior epigastric artery			
	Inferior epigastric artery	Inferior epigastric vein		
		Venous anastomosis between OV and inferior epigastric vein		
	Inferior gluteal artery			
	Internal pudendal artery			
	Iliolumbar artery			
	Double origin			

OA: Obturator artery, OV: Obturator vein, ON: Obturator nerve

patients.[35] When the obturator externus muscle stays attached during dislocation of the head of the femur and when tenotomy of the muscle insertions is around the proximal femur, including when circumferential capsulotomy is performed, the muscle protects the deep branch of the medial femoral circumflex artery from stretching or disruption that potentially causes avascular necrosis of the head of the femur.[36] Complete rupture of the obturator externus muscle after acetabular fractures determined on preoperative magnetic resonance imaging scans is a prognostic factor for the development of avascular necrosis of the femoral head.[37] The muscles receive the innervation from the third and fourth lumbar nerves through the obturator nerve.[14]

Obturator artery and obturator vein: Anatomy with clinical aspects

The origin of the obturator artery is principally variable.[2,3,9,38] It originates commonly from the common iliac artery or against the anterior division of the internal iliac artery in more than one-third of cases. Sometimes, it originates from the inferior epigastric artery, at times from the superior gluteal artery, and occasionally from the internal pudendal trunk. It comes from the inferior gluteal artery, every so often from the external iliac artery, and along periodically from the posterior division of the internal iliac artery. As is usual, the artery is accompanied by two veins. Veins followed the same course as the arteries almost always drain into the internal iliac vein, commonly within the inferior epigastric or approximately toward the external iliac vein [Table 1 and Figures 4 and 5].[1,7,27-29]

Anatomical knowledge and understanding of vascular alteration had always been interesting concerning obturator topography, because of its clinical significance in the therapeutic and diagnostic maneuvers.[4] This type of vasculature may disturb pelvic laparoscopy or invasive procedures in the pelvis. Advantages of the possible vascular variations can be achieved in embolization and revascularization procedures for patients with aortoiliac occlusive diseases.[39] There is a terminological variety in defining the term aberrant obturator vessel among some authors. The term describes the different course of the blood vessel, entering atypically the obturator canal or as additional to another existing obturator vein, respectively, artery. Some authors define as obturator any vessel entering the obturator canal as a result of unequal anastomoses between the external and internal iliac vessels.[4,8,27,28,40] Their unexpected presence through open or laparoscopic surgery,[41] pelvic fractures, or interventional various

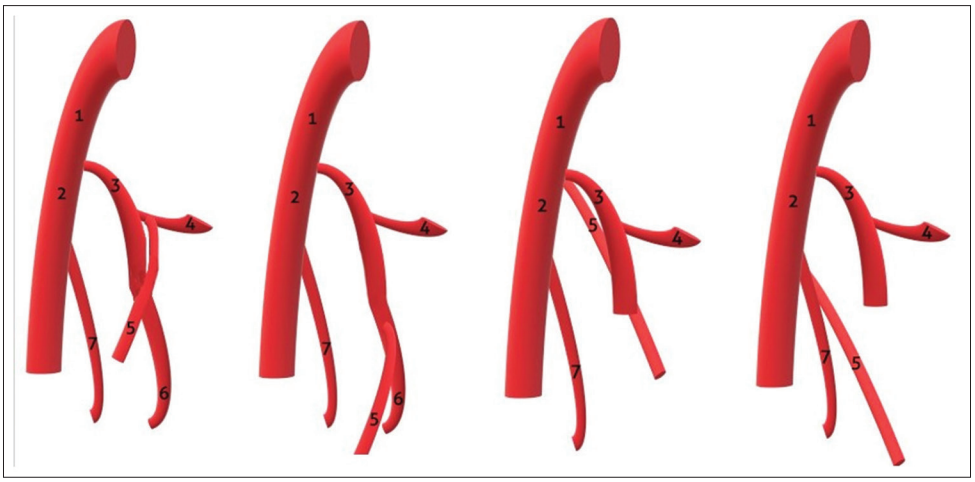

Figure 4: Obturator artery and variations. 1: Iliac common artery, 2: Iliac external artery, 3: Iliac internal artery, 4: Superior gluteal artery, 5: Obturator artery, 6: Inferior gluteal artery, 7: Inferior epigastric artery

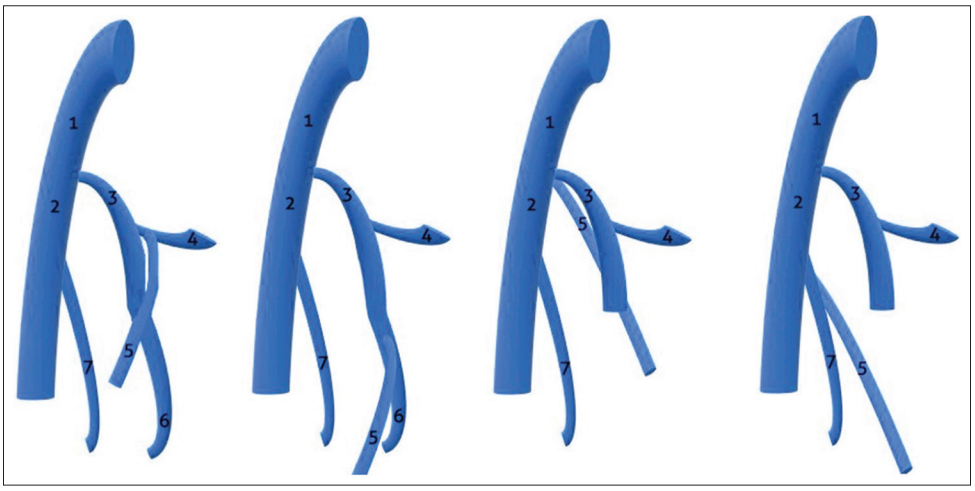

Figure 5: Obturator vein and variations. 1: Iliac common vein, 2: Iliac external vein, 3: Iliac internal vein, 4: Superior gluteal vein, 5: Obturator vein, 6: Inferior gluteal vein, 7: Inferior epigastric vein

minimally invasive procedures[42] can result in very serious complications as an obturator vessel can be unintentionally cut.[1] According to the literature, the persistence of all reported variable origins of the obturator artery or any anomalous vascular connection between the obturator artery and the other vessels from the iliac artery have to be considered before surgical procedures to avoid potentially accidental hemorrhage.[9] There are many reports of such a one collateral circulation between the obturator and external iliac vessels or terminal small vessels indicates the importance of this anastomosis and is considered as heterogeneous corona mortis [Table 2].[4,8,43,44] Anatomical variation of corona mortis may differ concerning its contralateral side, not only in distance[45] but also differs in size[39,46] and length.[6,46] Clinically, it is important due to the potential risk of bleeding in pelvic fractures, pelvic and acetabular operations, during fixation of the mesh on Cooper's ligament, surgery for urinary incontinence, oncogynecological procedures, and laparoscopic hernia repair in the inguinofemoral region.[8,28,40,43-51]

Obturator nerve: Anatomy with clinical aspects

The obturator nerve is formed within the psoas major muscle by the anterior divisions of the anterior primary rami of L2-L4 spinal nerves.[52] The obturator nerve emerges from the medial border of the psoas major and passes into the lesser pelvis and before entering the obturator canal[39,51] gives off branches to the obturator artery, periosteal nerve branches, and the nerve to obturator externus muscle. The posterior and anterior divisions of the obturator nerve arise into the tight anterior to the obturator externus muscle and its fascia near the obturator foramen, within the obturator canal, at the exit from the obturator canal or at the proximal border of the adductor brevis muscle. The posterior branches innervate the obturator externus, the adductor brevis, and the anterior part of the adductor magnus muscles. The anterior and posterior obturator divisions are accompanied by the branches of the obturator artery and vein.[6,20] The course of the obturator nerve is relatively constant from its origin to the obturator

Table 2: Various combinations of vascular distribution, arterial and venous coronae mortis

Vascular distribution	Arterial component	Venous component
Crossing the superior pubic ramus (any vessel)	Anastomosis OA-to-IEA	OV draining into IEV anastomosis OV-to-IEV
Any vessel diameter >4 mm	OA from EIA	Anastomosis OV-to-IEV
Arterial anastomosis	Anastomosis OA-to IEA	OV draining into IEV
Multiple arterial anastomosis	OA from IEA	Anastomosis OV-to-IEV
Multiple venous anastomoses	Anastomosis OA-to-IEA	Anastomosis OV-to-IEV
More than one vessel (vein, artery, or both)	Pubic branches of OA	OV draining into EIV
Bilateral vascular abnormalities	Anastomosis OA-to-IEA	Anastomosis OV-to-IEV
Bilateral symmetry in the vascular distribution	OA from IEA	Anastomosis of the OV and EIV
Aberrant OA from external iliac artery	OA from IEA	OV draining into EIV
Aberrant OV from external iliac vein	OA from IEA	Anastomosis OV-to-IEV

OA: Obturator artery, OV: Obturator vein, IEA: Inferior epigastric artery, EIA: External iliac artery, IEV: Inferior epigastric vein, EIV: External iliac vein

canal, by comparison of the obturator artery and obturator vein to their origins. Topographical variations in the course of the obturator nerve consist of (i) obturator nerve separated from the obturator artery and obturator vein in the lateral pelvic wall, (ii) all three structures could be separated at the posterior pelvic wall and converge toward the obturator canal, (iii) obturator nerve could be separated from the obturator artery and obturator vein or only from the obturator vein, or (iv) all three structures could be twisted around each other [Table 1].[6,7,10,20,27-29]

The presence of the obturator vessels at the side of the obturator nerve divisions within the obturator canal might increase the risk of pathological processes to these structures. As an illustration avascular necrosis of the head of the femur pathologies from the hip may refer to pain to the knee and entrapment neuropathy might result in anatomic relationships between the obturator nerve and accompanying obturator vessels.[6] Just as pelvic fractures, pelvic hematomas, intrapelvic tumors, and local inflammatory of infectious processes in the adjacent pubic bones[5,10,53] may involve the region of the obturator foramen, causing obturator nerve entrapment syndrome.[6,10,52,54] Similarly, complications of gynecological or orthopedic surgery, inflammatory changes in the adjacent pubic bone in osteitis pubis, and obturator hernia are characterized by pain and/or loss of function of the obturator nerve. A complex intraoperative functional accident of obturator nerve results, especially in patients with endometriosis and genitourinary malignancies,[55] massive hemorrhage of the obturator artery during transurethral bladder surgery with bladder perforation, and orthopedic complications.[6,10] In addition, other neuropathy[56] in the lower abdomen and pelvic region can be also present as pain and loss of sensation, and identifying an isolated obturator nerve lesion could be overlooked. Obturator neuropathy should be effectively differentiated from lumbar plexopathy, diabetic polyneuropathy, and lumbar neuropathy.[10] Diagnosing the possible chronic pain in the distribution of the obturator nerve requires multi-disciplinary knowledge and good clinical experience to prevent avoidable complications.[51]

Conclusions

Based on the anatomical knowledge, the highly variable structures of the obturator region can potentially cause serious complications and different outcomes of the procedures done in this area. Understanding topographical relationships between anatomical structures and anatomical variations in the obturator region are clinically important in a great variety of medicine, from radiology, orthopedic surgery, vascular surgery, and abdominal surgery to urogynecology and necessary to avoid coincidental harm.

Financial support and sponsorship

Nil.

Conflicts of interest

There are no conflicts of interest.

References

1. Nagabhooshana S, Vollala VR, Rodrigues V, Bhat S, Pamidi N, Lobo SW. Anatomical variation of obturator vessels and its practical risk: A case report from an anatomic study. J Vasc Bras 2008;7:275-7.
2. Kumari S, Trinesh Gowda MS. A study of variations of origin of obturator artery: Review in south Indian population. J Anat Soc India 2016;65 Suppl 1:S1-4.
3. Biwas S, Bandopadhyay M, Adhikari A, Kundu P, Roy R. Variation of origin of obturator artery in eastern indian population – A study. J Anat Soc India 2010;59:168-72.
4. Rusu MC, Cergan R, Motoc AG, Folescu R, Pop E. Anatomical considerations on the corona mortis. Surg Radiol Anat 2010;32:17-24.
5. Koo S, Fan CM. Pelvic congestion syndrome and pelvic varicosities. Tech Vasc Interv Radiol 2014;17:90-5.
6. Kumka M. Critical sites of entrapment of the posterior division of the obturator nerve: Anatomical considerations. J Can Chiropr Assoc 2010;54:33-42.
7. Pai MM, Krishnamurthy A, Prabhu LV, Pai MV, Kumar SA, Hadimani GA. Variability in the origin of the obturator artery. Clinics (Sao Paulo) 2009;64:897-901.
8. Ates M, Kinaci E, Kose E, Soyer V, Sarici B, Cuglan S, *et al.* Corona mortis: *In vivo* anatomical knowledge and the risk of injury in totally extraperitoneal inguinal hernia repair. Hernia 2016;20:659-65.

9. Jusoh AR, Abd Rahman N, Abd Latiff A, Othman F, Das S, Abd Ghafar N, *et al.* The anomalous origin and branches of the obturator artery with its clinical implications. Rom J Morphol Embryol 2010;51:163-6.
10. Jo SY, Chang JC, Bae HG, Oh JS, Heo J, Hwang JC. A morphometric study of the obturator nerve around the obturator foramen. J Korean Neurosurg Soc 2016;59:282-6.
11. Skandalakis LJ, Skandalakis PN, Colborn GL, Skandalakis JE. Obturator hernia: Embryology, anatomy, surgery. Hernia 2000;4:121-8.
12. Von Lanz T, Wachsmuth W. Praktische Anatomie. Ein Lehr-und Hilfsbuch der Anatomischen Grundlagen Ärztlichen Handelns, Bein und Statik. Berlin, Heidelberg: Springer-Verlag; 1938.
13. Bendavid R, Abrahamson J, Arregui ME, Flament JB, Phillips EH. Abdominal Wall Hernias: Principles and Management. New York: Springer-Verlag; 2001.
14. Williams PL, Warwick R. Gray's Anatomy. 36th ed. Edinburgh: Churchill Livingstone; 1980.
15. Bierry G, Le Minor JM, Schmittbuhl M. Oval in males and triangular in females? A quantitative evaluation of sexual dimorphism in the human obturator foramen. Am J Phys Anthropol 2010;141:626-31.
16. Petrie A, Tubbs RS, Matusz P, Shaffer K, Loukas M. Obturator hernia: Anatomy, embryology, diagnosis, and treatment. Clin Anat 2011;24:562-9.
17. Testut L, Latarjet A. Traité D'anatomie Humaine, Tome 1. Paris: G Doin; 1948.
18. Bogusiewicz M, Rosińka-Bogusiewicz K, Drop A, Rechberger T. Anatomical variation of bony pelvis prom the viewpoint of transobturator sling placement for stress urinary incontinence. Int Urogynecol J 2011;22:1005-9.
19. Ridgeway BM, Arias BE, Barber MD. Variation of the obturator foramen and pubic arch of the female bony pelvis. Am J Obstet Gynecol 2008;198:4.e1-4.
20. Nyangoh Timoh K, Bader G, Fauconnier A, Barrau V, Delmas V, Touboul C. Determination of a central avascular triangle within the obturator foramen: A radioanatomic study. PLoS One 2015;10:e0143642.
21. Das S, Suri R, Kapur V. A triplicate obturator foramen. Folia Morphol (Warsz) 2006;65:164-6.
22. Losanoff JE, Richman BW, Jones JW. Obturator hernia. J Am Coll Surg 2002;194:657-63.
23. Ersoy M, Sagsoz N, Bozkurt MC, Apaydin N, Elhan A, Tekdemir I. Important anatomical structures used in paravaginal defect repair: Cadaveric study. Eur J Obstet Gynecol Reprod Biol 2004;112:206-13.
24. Kim DI, Joh JH. A vase report of bilateral obturator foramen bypass. EJVES Extra 2005;10:31-2.
25. Rabbani A, Moini M, Rasouli MR. Obturator bypass as an alternative technique for revascularization in patients with infected femoral pseudoaneurysms. Arch Iran Med 2008;11:50-3.
26. Ahn SS, Daniels E. Arterial bypass via the obturator canal. Perspect Vasc Surg Endovasc Ther 2000;12:95-102.
27. Rajive AV, Pillay M. A study of variations in the origin of obturator artery and its clinical significance. J Clin Diagn Res 2015;9:C12-5.
28. Tantchev LS, Gorchev GA, Tomov ST, Radionova ZV, Velkova AS. Aberrant obturator vessels in minimally invasive pelvic lymph node dissection. Gynecol Surg 2013;10:273-8.
29. Won HS, Kim JH, Lee UY, Rha KH, Kim DK. Topographical relationships between the obturator nerve, artery, and vein in the lateral pelvic wall. Int Urogynecol J 2016;27:213-8.
30. Moore KL, Dalley AF. Clinical Oriented Anatomy. 5th ed. Baltimore: Lippincott Williams & Wilkins; 2006.
31. Talreja DR, Talerja RR, Talreja RS. The Internal Medicine Peripheral Brain. Baltimore, Philadelphia: Lippincott Williams & Wilkins; 2005.
32. Gudena R, Alzahrani A, Railton P, Powell J, Ganz R. The anatomy and function of the obturator externus. Hip Int 2015;25:424-7.
33. Kumar A, Anderson D. Primary obturator externus pyomyositis in a child presenting as hip pain: A case report. Pediatr Emerg Care 2008;24:97-8.
34. Fowler T, Strote J. Isolated obturator externus muscle abscess presenting as hip pain. J Emerg Med 2006;30:137-9.
35. Arpaci T, Sasmaz I, Akbas T, Eken A, Ozgur A, Antmen B. Bilateral recurrent external obturator muscle hematoma: An unusual cause of pelvic pain in hemophilia. Mol Clin Oncol 2016;4:622-4.
36. Gautier E, Ganz K, Krügel N, Gill T, Ganz R. Anatomy of the medial femoral circumflex artery and its surgical implications. J Bone Joint Surg Br 2000;82:679-83.
37. Maini L, Kumar S, Batra S, Gupta R, Arora S. Evaluation of the muscle morphology of the obturator externus and piriformis as the predictors of avascular necrosis of the femoral head in acetabular fractures. Strategies Trauma Limb Reconstr 2016;11:105-11.
38. Nayak SB, Shetty SD, Sirasanagandla SR, Vasanthakumar P, Jetti R. Multiple variations in the pelvic vasculature – A case report. J Clin Diagn Res 2015;9:D01-2.
39. Deshmukh V, Singh S, Sirohi N, Baruhee D. Variation in the obturator vasculature during routine anatomy dissection of a cadaver. Sultan Qaboos Univ Med J 2016;16:e356-8.
40. Sañudo JR, Mirapeix R, Rodriguez-Niedenführ M, Maranillo E, Parkin IG, Vázquez T. Obturator artery revisited. Int Urogynecol J 2011;22:1313-8.
41. Umeoka S, Koyama T, Togashi K, Kobayashi H, Akuta K. Vascular dilatation in the pelvis: Identification with CT and MR imaging. Radiographics 2004;24:193-208.
42. Granite G, Meshida K, Wind G. Frequency and clinical review of the aberrant obturator artery: A cadaveric study. Diagnostics (Basel) 2020;10:E546.
43. Darmanis S, Lewis A, Mansoor A, Bircher M. Corona mortis: An anatomical study with clinical implications in approaches to the pelvis and acetabulum. Clin Anat 2007;20:433-9.
44. Lau H, Lee F. A prospective endoscopic study of retropubic. Surg Endosc 2003;17:1376-9.
45. Stavropoulou-Deli A, Anagnostopoulou S. Corona mortis: Anatomical data and clinical considerations. Aust N Z J Obstet Gynaecol 2013;53:283-6.
46. Pinochet J, Molina CR, Flores EY. Bilateral variation of the venous corona mortis with a presentation previously undescribed. Folia Morphol (Warsz) 2016;75:409-12.
47. Daeubler B, Anderson SE, Leunig M, Triller J. Hemorrhage secondary to pelvic fracture: Coil embolization of an aberrant obturator artery. J Endovasc Ther 2003;10:676-80.
48. Engin C, Posacioglu H, Ayik F, Apaydin AZ. Management of vascular infection in the groin. Tex Heart Inst J 2005;32:529-34.
49. Karakurt L, Karaca I, Yilmaz E, Burma O, Serin E. Corona mortis: Incidence and location. Arch Orthop Trauma Surg 2002;122:163-4.
50. Pellegrino A, Damiani GR, Marco S, Ciro S, Cofelice V, Rosati F. Corona mortis exposition during laparoscopic procedure for gynecological malignancies. Updates Surg 2014;66:65-8.
51. Yoon W, Kim JK, Jeong YY, Seo JJ, Park JG, Kang HK. Pelvic arterial hemorrhage in patients with pelvic fractures: Detection

with contrast-enhanced CT. Radiographics 2004;24:1591-605.
52. Tipton JS. Obturator neuropathy. Curr Rev Musculoskelet Med 2008;1:234-7.
53. Leiber LM, Thouveny F, Bouvier A, Labriffe M, Berthier E, Aubé C, *et al.* MRI and venographic aspects of pelvic venous insufficiency. Diagn Interv Imaging 2014;95:1091-102.
54. Lopez AJ. Female pelvic vein embolization: Indications, techniques, and outcomes. Cardiovasc Intervent Radiol 2015;38:806-20.
55. Harma M, Sel G, Açıkgöz B, Harma Mİ. Successful obturator nerve repairing: Intraoperative sural nerve graft harvesting in endometrium cancer patient. Int J Surg Case Rep 2014;5:345-6.
56. Wada K, Goto T, Tezuka F, Tamaki S, Hamada D, Tsutsui T, *et al.* Variations in the obturator artery around the obturator foramen assessed by three-dimensional computed tomographic angiography and prevention of vascular-related complications in rotational acetabular osteotomy. Int Orthop 2017;41:133-9.

Case Report

True Hermaphrodite of Ovotestis in a 5-Year-Old Child

James Joseph Yahaya[1,2]

[1]*Department of Pathology, Makerere University College of Health Sciences, Makerere University, Kampala, Uganda,* [2]*Department of Biomedical Science, College of Health Science, The University of Dodoma, Dodoma, Tanzania*

Abstract

Assigning possible and correct sex of individuals born with ambiguous genitalia, notably those with true hermaphroditism (TH) at their neonatal stage, is of paramount psychosocial advantage. A 5-year-old child with karyotype of 46, XX who was reared as male is herein presented. The right testicle was neither palpable in the scrotal sac nor in the inguinal canal. The left testicle was palpable in the scrotum and was of adequate size according to the child. A hormonal profile showed a testosterone level of 2.30 ng/dl (normal value: 30–50 ng/dl). Both testicular and ovarian tissues were found on one side (ovotestis), hence TH of ovotestis was confirmed. It is important to assign true sex for patients with an intersex disorder particularly those with TH so as to give positive psychosocial benefits for them as well as removing gonadal tissues which would lead to the development of gonadal malignancies.

Keywords: *Hermaphrodite, orchidectomy, testicle, undescended*

Introduction

True hermaphroditism (TH) refers to simultaneous presence of both gonadal tissues (testicular and ovarian tissue) regardless of the patient's karyotype and other ancillary tests such as determination of SRY gene in the blood of the individual.[1] TH is the rarest form of the disorders of sexual differentiation (DSD) whose originality of the term hermaphrodite connoted from the Greek belief of the typical resemblance of a person with both sexes who resulted from joining of the nymph of Fountain of Salmacis with the son of Hermes and Aphrodite. The incidence of TH among the DSDs is 5%.[2] It has also been reported that 1 out of either 4500 or 5000 live-born babies have a chance of being a TH or sometimes called ovotesticular DSD and even the incidence may range up to 10% and about 75 cases of TH have been reported in the literature.[1,3]

Case Report

A 5-year-old child was presented by his mother at the outpatient department with the chief complaint of undescended right testicle. The child was reared as male and had an uneventful history since birth. On physical examination, the right testicle was neither palpable in the scrotal sac nor in the inguinal canal. The left testicle was palpable in the scrotum and was of adequate size according to the age of the child. The meatal opening was present at normal position. The penis was measuring approximately 3.8 cm long with 1.7 cm in girth. All routine investigations were within normal range. A hormonal profile showed a testosterone level of 2.30 ng/dl (normal value: 30–50 ng/dl). Sex chromatin testing using buccal smear was found negative. Karyotype analysis was done and it revealed 46, XX. Molecular test to determine the SRY gene in this case was not done.

Ultrasound report revealed undescended right testicle which was not visible in the inguinal canal or abdomen. A clinical diagnosis of undescended testicle (UDT) was established. Intraoperative exploration revealed both ovaries, left fallopian tube, a viable testicle on the right side, and uterus. Orchidectomy and removal of other Mullerian structures were done at surgery and sent for histological evaluation. The histopathological report confirmed the presence of ovarian, testicular, uterine, and fallopian tissue [Figure 1], testicular tissue [Figure 2], and uterine tissue [Figure 3]. Based on the findings, a diagnosis of TH was confirmed, and the mother was finally counseled to rear the child as a male due to predominant male phenotype.

How to cite this article: Yahaya JJ. True hermaphrodite of ovotestis in a 5-year-old child. J Anat Soc India 2022;XX:XX-XX.

Article Info

Received: 16 May 2020
Revised: 08 February 2022
Accepted: 02 April 2022
Available online: ***

Address for correspondence:
Dr. James Joseph Yahaya, Department of Biomedical Science, College of Health Science, The University of Dodoma, Dodoma, Tanzania. E-mail: mashimba2009@yahoo.com

Access this article online

Website: www.jasi.org.in
DOI: 10.4103/JASI.JASI_90_20
Quick Response Code:

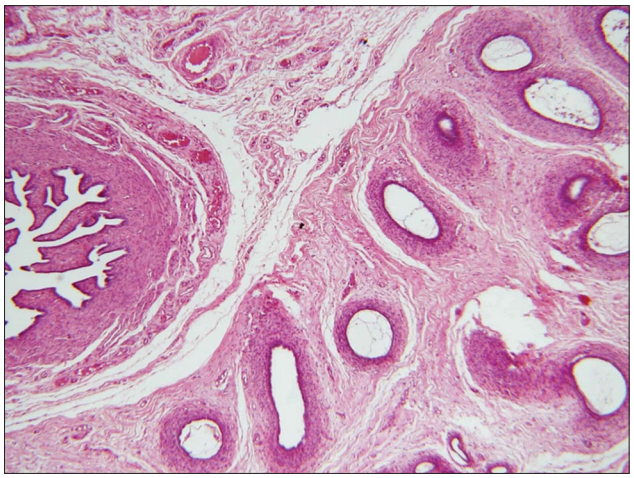

Figure 1: Fallopian tube and ovarian tissue were fused together (H and E, ×40)

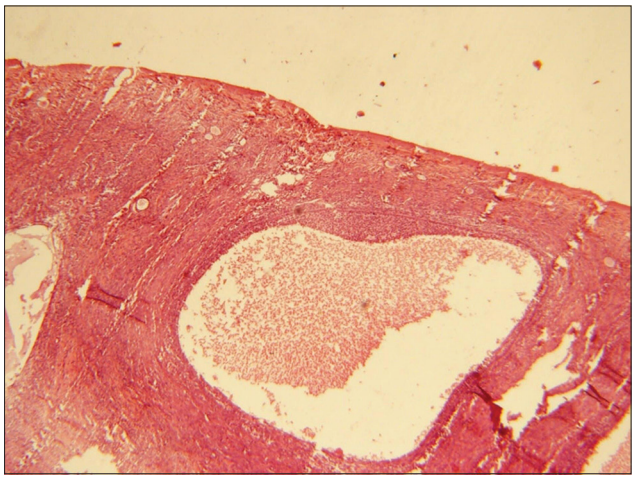

Figure 2: Testicular tissue (H and E, ×40)

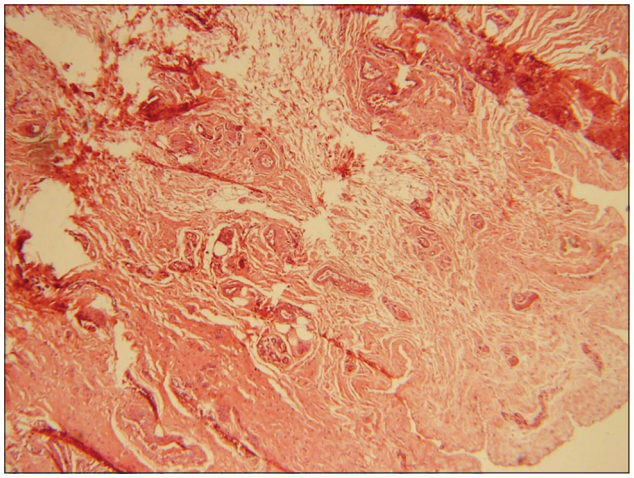

Figure 3: Uterine tissue showing myometrial fibers (H and E, ×40)

Discussion

The pathogenesis of TH has not been fully elucidated. Studies have shown that the presence of both Müllerian and Wolffian structures in individuals with TH could be a result of inappropriate timing of adequate Mullerian-inhibiting factor effect but also inadequate capacity of the Leydig cells to synthesize testosterone.[4,5] Another mechanism leading to TH is mutation of the sex-determining region Y (SRY) gene, which contributes to 10% and especially of 46 XX karyotypes.[5,6]

Patients with TH can be divided into three categories. Unilateral, if there are both testicular and ovarian tissues (forming one ovotestes or two separated gonads) on one side, and a testis or an ovary in the other side; if there is no gonadal tissue in this latter side, unilateral hermaphroditism is incomplete; (2) bilateral, if testicular and ovarian tissues are present on both sides of the body; and (3) alternate, if there is a testis on one side, and an ovary on the other side.[7] Majority of patients with TH present clinically with ambiguous genitalia, UDT, abdominal pain, hypospadias, cyclic hematuria, amenorrhea, and chordee.[5-7] Other cases of TH are phenotypically normal, and as they attain maturity, they begin to present with abnormalities such as gynecomastia.[5]

Imaging tests such as pelvic ultrasound and laparoscopic exploration are the commonly routine diagnostic methods in patients with TH. Histological evaluation of the sampled tissues from the patient helps to determine the sex of the patient regardless of the results of karyotype.[1] Cytomolecular tests are performed to study the patient's genetic sex; however, karyotypes are not suitable for selecting the rearing sex of the patient.[3,4] These tests involve the easiest cytological test such as Barr body testing and other molecular tests such as karyotype analysis, chromatin test, and DNA analysis for detection of SRY gene mutation.[3]

Endocrinological testing for androgen sensitivity assessment and other hormones of reproductive role is also normally considered. Gonadotropin-releasing hormone agonist (GnRHag) for females and anti-Mullerian hormone (AMH) levels for male need to be included in the panel. These two tests are done to evaluate the function of the gonads by comparing the baseline data and after the removal of the aberrant gonadal tissue.[3,4] The GnRHag test comprises a group of hormones including testosterone, estradiol, luteinizing hormone, follicular stimulating hormone, AMH, and 17-OH progesterone.[5,6] Assigning sex for which the child will be reared from the beginning has been reported to be a very crucial step in the process of management. The team of health-care professionals consisting of different medical specialists meets with parents or guardians and assigns a sex of rearing based on genital, gonadal, and genetic factors.[1]

The sex of rearing the child is influenced by quite many factors. The fat distribution, pubic hair distribution, and phallus size are the physical features that can be augmented in the process of assigning sex.[4] For example, female sex of rearing is the likely choice when phallic length is below

1.5 cm because an adequate and functional vagina can be more reliably constructed in that setting than a functional penis.[4,8] Surgical options for reconstruction of a functional sexual organ have been reported to have success in these days compared to the previous time. Different surgical interventions have been put in place for possible corrections of aberrant gonadal organs such as reduction of clitoromegaly as well as the removal of gonads for prevention of occurrence of malignant tumors. Surgical repair techniques including orchidopexy, urethroplasty, and chordee correction have been invented to manage patients with DSD.[9,10]

Conclusion

Assigning true sex for patients with intersex disorders especially those with TH brings positive psychosocial benefits as well as prompting removal of gonadal tissues which would lead to the development of gonadal malignancies.

Acknowledgments

We would like to show appreciation for the child's mother, physicians, and the surgeons for their cooperation at the time of gathering the necessary information which was required in the process of preparing the manuscript.

Informed Consent

Written informed consent was first obtained from the mother and a copy of it has been kept by the authors.

Declaration of patient consent

The authors certify that they have obtained all appropriate patient consent forms. In the form, the legal guardian has given her consent for images and other clinical information to be reported in the journal. The guardian understands that name and initials will not be published and due efforts will be made to conceal identity, but anonymity cannot be guaranteed.

Financial support and sponsorship

Nil.

Conflicts of interest

There are no conflicts of interest.

References

1. Tomaselli S, Megiorni F, De Bernardo C, Felici A, Marrocco G, Maggiulli G, *et al.* Syndromic true hermaphroditism due to an R-spondin1 (RSPO1) homozygous mutation. Hum Mutat 2008;29:220-6.
2. Bandopadhyay D, Yogesh R, Arundhati S. Genetic analysis in a true hermaphrodite: A case report. IJBAR 2013;4:933-6.
3. Grimes CK, Rosenbaum DM, Kirkpatrick JA Jr. Pediatric gynecologic radiology. Semin Roentgenol 1982;17:284-301.
4. McDonough PG, Byrd JR, Tho PT, Otken L. Gonadoblastoma in a true hermaphrodite with a 46, XX karyotype. Obstet Gynecol 1976;47:355-8.
5. Mieszczak J, Houk CP, Lee PA. Assignment of the sex of rearing in the neonate with a disorder of sex development. Curr Opin Pediatr 2009;21:541-7.
6. Hadjiathanasiou CG, Brauner R, Lortat-Jacob S, Nivot S, Jaubert F, Fellous M, *et al.* True hermaphroditism: Genetic variants and clinical management. J Pediatr 1994;125:738-44.
7. Salas-Cortés L, Jaubert F, Bono MR, Fellous M, Rosemblatt M. Expression of the human SRY protein during development in normal male gonadal and sex-reversed tissues. J Exp Zool 2001;290:607-15.
8. Heier J. A review of anatomical presentation and treatment in true hermaphroditism. Best Integr Writ 2014;1:12.
9. Al-Salem AH, Abusrair HA. True hermaphroditism. Ann Saudi Med 2000;20:40-2.
10. Greeley SA, Littlejohn E, Husain AN, Waggoner D, Gundeti M, Rosenfield RL. The effect of the testis on the ovary: Structure-function relationships in a neonate with a unilateral ovotestis (ovotesticular disorder of sex development). Horm Res Paediatr 2017;87:205-12.

Case Report

Bilateral Tripartite Dural Septation of the Jugular Foramen

Joastin Naidoo, Carmen Olivia Rennie, Lelika Lazarus

Discipline of Clinical Anatomy, School of Laboratory Medicine and Medical Sciences, College of Health Sciences, University of KwaZulu-Natal

Abstract

We present a case of bilateral tripartite dural septation on the internal aspect of the jugular foramen (JF) in a 71-year-old White South African male. Dura mater at the intracranial aspect of the JF forms the neurovascular compartment, which houses the cranial nerves (*viz.* glossopharyngeal (9th), vagus (10th), and accessory (11th) cranial nerves), as well as the jugular vein. In the present case, a dural septation was seen between the 9th and 10th cranial nerves and between the 10th and 11th cranial nerves; therefore, the 9th cranial nerve traversed the anterior compartment, the 10th cranial nerve traversed the intermediate compartment, and the 11th cranial nerve traversed the posterior compartment. Clinical implications of this variation of the JF arise due to the occurrence of glomus jugulare tumors, as well as other pathologies such as meningiomas and neuroinomas, and these tumors occur in the region in which the neurovasculature exits the cranium. The tumors then lead to compression of these structures within the foramen. Since two dural septa at the intracranial aperture of the JF are reported bilaterally, the rootlets of the cranial nerves were more tethered within the JF. This has surgical implications as substantial tethering of these rootlets requires additional dissection during surgery, thereby increasing the risk of iatrogenic injury to the cranial nerves. It has also been reported that compartmentalization of the JF accentuates the clinical presentation of the glomus jugulare tumor. Thus, a knowledge of variations within the JF becomes imperative to ENT and neurosurgeons.

Keywords: *Cranial nerves, dural septation, glomus jugulare tumor, jugular foramen, Vernet's syndrome*

Introduction

Foramina are anatomically considered openings which transmit various structures such as nerves, arteries, and veins.[1] The jugular foramen (JF) has been considered the most complex cranial foramen and the foramen with the most difficult surgical access; this is due to the location of the foramen which lies as a canal between the petrous part of the temporal bone and the occipital bone.[2,3] Various neurovascular structures traverse the JF including the glossopharyngeal, vagus, and accessory cranial nerves.[4,5] Therefore, due to the location of the JF and the cranial nerves passing through, among other structures such as the internal jugular vein and inferior petrosal sinus, safe surgical access to the foramen is encumbered.[2]

Tubbs *et al*. highlighted the paucity of the literature with respect to detailed anatomical studies defining the dural septations of the intracranial aspect of the JF and thus aimed to "fill the gap" in the literature. Tubbs *et al*. also stated that the dura mater at the inner aperture of the JF formed compartments housing neurovasculature; the study conducted by Tubbs *et al*. then classified the dural septations of the JF on the premise that these dural relationships are of interest in the surgical treatment of meningiomas associated with the JF, as well as providing additional knowledge to assist the neurosurgeon in manipulating the nerves as they enter the JF.

Clinically, a thorough knowledge of the anatomy of the JF and the variations thereof become relevant when dealing with cases such as glomus jugulare tumors, as well as other pathologies such as meningiomas and neurinomas, since careful preoperative investigations and planning are important due to the complexity of the JF.[3,6,7]

Case Report

A case of bilateral tripartite dural septation on the internal aspect of the JF in a 71-year old White South African male is found during dissection in an anatomy laboratory.

How to cite this article: Naidoo J, Rennie CO, Lazarus L. Bilateral tripartite dural septation of the jugular foramen. J Anat Soc India 2022;XX:XX-XX.

Article Info

Received: 04 September 2019
Revised: 10 March 2021
Accepted: 24 November 2021
Available online: ***

Address for correspondence:
Prof. Lelika Lazarus, Discipline of Clinical Anatomy, School of Laboratory Medicine and Medical Sciences, College of Health Sciences, University of KwaZulu-Natal, Natal Westville Campus, Private Bag X54001, Durban 4000, South Africa.
E-mail: ramsaroopl@ukzn.ac.za

Access this article online

Website: www.jasi.org.in
DOI: 10.4103/JASI.JASI_123_19
Quick Response Code:

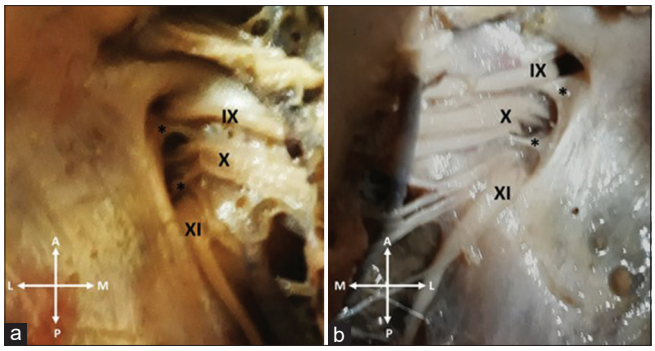

Figure 1: Bilateral tripartite dural septation of the jugular foramen. (a) Left jugular foramen, (b) right jugular foramen, IX: Glossopharyngeal nerve, X: Vagus nerve, XI: Accessory nerve, *: Dural septa

Each cranial nerve is seen to be passing through its own compartment. A dural septation was seen between the glossopharyngeal and vagus nerves and between the vagus and accessory nerves; therefore, the glossopharyngeal nerve traversed the anterior compartment, the vagus nerve traversed the intermediate compartment, and the accessory nerve traversed the posterior compartment. The anteroposterior diameter of the right JF was 9.87 mm, and the mediolateral diameter was 4.54 mm; the anteroposterior diameter of the left JF was 9.39 mm and the mediolateral diameter was 3.28 mm.

Discussion

The JF has been an area that has attracted the attention of radiologists, ear, nose, and throat (ENT) surgeons, and neurosurgeons since safe surgical access to the JF is hindered by the contents of the foramen and local surrounding structures.[2,7] Dura mater at the intracranial aspect of the JF forms a distinct compartment for the venous structures and cranial nerves that traverse the foramen.[3] These dural relationships are of potential interest with respect to surgical treatment of lesions associated with the JF, such as paragangliomas.[3]

Dural septations divide the intracranial JF into three compartments; dura overlying the intrajugular compartment has two perforations, one of which is the glossopharyngeal meatus and the other being the vagal meatus.[2] The glossopharyngeal nerve passes through glossopharyngeal meatus, whereas the vagus and accessory nerves pass through the vagal meatus; these are separated by a dural septum which provides a clear separation of the glossopharyngeal and vagus nerves as they enter the JF.[2] Sethi *et al*. stated that the compartmentalization of the foramen could be the reason for compression on the structures traversing the foramen, which presents as various symptoms that are grouped together as the JF syndrome, also known as Vernet's syndrome.

Findings of the study conducted by Tubbs *et al*. indicated four types of dural septation of the JF. A single septation present between the glossopharyngeal nerve (anteriorly) and the vagus and accessory nerves (posteriorly) was considered Type 1, no septations present was considered Type 2, a single septation present between the glossopharyngeal and vagus nerves (anteriorly) and the accessory nerve (posteriorly) was considered Type 3, and multiple septations (ranging from three to seven septa) was considered Type 4.

The tripartite septation of the present study, in which three dural septa are present [Figure 1]; thus, falls under the category of Type 4 septation as defined by Tubbs *et al*. who recorded this variation in 25% of the sample size. However, this study reports on a bilateral occurrence of the tripartite septation.

Tubbs *et al*. further noted that the meningeal relations of a Type 4 septation have smaller rootlets of each of the cranial nerves of the JF that were septated and thus are more tethered within the JF. This significant tethering would then require additional dissection, thereby increasing the risk of iatrogenic injury to the cranial nerves following manipulation of the nerves by the surgeon.[3] Furthermore, due to the differences with regard to intracranial dural sleeves of the JF, tumors in this region may have different growth patterns, for example, the Type 4 septation, or tripartite septation in the present study, has a likelihood of inhibiting significant growth of tumors into the JF.[3]

Glomus jugulare tumors, which are found in the tunica adventitia of the jugular bulb, grow in and around the JF and cause compression of the structures that traverse the foramen.[7] The compression of the neurovasculature results in difficulty swallowing, loss of voice, facial palsy, and pulsatile tinnitus.[7,8] Sethi *et al*. stated that compartmentalization of the JF may heighten the clinical presentations of the glomus jugulare tumor. Daley and Colliver theorized that Vernet's syndrome was caused by compression of the cranial nerves at the JF; however, Shapiro stated that large neurinomas of the glossopharyngeal, vagus, and accessory nerves passing through the JF may enlarge the JF.

The present study also recorded anteroposterior and mediolateral diameters of the JF. The right JF had an anteroposterior diameter of 9.87 mm and a mediolateral diameter of 4.54mm, whereas the left JF had an anteroposterior diameter of 9.39 mm and a mediolateral diameter of 3.28mm. This supports the trend of the previous studies in which the right JF is larger than the left JF such as Tahir and Anil (61.7%) and Sethi *et al*. (53.5%). Tahir and Anil reported that the size of the JF is related to the size of the transverse sinus; thus, the right JF appears to be larger than the left since the superior sagittal usually drains into the right transverse sinus.[9-11]

Conclusion

The bilateral occurrence of the tripartite dural septation, as reported in the present study, highlights the importance of

knowledge of the variant anatomy of the JF. Furthermore, due to the complexity of the JF and the paucity of the literature regarding the intracranial dural septations of the JF, a knowledge of this area becomes imperative to ENT surgeons and neurosurgeons in the preoperative planning of cases such as Vernet's syndrome and glomus jugulare tumors to minimize iatrogenic injury.

Declaration of patient consent

The authors certify that they have obtained all appropriate patient consent forms. In the form the patient (s) has/have given his/her/their consent for his/her/their images and other clinical information to be reported in the journal. The patients understand that their names and initials will not be published and due efforts will be made to conceal their identity, but anonymity cannot be guaranteed.

Financial support and sponsorship

Nil.

Conflicts of interest

There are no conflicts of interest.

References

1. Sakthivel KM, Balaji TK, Moni AS, Narayanan G, Sathish Kumar K. Study of jugular foramen – A case report. IOSR-JDMS 2014;13:63-7.
2. Tummala RP, Coscarella E, Morcos JJ. Surgical anatomy of the jugular foramen. Oper Tech Neurosurg 2005;8:2-5.
3. Tubbs RS, Griessenauer CJ, Bilal M, Raborn J, Loukas M, Cohen-Gadol AA. Dural septation on the inner surface of the jugular foramen: An anatomical study. J Neurol Surg B Skull Base 2015;76:214-7.
4. Moore KL, Dalley AF. Clinically Oriented Anatomy. 5th ed. Philadelphia: Lippincott Williams & Wilkins; 2006. p. 897.
5. Jasuja VR, Kulkarni PG, Borate SM, Wadekar PR, Punyani SR. Morphometric and morphologic, study of jugular foramen in western Maharashtra region of India. Int J Anat Res 2016;4:2085-9.
6. Watkins LD, Mendoza N, Cheesman AD, Symon L. Glomus jugulare tumours: A review of 61 cases. Acta Neurochir (Wien) 1994;130:66-70.
7. Sethi R, Singh V, Kaul NV. Morphological variations of a jugular foramen in North Indian human adult skulls. Indian J Otol 2011;17:14-6.
8. Kocur D, Ślusarczyk W, Przybyłko N, Hofman M, Jamróz T, Suszyński K, *et al.* Endovascular approach to glomus jugulare tumors. Pol J Radiol 2017;82:322-6.
9. Daley NC, Colliver EB. A case of vernet syndrome associated with internal jugular phlebectasia. PM R 2014;6:1163-5.
10. Shapiro R. Compartmentation of the jugular foramen. J Neurosurg 1972;36:340-3.
11. Hatiboğlu MT, Anil A. Structural variations in the jugular foramen of the human skull. J Anat 1992;180:191-6.

Case Report

Multiple Intracranial Vessel Fenestrations: A Report of Two Cases from a Tertiary Care Center

Amlan Kusum Datta, Subhadeep Gupta

Department of Neurology, Bangur Institute of Neurosciences, Institute of Post Graduate Medical Education and Research, Kolkata, West Bengal, India

Abstract

Intracranial vascular fenestrations are unique anatomical anomalies, consequential to developmental perturbations in vessel embryology. The importance of identification rests on its frequent association with disturbed cerebral flow dynamics and intracranial pathologies. Herein, we report two cases from the same institute of such an association. One presented with an isolated intraventricular hemorrhage, found to have basilar artery fenestrations, whereas the other presented with subarachnoid hemorrhage, with fenestrations involving both the anterior and posterior circulations. Neither of the two patients had any evidence of aneurysms, arteriovenous malformations, or dissections and were managed conservatively. Being acquainted with the anatomy and pathophysiology of these vascular aberrations are paramount in achieving optimal patient outcomes in certain vascular catastrophes.

Keywords: *Angiography, embryology, fenestrations, neuroanatomy, subarachnoid hemorrhage*

Introduction

A "fenestration" refers to an anatomical aberration, wherein a vessel segregates into two or more vascular channels, which fuse into a single lumen along its distal course. The high degree of variability in the reported prevalence of intracerebral arterial fenestrations, with rates ranging from <1% up to as high as 60%,[1] may be attributed to the lack of uniformity among the nature of imaging modalities, ranging from noninvasive angiograms to more advanced high-resolution three-dimensional digital subtraction angiography (DSA) techniques. Apart from the intriguing embryological aspect, interest in fenestrations stem from their propensity to be associated with intracranial pathologies such as subarachnoid hemorrhages (SAH), strokes, and dissections.[2] Albeit controversial, it is sumptuous to assume arterial fenestrations to be a marker of neurovascular pathologies owing to their supposed ability to alter microvascular flow dynamics. Herein, the authors report two cases of isolated intracranial vascular events associated with intracranial arterial fenestrations, without any other identifiable bleeding sources.

Case Report

Patient 1

A 40-year-old male, without known vascular risk factors, presented with a thunderclap headache. Neurological examination revealed the presence of neck stiffness without any other focal deficits. Computed tomography (CT) scan, which was done at our institute approximately a week after the initial event, revealed an intraventricular hemorrhage in the fourth ventricle, with the presence of hydrocephalus [Figure 1]. Magnetic resonance angiography (MRA), using a 3 Tesla magnetic resonance imaging scanner, Time of flight sequence of intracranial vessels revealed two fenestrations of the basilar artery [Figure 1b] with the presence of bilateral fetal posterior cerebral arteries (fPCAs). No other pathologies such as aneurysms, dissection, or arteriovenous malformations were noted. In absence of any therapeutic scope, the patient was managed conservatively, and an invasive angiographic study was not performed. He was discharged in hemodynamically stable condition and followed up for 1 year, till which he has remained asymptomatic.

Patient 2

A 35-year-old nonhypertensive male, presented with "thunderclap headache," followed by transient loss of consciousness,

How to cite this article: Datta AK, Gupta S. Multiple intracranial vessel fenestrations: A report of two cases from a tertiary care center J Anat Soc India 2022;XX:XX-XX.

Article Info

Received: 30 September 2021
Revised: 17 April 2022
Accepted: 09 June 2022
Available online: ***

Address for correspondence:
Dr. Amlan Kusum Datta, Department of Neurology, Bangur Institute of Neurosciences, Institute of Post Graduate Medical Education and Research, 52 1/A Sambhu Nath Pandit Street, Bhowanipore, Kolkata - 700 020, West Bengal, India.
E-mail: amlankd@gmail.com

Access this article online

Website: www.jasi.org.in
DOI: 10.4103/jasi.jasi_167_21
Quick Response Code:

without any focal neurological deficit. Noncontrast CT brain showed the presence of subarachnoid hemorrhage involving the right Sylvian fissure [Figure 1d]. Since MRA was unremarkable, DSA of intracranial vessels was conducted, after obtaining prior informed patient consent. Although no aneurysms could be detected, following injection of contrast into the left vertebral artery, a fenestration was noted in the same vessel. Another fenestration was seen involving the proximal right middle cerebral artery (MCA), following injection into the right internal carotid artery (ICA). Like the previous patient, he too was managed conservatively and made an uneventful recovery. He is into the 9th month of follow-up and his course has been uneventful to date.

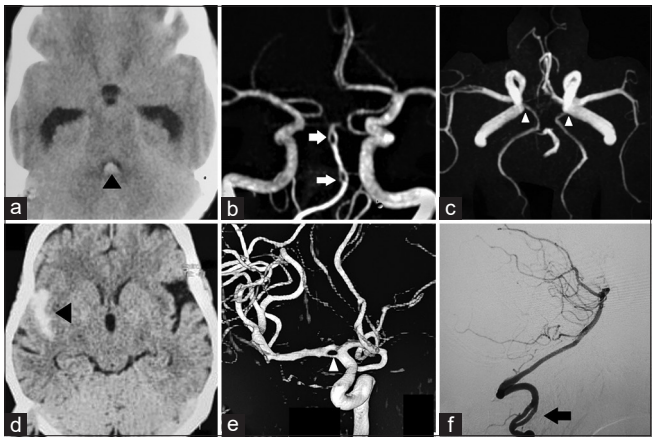

Figure 1: Upper panel: Noncontrast CT Brain (a) blood in the fourth ventricle (black arrowhead) and dilatation of temporal horn of lateral ventricle suggestive of hydrocephalous. Time of flight MR angiography, (b and c) left VA terminating as a left posterior inferior cerebellar artery, two fenestrations in the basilar artery (white arrow), bilateral fetal PCA originating from ICA (white arrowhead), and hypoplastic A1 segment of right ACA. Lower panel: Noncontrast CT Brain, (d) blood in Sylvian fissure (black arrowhead). 3D DSA after right ICA injection, (e) reveals fenestration of M1 segment of the right middle cerebral artery (white arrowhead). DSA after left VA injection, and (f) large distal left vertebral artery fenestration (black arrow). CT: Computed tomography, MR: Magnetic resonance, VA: Vertebral Artery, PCA: Posterior Cerebral artery, ICA: Internal carotid artery, ACA: Anterior cerebral artery, DSA: Digital subtraction angiography

Discussion

Recent advances in angiographic techniques, particularly with the development of three-dimensional DSA techniques, have enabled the better demonstration of thin fenestration channels, which previously remained occult on traditional angiographic methods despite evidence of their more frequent existence from postmortem and surgical series[3-5]

Fenestrations may arise due to either failure of fusion of paired embryological vessels or from a failure of complete obliteration of a primitive vascular anastomotic network.[6] Naturally, the duplicated vascular channels comprise distinct endothelial and muscular layers, occasionally sharing a common adventitia.[6] As with other morphological variations, fenestrations too are located frequently at or near the midline, with the anterior communicating and basilar arteries (BA) being most involved.[1] BA fenestrations, believed to be the result of a failure of fusion of paired longitudinal neural arteries, can occur anywhere along its course, with the vertebral-basilar junction being the favored location[2,6] [Figure 2a]. The presence of bilateral fPCAs as noted in the first case [Figure 1c], perhaps represent an attempt to compensate for the perturbed basilar artery flow.

The primitive ICA divides into a cranial and caudal division, the latter of which gives rise to the primitive anterior choroidal artery (ACho). Numerous arterial twigs develop distal to the ACho, which subsequently form the MCA. Errors in the regression of one or more of these vascular channels result in the origin of MCA fenestrations[7] [Figure 3]. The coexistence of multiple fenestrations, that too, arising from posterior and anterior circulations, is an extremely unlikely event.[1] Double fenestrations of BA, as in the first case, involving its proximodistal segments represent fusion anomalies of both the caudal rami of ICA and paired longitudinal arteries [Figure 2].[6] Therefore, although the adult morphological predisposition mimics an isolated posterior circulation

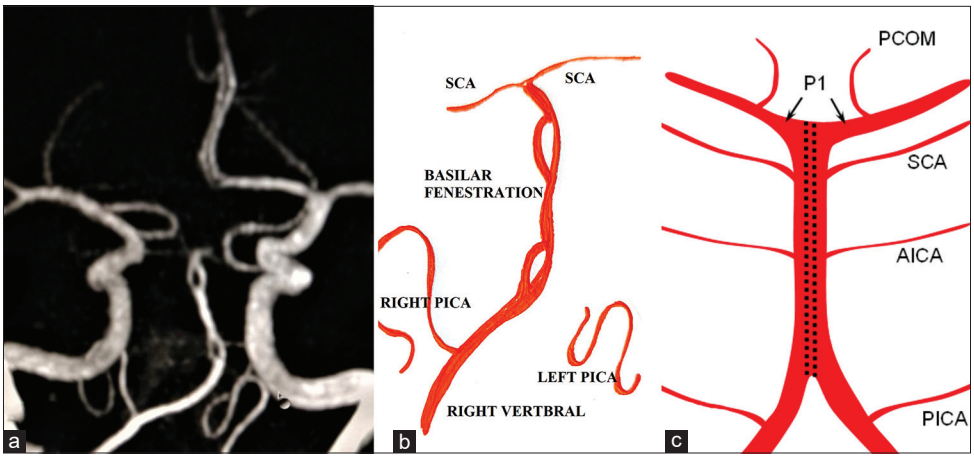

Figure 2: (a) DSA image depicting basilar artery fenestration with corresponding. (b) Line diagram showing a fenestration of the BA, adjacent to the site of origin of the AICA, proximal to origins of SCA and PCA, distal to the origin of PICA. (c) Line of normal embryologic fusion along midline of two longitudinal neural arteries to form the basilar artery. DSA: Digital subtraction angiogram, BA: Basilar artery, AICA: Anterior inferior cerebellar artery, SCA: superior cerebellar artery, PCA: Posterior cerebral artery, PICA: Posterior inferior cerebellar artery

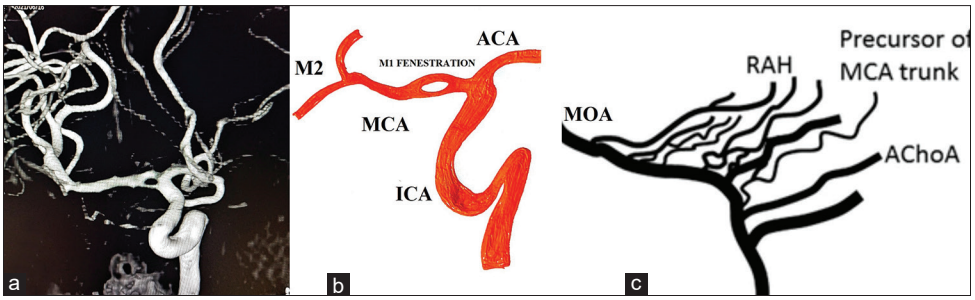

Figure 3: (a) Digital subtraction angiography image depicting fenestration of MCA with corresponding. (b) Line diagram showing fenestration of proximal right MCA (M1). (c) normal fetal development of the MCA from arterial twigs arising from the ICA, distal to the ACA. MCA: Middle cerebral artery, ICA: Internal carotid artery, ACA: Anterior cerebral artery

developmental aberration, it might actually represent a fusional defect of both the anterior and posterior circulation.

The frequent association of fenestrations with intracranial pathologies may be attributed to altered microvascular flow dynamics and histopathological aberrations of fenestrated vessels.[8] Although generally believed to be caused by aneurysmal rupture, in 5%–15% of cases of SAH, no bleeding source can be delineated.[9] Hudák *et al*.[8] had previously reported a high incidence of arterial fenestrations in cases of angiographically negative SAH. Even though autopsy studies have revealed the presence of muscular defects in walls of arteries affected by fenestrations,[10] definite evidence implicating fenestrations as a cause of SAH is lacking.

The presence of an unexplained intracranial vascular pathology might be a compelling reason to thoroughly search for intracranial fenestration anomalies using high-resolution invasive angiography techniques if need be. However, larger population-based studies are needed before assuming that these defects may prospectively give rise to *de novo* intracranial bleeding or other pathologies.

Consent

Informed consent obtained.

Declaration of patient consent

The authors certify that they have obtained all appropriate patient consent forms. In the form, the patients have given their consent for their images and other clinical information to be reported in the journal. The patients understand that their names and initials will not be published and due efforts will be made to conceal their identity, but anonymity cannot be guaranteed.

Acknowledgment

Our sincere gratitude to the patients and their kin for their kind cooperation.

Financial support and sponsorship

Nil.

Conflicts of interest

There are no conflicts of interest.

References

1. Cooke DL, Stout CE, Kim WT, Kansagra AP, Yu JP, Gu A, *et al*. Cerebral arterial fenestrations. Interv Neuroradiol 2014;20:261-74.
2. Vasović L, Trandafilović M, Jovanović I, Ugrenović S, Antović A, Karadžić R, *et al*. Human basilar artery abnormalities in the prenatal and postnatal period. World Neurosurg 2013;79: 23. e15-23.
3. Gomes FB, Dujovny M, Umansky F, Berman SK, Diaz FG, Ausman JI, *et al*. Microanatomy of the anterior cerebral artery. Surg Neurol 1986;26:129-41.
4. Sanders WP, Sorek PA, Mehta BA. Fenestration of intracranial arteries with special attention to associated aneurysms and other anomalies. AJNR Am J Neuroradiol 1993;14:675-80.
5. Serizawa T, Saeki N, Yamaura A. Microsurgical anatomy and clinical significance of the anterior communicating artery and its perforating branches. Neurosurgery 1997;40:1211-6.
6. Kathuria S, Gregg L, Chen J, Gandhi D. Normal cerebral arterial development and variations. Semin Ultrasound CT MR 2011;32:242-51.
7. Uchiyama N. Anomalies of the middle cerebral artery. Neurol Med Chir (Tokyo) 2017;57:261-6.
8. Hudák I, Lenzsér G, Lunenkova V, Dóczi T. Cerebral arterial fenestrations: A common phenomenon in unexplained subarachnoid haemorrhage. Acta Neurochir (Wien) 2013;155:217-22.
9. Andaluz N, Zuccarello M. Yield of further diagnostic work-up of cryptogenic subarachnoid hemorrhage based on bleeding patterns on computed tomographic scans. Neurosurgery 2008;62:1040-6.
10. Finlay HM, Canham PB. The layered fabric of cerebral artery fenestrations. Stroke 1994;25:1799-806.